A Power System Emergency Control Scheme in the Presence of High Wind Power Penetration

Hoseinzadeh, Bakhtyar

Publication date:
2015

Document Version
Publisher's PDF, also known as Version of record

A Power System Emergency Control Scheme in the Presence of High Wind Power Penetration

by

Bakhtyar Hoseinzadeh

A Dissertation Submitted to
the Faculty of Engineering and Science at Aalborg University
in Partial Fulfillment for the Degree of
Doctor of Philosophy in Electrical Engineering

May 2015
Aalborg, Denmark

Aalborg University
Department of Energy Technology
Pontoppidanstraede 101
Aalborg East, DK-9220
Denmark
Phone: +45 99 40 92 40
Fax: +45 98 15 14 11
http://www.et.aau.dk

Printed in Denmark by Uniprint
First Edition (March 2015)
Second Edition (June 2015)
ISBN: 978-87-92846-65-5

The professional softwares utilized in the current research:

- **PowerFactory**® is a trademark of **DIgSILENT GmbH** used for simulations;
- **MATLAB**® is a trademark of **MathWorks**, Inc used for plotting the simulation results;
- **Visio**® is a trademark of **Microsoft** Corporation used for drawings;
- **AutoCAD**® is a registered trademark of **Autodesk** used for drawings;
- **TeXstudio** is a free **LaTeX** editor used for dissemination of papers and thesis.

Thesis Details

1. Thesis Title: A Power System Emergency Control Scheme in the Presence of High Wind Power Penetration

2. Ph.D. Student: Bakhtyar Hoseinzadeh

3. Supervisor/s: Prof. Claus Leth Bak, Assoc. Prof. Filipe Faria da Silva

4. Opponents: Prof. Dr. Göran Andersson, ETH zürich, Switzerland, Prof. Ivan M. Dudurych, EirGrid Consulting Group, Ireland, Assoc. Prof. Jayakrishnan R. Pillai, Aalborg University.

5. Moderator: Prof. Birgitte Bak Jensen

6. Publications:

Paper 1: **B. Hoseinzadeh**, F. F. Silva, and C. L. Bak, "Decentralized Coordination of Load Shedding and Plant Protection with High Wind Power Penetration,"*Power Systems, IEEE Transactions on*, Under Review.

Paper 2: **B. Hoseinzadeh**, F. F. Silva, and C. L. Bak, "Adaptive tuning of frequency thresholds using voltage drop data in decentralized load shedding,"*Power Systems, IEEE Transactions on*, 2014.

Paper 3: **B. Hoseinzadeh**, F. F. Silva, and C. L. Bak, "Decentralized Power System Emergency Control in the Presence of High Wind Power Penetration,"*PES General Meeting | Conference Exposition, 2015 IEEE*, 2015.

Paper 4: T. Kalogiannis, E. M. Llano, **B. Hoseinzadeh**, and F. F. Silva, "Impact of High Level Penetration of Wind Turbines on Power System Transient Stability,"*POWERTECH Conference, 2015 IEEE*, 2015.

Paper 5: **B. Hoseinzadeh**, F. F. Silva, and C. L. Bak, "Active Power Deficit Estimation in Presence of Renewable Energy Sources,"*PES General Meeting | Conference Exposition, 2015 IEEE*, 2015.

Paper 6: **B. Hoseinzadeh**, F. F. Silva, and C. L. Bak, "Malfunction Operation of LVRT Capability of Wind Turbines Under Islanding Conditions,"*POWERTECH Conference, 2015 IEEE*, 2015.

Paper 7: **B. Hoseinzadeh**, F. F. Silva, and C. L. Bak, "Coordination of Voltage and Frequency Feedback in Load-Frequency Control Capability of Wind Turbine,"*Industrial Electronics Society (IECON), 2014 IEEE*, 2014.

Paper 8: **B. Hoseinzadeh**, F. F. Silva, and C. L. Bak, "Decentralized & Adaptive Load-Frequency Control Scheme of Variable Speed Wind Turbines,"*The 13th International Workshop on Large-Scale Integration of Wind Power into Power Systems as well as on Transmission Networks for Offshore Wind Power Plants*, 2014.

Paper 9: **B. Hoseinzadeh**, F. F. Silva, and C. L. Bak, "Power System Stability Using Decentralized Under Frequency and Voltage Load Shedding,"*PES General Meeting | Conference Exposition, 2014 IEEE*, 2014.

Paper 10: **B. Hoseinzadeh**, and Z. Chen, "Intelligent Load-Frequency Control Contribution of Wind Turbine in Power System Stability,"*EUROCON Conference, 2013 IEEE*, pp. 1124–1128, 2013.

7. This present report combined with the above listed scientific papers has been submitted for assessment in partial fulfilment of the PhD degree. The scientific papers are not included in this version due to copyright issues. Detailed publication information is provided above and the interested reader is referred to the original published papers. As part of the assessment, co-author statements have been made available to the assessment committee and are also available at the Faculty of Engineering and Science, Aalborg University.

"Many of life's failures are people who did not realize how close they were to success when they gave up."

Thomas A. Edison

To:

my parents,

my wife

and my children

for their exceptional love in my life

Preface

This thesis is written according to the project entitled "*A Power System Emergency Control Scheme in the Presence of High Wind Power Penetration*". The Ph.D. project is supported mainly by Ministry of science, Research and Technology of Iran and partially by the Department of Energy Technology, Aalborg University, Denmark. Acknowledgments are given to the above-mentioned institutions, as well as the Center Of Modern Power Transmission System (MPTS) and Otto Mønsteds Fond, who supported me for conference participation several times through my Ph.D. study. Special thanks to the head of the Department of Energy Technology John K. Pedersen, and prof. Zhe Chen for their kind support and tremendous help.

This research project was done under the supervision of prof. Claus Leth Bak from the Department of Energy Technology, Aalborg University, Denmark. First and foremost, I would like to express my deepest gratefulness to my supervisor, prof. Leth Bak, for his professional and patient guidance with his open-mindedness and earnestness during the Ph.D. project period. I do believe that the encouragement, which I received from prof. Leth Bak during my Ph.D. study will be of great support for my career and through my future life.

Also, I would like to place on record my gratitude to my co-supervisor, associate prof. Filipe Faria da Silva for being generous in sharing his research experiences, excellent and professional co-supervision during my study regarding his availability, helpful comments, view points and discussions during my PhD program. He undoubtedly offered me valuable technical and methodological advices in my research. Indeed, he taught me how to become a successful researcher and membership in his research team and working under his direct guidance was my pleasure, honor, an opportunity and a turning point in my academic career.

Additionally, I owe special thanks to my dear colleague, prof. Hassan Bevrani at University of Kurdistan for his infinite encouragement, support and aid during my academic career.

In particular, I take this opportunity to record my since gratefulness to all my colleagues from the Department of Energy Technology, Aalborg University, Denmark, for cooperation, lovely and pleasant environment and the endless friendship with unforgeable memories. I also would like to thank my close friends Mostafa Astaneh, Hamid Soltani, Amir Sajad Bahman, Reza Ahmadi and Qobad Shafiee. Moreover, much special appreciations are extended to Tina Lisbeth Larsen, Mette Skov Jensen, Corina Busk Gregersen and Casper Jørgensen for their assistance in many different ways. I would also like to express my gratitude to the assessment committee for the Ph.D. defense.

Finally, the most important and the sincerest gratitude to my parents for their exceptional love to the family and their encouragement through my life, to my lovely brother, sisters and their families for the support, concerns and understanding. All the best for our future.

Bakhtyar Hoseinzadeh
Aalborg University, November 18, 2015

Abstract

The main goal of the project is to improve existing protection technology by localizing the load shedding scheme in grids with high share of dispersed generation dominantly provided by renewable energy sources, i.e. wind, wave, solar, biomass, etc.

The higher complexity and lower predictability of grids with a high penetration of renewable energies makes it difficult to overseen and overcome widespread range of combinational and cascading events, just by relying on conventional protection systems, which generally do no coordinate different grid variables in the respective protection schemes. Utilization of all of locally measurable variables, e.g. frequency, its rate of change, voltage drop, power flow direction under an integrated decentralized plan is done in this project, in order to improve the grid reliability.

The proposed scheme benefits from a decentralized strategy, which reduces the burden of central control by decreasing the amount of data processing and more important, by avoiding any control problems in the system due to loss of communication link resulting from accidents of *Cyber Security* attacks, which have been recently located in the center of attention. The algorithms developed in this project may also constitute the lower level of a hierarchical control strategy, which can be activated in case of losing the communication with the control center.

Modern power protection relays often provide several protection schemes inside of one common package. However, they normally operate without coordination even when they are implemented inside a same module. This project intends to benefit from the fact that the existing technology already uses, all the required data as input to coordinate distinct plans under an integrated and versatile scheme. The proposed scheme automatically updates the frequency set points, stage time delays used for load shedding as a function of fault location and severity of the disturbance/s. It is a comprehensive solution for all possible combination of contingencies including outages, cascading events and islanding. The proposed methods not only are efficient for conventional power systems, but also for the time-variant structure and dispatch of grids with high share of renewable energy sources.

In order to achieve an efficient, fast and optimal load-generation balance following the under frequency contingencies in the power system, both load and generation sides

should contribute in the efforts. The load-frequency control as an ancillary service provided by renewable energy sources and load shedding as an emergency control should be localized. It means that the active power deficit should be compensated locally at vicinity of event location in order to avoid transferring the demanded active power from distant units to the incidence place. In this thesis, localization of both load-frequency control an load shedding are fulfilled using locally measured voltage drop data in the decentralized control strategy.

The proposed load shedding scheme is coordinated with existing plant protection relays, which are normally installed on the conventional synchronous machines. Considering the frequency-time characteristic of plant protection relays in the load curtailing plan makes the proposed scheme preventive against successive outage of generation units by them, which worsen the stability of power system.

Moreover, preventive aspect of proper control decisions are further improved by considering early outage of renewable energy sources due to malfunction operation of LVRT grid code under the islanding situations, even though the wind turbine is not under stress neither electrically or mechanically.

Since the actual active power deficit may no longer be estimated properly due to outage of synchronous machines in cascading events or in the presence of renewable energy sources due to employed power electronic converters, decoupled inertia of renewable source and hence reduction of total inertia of the grid. The current inertia of the power system and therefore the actual active power deficit is approximated/updated at each load shedding stage.

Resumé

Hovedformålet med projektet består i, at forbedre eksisterende frekvensaflastning rutiner ved at minimere mængden af frekvensaflastet belastning i net med en høj andel decentral produktion, der primært er domineret af fornybare kilder som vind, bølge, sol, biomasse, osv.

Elnet med en høj andel af fornybare er mere komplekse og ikke så forudsigelige som traditionelle elnet, der primært har central produktion. Dette gør det næsten praktisk umuligt, at forudsige konsekvenserne af koblingsmuligheder, parameterændringer samt kaskadehændelser og dermed i praksis meget svært at lægge en alment dækkende frekvensaflastning plan. Anvendes lokale data som frekvens og dens ændringstendens, spænding og dennes ændringstendens samt effektretninger kan frekvensaflastning optimeres til netop kun at udkoble et minimalt antal belastninger i netop den lokalitet, der giver en optimal frekvensgenopretning og dermed bedst mulig net genopretning efter fejl.

Det foreslåede koncept er fordelagtigt på grund af den decentrale opbygning, hvilket begrænser nødvendigheden af centralt styrende enheder til koordinering af aflastnings sekvensen. Derved skal udføres mindre databehandling og, mere vigtigt, systemet bliver ufølsomt over fejl på kommunikationsforbindelser, der kan skyldes cyber kriminalitet. Netop data-cyber kriminalitet er i medier og operatørers fokus for tiden.

Den udviklede algoritme muliggør, via sin decentrale opbygning, ligeledes en mindre hierarkisk opbygning af kontrol anlæg og strategi i forbindelse med datafejl på kommunikationsforbindelser da enhederne fungerer som selvstændige enheder i normal drift.

Moderne beskyttelse relæer har ofte flere sikringsanordninger i en fælles pakke. Men normalt uden koordinering, selv når de er implementeret i samme modul. Dette projekt har til formål at drage fordel af, at den eksisterende teknologi, der allerede bruger, at alle de nødvendige data som input og koordinere forskellige strategier under en integreret og alsidig beskyttelses strategi. Den foreslåede strategi opdaterer automatisk frekvens set punkter, fase tidsforsinkelser anvendes til frakobling af belastning som funktion af fejlens placering og hvor alvorlig fejlen er. Det er en omfattende løsning til alle mulige kombination af uforudsete net udfald, kaskade hændelser og opdelinger i nettet på grund af fejl. De foreslåede metoder er ikke blot effektive for konventionelle el systemer, men

også for den tid-variant struktur og net md høj andel af vedvarende energikilder.

For at opnå en effektiv, hurtig og optimal balance af last og generation efter under frekvens hændelse i el systemet bør både belastnings- og generation sider bidrager. Belastnings frekvensstyring leveres son en sekundær ydelse af vedvarende energikilder og frakobling af belastning i en nødsituation bør styres lokalt. Det betyder, at den aktive effekt underskud bør kompenseres lokalt i nærhed af begivenhed for at undgå at overføre den krævede aktive effekt fra produktions enheder der er langt fra fejlen. I denne afhandling, er både frekvens og last bort kobling styret ved at forsyne den decentrale kontrol enhed med lokalt målte spændinger.

Den forslåede last bortkoblings strategi er koordineret med de eksisterende beskyttelsesrelæer der er beskytter synkronmaskinen. Ved at inddrage de eksisterende relæer i strategien gør den metode forslåede i denne afhandling det muligt at undgå at udkoble produktions enheder der kan medføre en forringelse af systemets stabilitet.

Acronyms

LS	Load Shedding
LFC	Load-Frequency Control
MPPT	Maximum Power Point Tracking
WT	Wind Turbine
WP	Wind Power
WPP	Wind Power Penetration
RES	Renewable Energy Source
ROCOF	Rate of Change of Frequency
PMSG	Permanent Magnet Synchronous Machine
DFIG	Doubly Fed Induction Machine
UFLS	Under Frequency Load Shedding
UVLS	Under Voltage Load Shedding
AUFVLS	Adaptive Under Frequency and Voltage Load Shedding
SM	Synchronous Machine
LVRT	Low Voltage Ride Through
GSC	Grid Side Converter
RSC	Rotor Side Converter
PCC	Point of Common Coupling
COI	Center of Inertia

PEC	Power Electronic Converter
DG	Dispersed Generation
LTC	Load Tap Changer
SFR	System Frequency Response
VSWT	Variable Speed Wind Turbine
SCADA	Supervisory Control and Data Acquisition

Table of Contents

List of Figures

List of Tables

Part I

Report

Chapter I

Preamble

1.1 Introduction

1.1.1 Background

Emergency control actions are required as the last firewall against blackout following disturbances. The role of dispersed generation, especially Renewable Energy Sources (RESs), e.g. wind power in emergency conditions has been slightly considered, investigated and reported. Frequency and voltage indices are determinant decision variables in the emergency control. Integration of wind power into the grid significantly influences the frequency and voltage behavior following the disturbances. Therefore, emergency control plans may require a revision in case of high share of wind energy.

Power systems undergo various disturbances, but only a few of them are led to blackout. Identification of disturbance severity with their proper analysis aids the power system operators to efficiently tune the emergency control factors on line.

Severe load-generation mismatch may lead to cascading events and hence, blackout. Utilizing the available and standby spinning reserve, starting up the generators and/or generator redispatching may not be always fast enough to overcome serious active power deficit, especially in presence of renewable energy sources, which are normally set on Maximum Power Point Tracking (MPPT) to extract maximum energy from wind power, with low or even zero spinning reserve.

Load shedding is the last and most expensive emergency control action used to shed the loads that cannot be supplied with a voltage and/or frequency laid inside the permissible range. The load shedding algorithms are implemented to shed the loads before losing the rest of the power system.

Numerous literatures recommend to analyze the penetration limit of wind power into power system considering its capacity, location and technology, from a protection perspective. Sufficient investigations should be carried out to identify mitigation strategies regarding system protection, which allow increment of penetration limit.

Since integration of wind power into distribution feeders remarkably alters the behavior of feeder as a load/consumer, it may generate blind zones of detection for protection devices or may affect/challenge coordination of different protection devices.

1.1.2 Project Motivation

As can be seen in Figs. 1.1 and 1.2, the fast global growth in energy demand and the widespread environmental concerns gradually leads the energy provision toward renewable energy sources [1], which implicitly highlights the outstanding role of the current project toward this energy goal. Secure, efficient and affordable usage of this kind of energy, which has a different nature from more traditional sources of electric energy, should be properly considered, in order to achieve a smart integration of renewable energies into the grid, as it is prioritized in the energy policy landscape of several countries.

Integration of renewable energy sources without consideration of their intermittent behavior and stochastic nature may challenge the reliability of the grid. The current project intends to improve the protection system by considering the side effects of dispersed generation.

The following major issues regarding integration of renewable energy sources into the grid, especially in case of high penetration, should be considered in the short and long term goals of grid stability, control and protection. Moreover, the validity of existing methods should be reassessed in the presence of renewable energy sources. The major issues regarding integration of renewable energy sources into power system are shortlisted as below:

- Multi direction of power flow

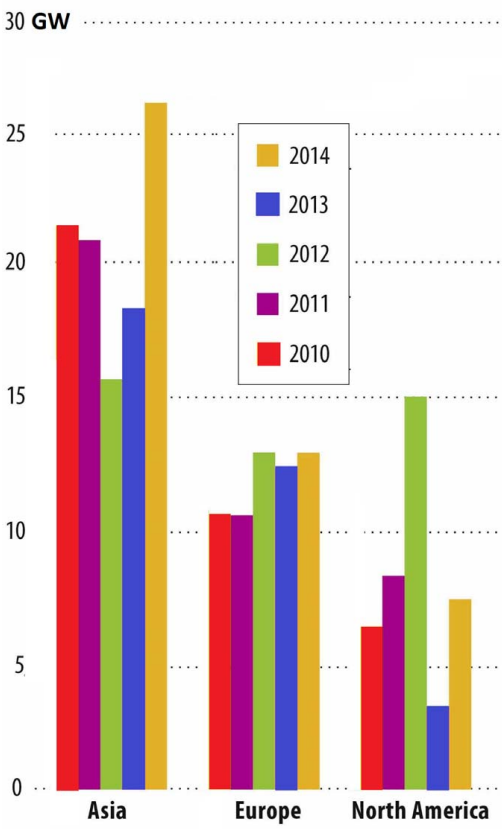

Fig. 1.1: Annual Installed Wind Power [1]

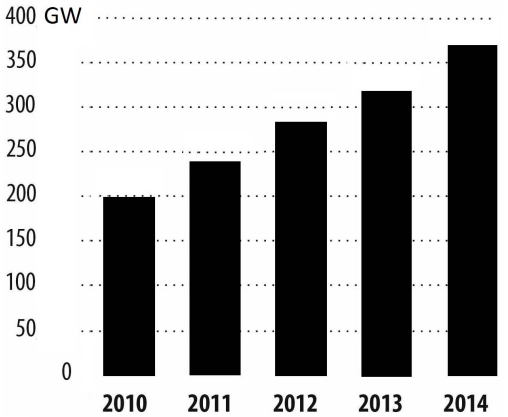

Fig. 1.2: Worldwide Installed Wind Power [1]

- Prevalence of harmonics, which may improperly trigger some of sensitive protection devices
- Reduction of grid inertia due to employed power electronic converters
- Low or no spinning reserve of renewable energy sources due to MPPT
- Coordination of existing independent protection schemes
- Contribution of renewable energy sources in Load-frequency control

1.1.3 Project Objectives

One of the objectives of the future smart grid is to enhance the protection system to improve efficiency, reliability and quality of the power delivery to the consumers. The self-healing automation in medium and low voltage grids should be carefully investigated, in order to improve the protection system of smart grid. One of the most significant and critical factors for power companies is the time, which is spent on fault localization and clearing, as a fast fault clearing reduces the required manpower and economic losses.

Modern power relays often provide several protection schemes inside of one common package. However, they normally operate without coordination even when they are inside a common module. This project intends to benefit from the fact that the existing technology already has access to all the required data, i.e. voltage, frequency and its rate of change, which can be utilized to coordinate distinct plans under an integrated and versatile scheme. The proposed scheme automatically updates different frequency thresholds used for load shedding in function of fault location and severity. It is a comprehensive solution for all possible combination of contingencies including cascading events and islanding. Moreover, the proposed solution is not only efficient for conventional power systems, but also for the time-variant structure and dispatch of grids resulting from high share of renewable energy sources.

The method proposed in this project can easily handle the structural changes of the network, due to the uncertain connectivity of the renewable energy sources, and paves the way toward Plug-and-Play (PnP) operation enabling the addition and removal of the system elements in a modular fashion way, by means of an automatic and adaptive updating of hardware settings according to the current state trajectory of the power system. This approach has the advantage on requiring minimal human intervention and it is especially advantageous in the large power systems, with time varying connectivity of dispersed generations and in which big data is required to be processed in the control center, besides the risk of communication lost and the increasing concern of Cyber Security.

The project objectives can be shortlisted as follows:

- To reduce the number of loads and feeders involved in the load shedding scheme

- Over frequency avoidance by preventing over load shedding
- Localized load shedding
- Automatic tuning of protection relay settings
- Decentralized and self-healing scheme
- Event location-oriented performance of smart relays
- Coordination of load shedding with existing plant protection relays

1.1.4 Project Limitations

There are many IEEE standard power systems available in the literatures to be used as case study, but only 9 and 39 bus IEEE standard test systems are considered in this project to assess the efficiency of proposed methods. The suggested methods developed in this project can later be evaluated for different test systems.

In this project, merely the wind power implemented by DFIG and/or PMSG type of wind turbine as a representative of renewable energy sources are considered to realize integration of dispersed generation into power system.

According to the literatures and IEEE standards, the simulation period of interest for emergency control is up to tens of seconds, the wind speed can be assumed constant during such a short period of time. It make sense, since the natural fluctuations of wind speed, which is considered as stochastic nature and intermittent behavior of renewable energy sources are to some extent suppressed by equivalent inertia of turbine and rotor as the incipient filter and at the next steps are further flatted by employed power electronic converters and the available DC link.

In order to highlight the efficiency of the proposed methods under the worst possible scenarios and to respect practical considerations, it is also assumed that there is no primary and/or secondary control due to depleting the spinning reserve of available generation units either conventional synchronous machines or wind turbines. It is noteworthy to remind that due to MPPT policy of operation point of renewable energy sources, their reserve capacity are typically adjusted at zero or close to zero in order to extract the maximum available energy from the source.

1.2 Thesis Outline

This thesis is presented in the form of collection of papers and it is organized by a report and a plurality of papers published from this project. The report is a brief summary of the research work done in the project, and is constituted by following chapters:

Chapter II: Adaptive Emergency Control

This chapter introduces the power system stability and its operation states including *normal*, *alert*, *emergency*, *restorative* and *extremis*. The possible countermeasures applicable in *emergency* state are studied and the load shedding scheme as the last and most expensive control action against blackout is especially described. Integration of dispersed generation, especially renewable energy sources into power system and its impacts on emergency control are investigated in brief. At the end, the determinant role of voltage dynamics in the power system stability are highlighted and its coordination with under frequency schemes are emphasized.

Chapter III: The State of the Art

This chapter will explore the recent literatures that are relevant to understanding the development of, and interpreting the results of this convergent study. This chapter presents the related literature and studies after the thorough and in-depth research done by the other researchers. This will also present the synthesis of the art, theoretical and conceptual framework, definition of terms and introduction of issues to fully understand and better comprehension of the research study.

Chapter IV: Wind Turbine Ancillary Services and Challenges

In this chapter the capabilities of wind turbines in providing ancillary services such as contributing in the load-frequency control and reactive power support/voltage regulation are investigated as an opportunity/strength to maintain the reliability of power system stability. Moreover, the weaknesses and threats regarding penetration of renewable energy sources into power system including malfunction operation of LVRT during islanding, reduction of network inertia, prevalence of harmonics, intermittent behavior and stochastic nature of renewable energy sources are highlighted.

Chapter V: Decentralized Load Shedding

In this chapter the decentralized strategy of emergency control of power system is addressed. Due to the significance of power system stability, the network should be adaptively/automatically recovered under any circumstances, e.g. combinational/cascading events, islanding and losing the communication with control center due to either natural system failure or Cyber Security attacks, which are recently in the center of attention.

Chapter VI: Load Shedding with High Share of Wind Power

In this chapter the load shedding is evaluated in the presence of high wind power penetration. Due to the expected high rage of frequency decline resulting from employed

power electronic converters and as a consequence, remarkably decrease of system inertia, proper coordination of scheme with the existing plant protection relays installed on conventional generators is analyzed.

Chapter VII: Conclusion

Finally, the report is summed up at chapter VI focusing on the research findings and the main contributions achieved by the documented project.

Chapter VIII: Future Works

The research perspective including the new challenges, improvements, weaknesses and the objectives, which are out of scope of this thesis are enumerated in this chapter.

1.3 List of Publications

A list of the papers derived from this project, which have been published, accepted or submitted are listed as follows. Moreover, the relationship between each chapter and its corresponding publications has been indicated in the Table. 1.1.

Table 1.1: The Relevance of the Thesis Chapters to the Publications

Chapter No.	Publications
4	C.2, C.4, C.5, C.6, C.8
5	J.2, C.7
6	J.1, C.1, C.3,

Journal Papers

[J.1] **B. Hoseinzadeh**, F. F. Silva, and C. L. Bak, "Decentralized Coordination of Load Shedding and Plant Protection with High Wind Power Penetration,"*Power Systems, IEEE Transactions on*, Under Review.

[J.2] **B. Hoseinzadeh**, F. F. Silva, and C. L. Bak, "Adaptive Tuning of Frequency Thresholds Using Voltage Drop Data in Decentralized Load Shedding,"*Power Systems, IEEE Transactions on*, pp. 1 –8, September, 2014.

Conference Papers

[C.1] **B. Hoseinzadeh**, F. F. Silva, and C. L. Bak, "Decentralized Power System Emergency Control in the Presence of High Wind Power Penetration,"*PES General Meeting | Conference Exposition, 2015 IEEE*, 2015.

[C.2] T. Kalogiannis, E. M. Llano, **B. Hoseinzadeh**, and F. F. Silva, "Impact of High Level Penetration of Wind Turbines on Power System Transient Stability,"*POWERTECH Conference, 2015 IEEE*, 2015.

[C.3] **B. Hoseinzadeh**, F. F. Silva, and C. L. Bak, "Active Power Deficit Estimation in Presence of Renewable Energy Sources,"*PES General Meeting | Conference Exposition, 2015 IEEE*, 2015

[C.4] **B. Hoseinzadeh**, F. F. Silva, and C. L. Bak, "Malfunction Operation of LVRT Capability of Wind Turbines Under Islanding Conditions,"*POWERTECH Conference, 2015 IEEE*, 2015.

[C.5] **B. Hoseinzadeh**, F. F. Silva, and C. L. Bak, "Coordination of Voltage and Frequency Feedback in Load-Frequency Control Capability of Wind Turbine,"*Proceedings of the 40th Annual Conference of IEEE Industrial Electronics Society, IECON 2014.*, pp. 1 –7, June, 2014.

[C.6] **B. Hoseinzadeh**, F. F. Silva, and C. L. Bak, "Decentralized & Adaptive Load-Frequency Control Scheme of Variable Speed Wind Turbines,"*The 13th International Workshop on Large-Scale Integration of Wind Power into Power Systems as well as on Transmission Networks for Offshore Wind Power Plants*, Energynautics, pp. 1 –7, 2014.

[C.7] **B. Hoseinzadeh**, F. F. Silva, and C. L. Bak, "Power System Stability Using Decentralized Under Frequency and Voltage Load Shedding,"*PES General Meeting | Conference Exposition, 2014 IEEE*, 2014.

[C.8] **B. Hoseinzadeh**, and Z. Chen, "Intelligent Load-Frequency Control Contribution of Wind Turbine in Power System Stability,"*EUROCON Conference, 2013 IEEE*, pp. 1124–1128, 2013.

Chapter II

Adaptive Emergency Control

When a power system operates at steady state with nominal frequency, the total input mechanical power from the prime movers of generators is equal to the sum of active power of all connected loads plus all active power losses in the system. Any significant disturbance applied to this balance causes frequency change. Huge rotating mass of generators acts as repositories of stored kinetic energy. When there is insufficient mechanical power input to the system, the rotors decelerate by supplying energy to the system. Conversely, when excess mechanical power is input, they accelerate by absorbing energy. Hence, any change in rotor speed causes frequency variation.

Governors sense speed variation resulting from gradual load changes and adjust the input mechanical power to the generator to maintain the frequency at its nominal value. Therefore, the extra load is supplies using available spinning reserve, i.e. the unused and standby capacity of generators operating and synchronized to the system. This will cause frequency to be stabilized again.

Rapid and large changes in generation due to loss of a key generator or a determinant transmission line may lead to a severe load-generation imbalance, resulting in a sharp frequency drop. Such fast frequency plunges that are often accompanied with severe overloads require impossible rapid governor and boiler reaction, which may cause system collapse. Proper selection of loads to curtail makes the system recovery possible, prevents prolonged supply interruption, and facilitates the customer service restoration with minimum delay.

As complete elimination of faults are almost impossible in the power systems, appropriate countermeasures should be foreseen in advance to avoid combinational and cascading events that may lead to system collapse. Since the system corruption financially affects the consumers and the utility. The power system operation and control should be designed robust against uncertainties, random faults with minimum interruption of consumer supply. This research project addresses the application of emergency control action to restore the system to a stable status following disturbance/s.

2.1 Power System Operation States

The operation states of power system can be classified into five major states including: *normal*, *alert*, *emergency*, *restorative* and last but not least *extremis* [4]. The transition flow chart between different states is depicted in Fig. 2.1. When the power system experiences the *normal* state, it means the entire system properly operates and the variables are in the predefined and expected range. The system is able to withstand disturbances, which may cause deviation of variables from their steady state value inside their corresponding constrain. If a system can withstand potential contingencies (such as a fault followed by line or generator trip) without violation of equipment limits or losing stability, then the system is in *normal* or *secure* state. A network configuration or loading state, which can withstand an element outage without loss of supply to any load is called *N-1* secure. Otherwise we classify the system as being *insecure* , i.e., in

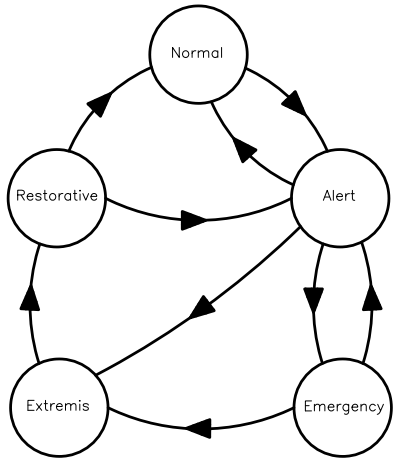

Fig. 2.1: Power system operation states

the *alert* state.

If the security degree of system degrades to a specific lower level due to higher probability of disturbance occurrence, the system transits to a new state called *alert* state. In *alert* state, all of variables are still inside the satisfactory limits and there is no boundary violation of variables, but the system is not strong enough as before and is prone to pass to other situations.

If a system operator infers from the operating data that a system is in an alert state, then preventive control actions are required to bring the system back to a normal state. However, it is possible that the system operator is unable to act in time before a contingency actually occurs. A grid may even operate insecurely (in an *alert* state) due to a high cost of preventive control or due to inadequate reserve margins. However this situation is undesired, since it may lead to blackouts (if emergency control actions fail), which can cause great economic loss. The classification of a system state as a normal or alert state is based on simulating some disturbances. Often, even though the system has been classified as being in a normal state, several improbable disturbances, which would not have been analyzed for doing this classification, may take place.

There are three states in front of the system to enter from *alert* state. The first state is the aforementioned *normal* state that is possible by coming the security grade back to the normal level. The second way is toward *emergency* state, which is selected by the system when contingencies initiate the excess burden of equipments. In this case the disturbance is sufficient enough to expel the variables from normal bounds. In this condition, some of equipment are partially overloaded, thus low level of voltage is consequently expected for some of buses. The third and most significant case happens

when the disturbance is very severe and moves the system directly to the *extremis* state. The result of being in *extremis* state without in time remedial actions is cascading events, outages and perhaps shutting down of power system in part or whole. The *restorative* state corresponds to a situation in which proper countermeasures have been taken early enough to restore the entire system from *extremis* state and pass the state to either *normal* or *alert* state based on system status.

2.1.1 Cascading Events

In recent years, power systems become larger due to fast and widespread growth of energy demand and large scale blackouts happen more frequently. The research on maintaining power system security and preventing cascading evens from more propagation is becoming one of the hot topics in power system area, especially after the US-Canada blackout on Aug. 14, 2003, which has demonstrated the vulnerability of modern power systems. Blackouts cause enormous economic losses, widespread panics and interruption of essential services.

Combinational and Cascading events are identified as root causes of recent large-scale blackouts around the world. Cascaded failures consist of a serial and radially occurrence of incidents, which in any individual is the cause of the consequence one/s [5]. Cascaded events follow a process like what depicted in Fig. 2.1. Typically, they are initiated by a single or several events. Their initiating events and root causes come from violation of power system variables from their normal and continuous operating constrains such as line overloading or generator over-excitation. The corresponding relays operate and cause transmission line or generator outage, respectively. Then the power system is lead from *normal* state into another state due to the newly happened cascading events. These successive outages reduce the reliability of power system more than before and can even cause more unpredicted incidents.

If the violations are not corrected in time, a significant mismatch between load and generation may come to exist. Frequency, voltage and rotor angle instability can take place when the network is undergone a massive disturbance, which may drive the system toward an uncontrolled system collapse. The excessive imbalance between supply and load eventually leads the system to a large-scale blackout.

When outage of an overloaded transmission line occurs, the power flow duty of tripped line switches to other neighbor transmission lines and as a result , the remaining transmission lines have to transport more power rather than their nominal capacity. Therefore one line over-load may convert to two or more line overloads. This process may rapidly propagate through the whole system and can trigger successive line or generation trip incidents, if they are not prevented in time. Initiating events in this context consist: natural catastrophe, power system equipment failure, protection malfunction, communication system failure, disturbance and human decision making mistake.

2.1.2 Security Assessment

To distinguish between a normal state and an alert state, a system operator carries out the following studies using the network configuration, load and generation values obtained from a static state estimation procedure:
Static Security Assessment: This involves continuous checking of post-disturbance system conditions regarding equipment rating and limit violations such as line thermal overloading ($S < S_{max} = I_{max} \cdot V_n$), line over voltage ($0.9 < V < 1.1pu$), etc.

Dynamic Security Assessment: it is associated with examining different categories of system stability, i.e. frequency and voltage stability [5]. To the best knowledge of authors, there is no comprehensive and widely used criterion for dynamic security assessment. The state trajectory of variables (the average deviation from their steady state values), the duration of being out of range, the rate of change of state variable and a combination of them may be considered as criterion. According to the defined security assessment criterion, if the security analysis shows that the system is *secure*, it is classified as a *normal* state.

2.1.3 Countermeasures

The different control objectives are followed among aforementioned power system operation states. In *normal* situation, objectives are based on achieving as much as optimal and efficient operation of power system with variables close to nominal values. In other states, objectives are determined in such a way to pass the system to the *normal* condition safe, smooth, and reliable. In order to reach the goals in different states, distinct control actions must be taken as countermeasures to lead the system toward satisfactory operation.

In *alert* state, the objective is to prepare the system for encountering eventually and uncertain events in future in a best possible way. Preventive action is implemented not only to avoid system from entering to *emergency* state, but at the same time to restore the power system to *normal* state. In other words, preventive mechanisms are to mitigate the impact of initiating events on power system. Typical preventive control actions are generation rescheduling, network switching and reactive power compensation.

In *emergency* state, which is mainly focused in current research, the power system is still intact and integrated and may be retrieved to the *alert* state, if proper emergency control actions initiated in time. Emergency controls, typically monitor the power system dynamics on-line to assessing whether there is the possibility of losing system integrity following of a severe disturbance. In this situation, time parameter has the highest priority and thus economical issues become secondary. To aim the corresponding objectives last resort actions are used to prevent partial or whole service interruption. Some typical emergency control actions include direct or indirect load shedding, generation shedding or network splitting.

2.2 Emergency Control

2.2.1 Emergency Control Characteristics

Much effort has been made to improve the reliability/security of power system such as preventive mechanisms, emergency controls, and restorative controls. As mentioned in section 2.1.3, preventive mechanisms are to mitigate the impact of initiating events on power systems and emergency controls are employed to prevent power systems from entering restorative states.

In previous section, different countermeasures suitable for power system states investigated. In this section the main focus is on special properties of *emergency* state and control actions, which should be considered throughout the control algorithm.

According to section 2.1.3, the system can transit from a perceived alert state to an emergency state if no preventive control actions are exercised, while a contingency occurs, or may directly transit to an emergency state from a perceived normal state if an unanticipated sequence of several contingencies occur. If the system enters into an emergency state, some equipment limits are exceeded, which may cause tripping of further equipments, thereby may worsen the situation and may lead to blackout.

Emergency control actions (manual or automatic) are required to retrieve the situation. If there is a thermal overload of equipment then there is some time to act and quick "heroic action" from a system operator would be needed. Since most of equipments can withstand a short-time thermal overload, there is a small window of time in which some manual emergency measures can be executed. For other emergency situations like instability, too short reaction time may be required and predesigned automatic emergency measures may be necessary. However in most cases one has to rely on automatic controls to quickly respond to such a situation.

The main characteristics of *emergency* state are as follows:

- The disturbance has been already happened and is certain but the trajectory of dynamic variables are often unknown and therefore the goal should be minimizing of the consequences by controlling the system dynamics.
- The emergency situations rarely happen, but this does not diminish there magnificence and it does not mean they should not be taken into account.
- The emergency control actions are basically expensive instantly, but they are affordable if they prevent system black out.
- The control strategy should be simple to be done in real time.
- Coordination of different control approaches or using of optimization algorithms may be impossible or difficult.

- The emergency control action may be implemented as closed loop to be more robust against unmodeled dynamics and uncertainties.
- Expensive control actions are direct load shedding, generation shedding and network splitting, whereas shunt capacitor/reactor switching and indirect load shedding (transformer tap changing) are cheap.
- Decision making time may be very short (msec to sec).
- Complexity of possible control operations must be simple in emergency control to be applicable in real-time.
- The disturbance is certain, but the state of the system is often only partially known and dynamic behavior is uncertain.
- Coordination of different control objectives is difficult.
- Strategy in emergency control is especially useful if it can handle also very unlikely events/situations.

2.2.2 Controlled Islanding

Large disturbances may cause Angular Instability, which means the synchronous grid cannot be operated in an integrated fashion if the generators fall in "out of step". If all generators are not in synchronism and are still connected to each other, then large variations in voltage and power may be resulted, which can damage equipment and render inter-connected operation inviable.

Fast emergency control (i.e. insertion of series capacitors, boosting the excitation of generators) can try to prevent angular instability, but if angular separation becomes too large and keeps increasing, the system has to be split into islands such that generators within an island are in synchronism. However, the emergency is not over - within an island load-generation has to be balanced to avoid large frequency variation. The splitting into islands may be uncontrolled (due to action of protective systems like distance relays) and sometimes very few, if any, islands survive, causing a blackout.

Emergency control measures under loss of synchronism conditions includes activation of a pre-designed islanding scheme (controlled system separation), and measures like under-frequency load shedding within islands with low generation.

Controlled Islanding, may be an efficient solution, as a disturbance can be contained and prevented from leading to cascading failures. Since outage of generators due to loss of synchronism is prevented, more generators remain connected to the network, fewer loads need to be interrupt and faster network recovery can be achieved.

For example, a sudden load tripping may cause overvoltages in long EHV lines especially if the transmission line loading goes significantly below the Surge Impedance Loading. This may cause line tripping on overvoltages. Emergency control can be in

the form of insertion of shunt reactive power absorbing devices.

Weakening of transmission system along with heavy reactive power demand and low reactive power generation margin may cause voltage instability. Emergency Control in the form of Under-voltage tripping of loads, disabling of tap changers in transformers may often be able to retrieve the situation.

2.3 Load Shedding

For a smooth growth of load, unit governors measure the speed decline and increase power input to the generator. Therefore, overload is compensated by using already provided of spinning reserve, the unused capacity of all generators operating and synchronized to the system. If all generators are operating at maximum production capacity and hence there is no available spinning reserve, the governors may be unable to relieve extra loads. In any case, the fast frequency plunges that accompany serious overloads require impossibly rapid governor and boiler reaction. To prevent such a drop in frequency, it is compulsory to intentionally and automatically release a portion of the load equal to or greater than the extra load. While the decline has been arrested and the frequency returned back to normal range, the disconnected load may be retrieved in small amounts, in order to allow the spinning reserve to become active and any additional available generators to have enough time to start up and being available.

The frequency information in an integrated system is same for all different voltage levels and all consumers are equally affected by a frequency event. Inversely, load curtailment at any voltage level will improve the status of the whole network. To stop the frequency decline and subsequently to rise the frequency back into the normal range, more load should be shed than corresponding shortage. It is worthy to shed as little as possible amount of load above absolute necessary quantity. Actually if so much load is curtailed, the system may be lead to an unstable condition. Thus a measure of proper control should be included.

When a load shedding procedure is designed for a given power system, several key factors must be determined to achieve the most effective and optimal solution. There are several key parameters should carefully be determined to minimize the amount of load to be curtailed, due to their significant effect on load shedding process. The total amount of load should be shed, the number of load shedding stages, the amount of load should be shed at each stage, frequency thresholds, the delay between stages and the location of load curtailment are important decision parameters which affect the load shedding process [6, 7].

Load shedding process can be done by traditional or new load shedding methods consisting of manual/SCADA (Supervisory Control and Data Acquisition system), automatic, local or wide area load shedding [8]. Serious frequency plunges can happen within a few seconds. Manual or operator/SCADA generally is unable to be fast enough to prevent partial or complete system collapse. Automatic schemes, which in relays with

frequency measurement are employed, have much better performance by shedding load blocks at discrete frequency or Rate of Change of Frequency (ROCOF) thresholds. In local load shedding application, the load curtailment is carried out at the same location of frequency measurement. Therefore, the communication system, which is accompany with expenses of implementation, reducing of the system reliability and adding eventually delays in communication is not needed at all. In a wide area method, communication system including telephone wire, cable, fiber-optic media or Global Positioning System (GPS) is an essential part of the proper operation of the whole power system.

2.4 Integration of RESs into Power System

2.4.1 Impact of RESs on Stability of Power System

The fast-growing energy demand and widespread concerns about global warming leads the energy provision trend toward RESs, which recently have attracted a great attention in terms of investment and development [9,10]. The replacement of central power plants with renewable energy sources, specially wind turbines, adds new and crucial challenges to existing issues of power system stability. Besides of their low or zero inertia in Variable Speed Wind Turbines (VSWTs), replacing of conventional generation with wind energy will dramatically influence the frequency response due to fluctuation in wind speed. Not only the ROCOF is increased, also magnitude of frequency excursion is augmented following a generation outage [11]. Higher level of wind penetration reduces the lower frequency threshold, and it may cause load shedding or even lead to a black-out. Especially in islanded grids, which already have a lower inertia than large integrated power systems, the frequency stability will be highly deteriorated when conventional generation is replaced by wind turbines [12, 13].

As the penetration level of RESs in the grid is remarkably augmented, their impacts on the power system operation and control can no longer be overlooked. The stochastic nature and intermittent behavior of RESs is inevitably imposed to the operation of the network and increases the uncertainty of energy sources, which challenges/alleviates the reliability of the grid [14]. Along with prevalence of harmonics (power quality issues), reduction of total inertia of the power system, which are the result of employed power electronic converters, should be added to the negative impacts of RESs on the power system [9, 15].

Since, inadequate reactive power compensation of wind turbine can cause voltage instability issues [16, 17], reactive power support of wind turbine is a major concern of power system researchers around the world [18, 19]. From inertia aspect of view, the active power provision of wind turbine differs from conventional synchronous machines. Internal control loops of wind turbine can be redesigned to emulate a virtual inertial response to support frequency stability, but have not been widely put in practice in power systems [11, 13]. The transient stability of rotor angle in the power system is

directly influenced by reactive power support of wind turbine and this capability can be useful in arresting the severe low voltage incidents as well as in minimizing angular separation of synchronized units [20].

More installation or replacing the conventional SMs by RESs result in a low inertia power system, which in case of a frequency drop yields a higher quantity of ROCOF and hence requires faster reaction of generation units that are contributing in the LFC action. Augmentation of ROCOF value, i.e. steeper frequency decline, is the result of lower inertia rather than higher active power deficit [9, 14, 15, 21]. In other words, a given ROCOF quantity in a low inertia power system estimates the active power deficit less than its actual value due to reduction of equivalent inertia in presence of RESs, i.e. an improper approximation of power imbalance magnitude. As a result, the resultant lower load shedding may lead the power system toward delayed recovery or even blackout. Therefore, the initial ROCOF in the presence of RESs may no longer be a proper indicator of load-generation mismatch as it is in the conventional power systems without contribution of RESs [8].

Normally, the VSWTs do not inherently contribute in the Load-Frequency Control (LFC) to support the grid during disturbance/s due to two major reasons. First, the employed PEC decouples their rotor inertia from grid frequency, i.e. low or no inertial response [9, 22]. Second, the operating point of VSWTs is typically set at MPPT to extract maximum power from wind and therefore they are unable to inject more power to the grid in case of further active power requirement, i.e. defective droop control [14, 22].

In order to equip the VSWTs with LFC capabilities similar to conventional SMs, necessary LFC control loops (both inertial and droop control) need to be implemented inside the PEC and some spinning reserve should be procured in the VSWT by shifting their operating point from MPPT to a suboptimal point with lower efficiency. Under any circumstances, the VSWTs are merely able to release the power up to 1.2 times of their rated power transiently during the events due to the limited MVA of their PECs, whereas the SMs may support the grid up to 2-3 times of their apparent power capacity in the transient state.

Typically, the spinning reserve around 5-10% of VSWT nominal power is considered in literatures [14, 21]. In power systems with high rate of WP penetration in which the WP becomes dominant generation and considering the aforementioned amount of reserve, the total available reserve in whole network may not be sufficient to overcome the entire range of severe contingencies especially the events with high level of active power shortage resulting from islanding event/s.

Reduction of total inertia is one of numerous WP outcomes, which remarkably affects the dynamical behavior of power system [8]. A high value of ROCOF during disturbances, which causes rapid decline of frequency is one of low inertia power system consequences and therefore requires shorter reaction time of corresponding control actions.

In conclusion, by penetrating the WP into the grid, following issues are inevitably

expected to be appear in power system dynamics/behavior:

- Lower power quality due to prevalence of harmonics produced by Power Electronic Converters (PECs);
- Bidirectional power flow in the load bus feeders;
- Lack of sufficient spinning reserve in VSWTs due to the Maximum Power Point Tracking (MPPT);
- Reduction of grid inertia due to employed power electronic converters;
- Steeper frequency decline (higher quantity of ROCOF);
- Wrong estimation of active power deficit (more) leading to overload shedding/over dispatching;
- Uncertainty of energy sources;
- Behavior of feeder: Load/source;
- Generate blind zones of detection for protection devices;
- Affecting/challenging coordination of existing independent protection schemes;
- Low or no spinning reserve in renewable energy sources due to MPPT.

2.4.2 Maximum Penetration of Wind Power

Nowadays, the wind energy industry development and its penetration to power system is inevitable due to public concern about global warming, limited energy sources and financial issues. Nevertheless, the security limits of power system restrict the share of wind energy in generation to prevent of being dominant below a specific percentage of whole demand [23]. The reason may be found in the intermittent nature and variable and stochastic generation of wind turbines in comparison to conventional power plants with constant and controlled output.

Although outstanding research has been done on determination of the maximum penetration level of Dispersed Generation (DG) into the grid, from power system stability aspect of view, the maximum possible level of wind power penetration is not well addressed yet in literatures and still is an open problem for investigation [23]. The authors in [24] used a transfer function approach to indicate that the normal fluctuations in wind power may cause serious problems for speed governor systems and system frequency.

From thermal and voltage limitation aspect of view, the maximum penetration level of wind energy in Crete Island has been studied in [25]. Investigation of impact of wind

energy on power system frequency in Iowa in [26] has shown that the increasing capacity of Doubly Fed Induction Generators (DFIGs) or Permanent Magnet Synchronous Generators (PMSGs) would worsen recovery of system frequency after a severe disturbance. The $N-1$ and $N-2$ line outage contingencies considering wind power penetration on the Irish power system are studied in [27] and as a result, decreasing wind power generation is proposed as a solution to prevent outage of conventional power plants, which would reduce overall system inertia. However, the power system stability considerations are left behind.

2.5 Integration of Voltage Data in Under Frequency Schemes

2.5.1 The Determinant Role of Voltage Data in Stability Analysis

A voltage collapse in a part of a power system indicates that the existing generators and transmission lines can not supply part of the load, which has gone beyond its normal operating range. More importantly, if this problem is not resolved in time by taking proper control actions, there is a risk of propagation of that local problem to a wider area or even to the entire network. Exploration of major blackouts, which happened in the late 1990s and early 2000s (the 1996 Western North America, the 2003-2004 Outages in Europe, 2003 eastern North America and others) demonstrated that the root cause of many of these blackouts is voltage collapse rather than the prevalent frequency event [28,29]. It can be seen that voltage collapse can be a leading symptom of impending power system contingencies. There are new design and security issues that should be considered in an Under Voltage Load Shedding (UVLS) scheme and merely relying on UFLS scheme and issuing a relevant control action can not be a remedial countermeasure for a wide range of disturbances especially disturbances with under voltage initiating events, since they may not be an appropriate countermeasure for voltage collapse situations.

Nowadays, power systems are much more prone to voltage collapse than in the past due to the tendency of increasing the distance between generation sources and load centers, which are intentionally located far from each other [30]. There are two major reasons promoting the distance. First, from a financial aspect of view, it is affordable to purchase the energy from cheap remote generations instead of expensive nearby sources. Therefore, the power is transfered through a long transmission line and as a consequence, the possibility of voltage collapse increases. Secondly, it is hard to convince the public to allow new central power plants to be set up at high density urban areas. These two factors boosts the dependency of power system operation on the transmission system. It also causes the augmented reactive power losses during transmission line trip. More-

over, building of new transmission systems between distant sources and loads may not be affordable because of environmental and economical constraints.

The load type is another determinant factor, which may cause rapid system voltage collapse. Many of new prevalent loads such as air conditioners are alike small single phase induction motors. During the hot weather condition, these motors encompass a high portion of the consumers. These kind of loads are susceptible to stall during voltage drops resulted from short circuit of transmission lines. The gradually tripping of stalled motors and the relatively slow re-acceleration of more robust motors may cause decline of system voltage when a transmission line failure is removed [31]. If the transmission line failure is removed by a time delay backup relay, the voltage drop and its influence on aforementioned loads deteriorate. The slow fault clearing during the voltage collapse resulted a blackout of the Memphis city in 1987 [32]. In conclusion, power systems with remarkable contribution of induction motors are prone to fast or short-term voltage instability.

The difference in the neighbor bus voltages allows the reactive power to flow through the transmission line and under the normal condition of power system, voltages are typically located in the small range of $\pm 5\%$ of nominal value in pu. This small voltage difference will not permit significant reactive power to transport to very far distances. Therefore, it is undesirable to transport the reactive power over long distances, especially under peak load condition, and it needs to be produced in the vicinity of the load center, whereas active power may be transported to the remote points of consumption through the interconnected grid.

A sudden outage of transmission lines may lead to instantaneous requirement of local reactive power close to the load center to compensate the surplus losses of transporting the same amount of power over the rest of remained transmission lines. If the required reactive power is not provided in time at the consumption point, the voltage will be diminished. Under such a condition, utilizing of automatic devices such as Load Tap Changers (LTCs) in order to load restoration may exasperate the situation by creating further voltage drop [4]. These mechanism may last for a few seconds of time and lead to long-term voltage instability [33].

Conventional emergency control schemes that merely use the frequency data in LS plan and coordination of frequency and voltage are rarely considered in protection schemes in practice. For the sake of the aforementioned reasons, voltage information alongside frequency data is recently taken into account as a key factor that shows if the power system is under stress or not [6]. Power system operators recognize that frequency may remain in normal range during the voltage sags before the entire system collapse and are going to employ the UVLS scheme as a complementary part of their existing UFLS scheme.

2.5.2 Coordination of UVLS and UFLS Schemes

According to [34] regarding impacts of voltage variation on UFLS scheme, a precise perception of the characteristics of both frequency and voltage collapse is necessary to establish a proper and effective coordination between underfrequency and undervoltage tripping schemes. Underfrequency and undervoltage collapse are to some extend independent incidents and may typically have distinct root causes such as loss of a huge generation for underfrequency or outage of a determinant transmission line for undervoltage collapse. Undervoltage event is identified as a local phenomena, whereas underfrequency event is classified as a global system incident. Generally, voltage collapse influence the frequency profile slightly, which may not be sufficient enough to make the underfrequency schemes to react.

A remarkable generation lost may namely lead to a load-generation imbalance throughout the whole system following by an underfrequency incident. The frequency starts to drop gradually with the event, but typically not as fast as undervoltage events due to long inertia time constants of system generators in conventional power systems.

Voltage incidents are generally associated with the local lack of reactive power. A slow voltage drop may come from reaching the generator to full capacity of available reactive power reserve and a fast voltage decline can be typically involved to serious disturbances such as transmission line short circuit or loss. Voltage collapse can come to exist in areas, which either the load is supplied by a faraway generation with restricted reactive power support or areas with a low level of local generation and a high portion of motor loads. Undervoltage events often happen in a shorter range of time in comparison to underfrequency events.

Undervoltage and underfrequency load shedding plans have different characteristics and are independently established in power system without any coordination. Study of UFLS scheme is often carried out using the System Frequency Response models (SFRs) [35–37]. The effects of voltage changes on the frequency deviation is not taken into account in these models. Contrariwise, the UVLS methods that have been proposed so far for setting of the UVLS relays, do not employ the frequency indices [7,38]. Combination of both schemes seems to be necessary in practice to achieve a more reliable/effective LS scheme. Any individual use of these indices may lead the power system toward over load shedding or blackout. Decentralized UVLS scheme may be employed to avoid local voltage collapse at many substations. By sharing the existing software and hardware between both undervoltage and underfrequency protection schemes, the UVLS scheme can be implemented in parallel with underfrequency in order to be financially affordable.

2.5.3 LS Localization Using Voltage Drop Data

Determining the locations of LS is one of the most important key factors, which needs to be selected carefully. In order to obtain a more reliable/efficient LS plan during emer-

gency conditions, the event location must be properly included in the decision making process, whereas in the conventional UFLS schemes, the loads, which should be dropped in case of need to LS are already determined independent of contingency location and current status of power system [35, 39]. Discarding the loads, which are distant from the event location, may cause overloading of tie-lines, power factor reduction and even worse voltage profiles [40]. Inversely, dropping the loads located inside the neighborhood of disturbance point may recover the voltage of affected load buses and is strongly recommended by many literatures [8, 37, 41].

The loads may be prioritized to discard based on their voltage decay, i.e. the loads with larger voltage decay are curtailed sooner than the others. The LS process begins to be triggered from the failure zone and radially proliferates in the network in such a way that not only the frequency downfall is stopped in time, but also the frequency comes back into the permissible range [8, 42]. Therefore, according to [36, 41], in order to find the most appropriate locations for the LS plan, the deviation of the load bus voltages may be a proper and effective criterion of proximity to the event location.

The voltage data involved in the proposed method are accessible even in the conventional LS relays. In the present decentralized UFVLS scheme, the expenses and vulnerability of communication system are avoided and by sharing the existing software and hardware available inside the LS relays between both UVLS and UFLS schemes, practical implementation of approach may financially be affordable [39, 43].

Chapter III

The State of the Art

3.1 Literature Review

3.1.1 Traditional Load Shedding

Load shedding to avoid frequency collapse is a conventional emergency approach in the power system stability area. There are different types of UFLS scheme comprising traditional, semi-adaptive, and adaptive [41, 44]. The traditional load shedding is often employed among the others, due to its simplicity in manufacturing of relays [41]. The traditional scheme curtails a specific amount of load when the frequency declines below a predetermined threshold. If this amount of load shed is enough, the frequency will become stable due to load-frequency control capability of generators, otherwise the frequency continuously declines slower than before. When the frequency crosses the next threshold, the next load shed stage is executed. This procedure is going on until the frequency drop is stopped or all the relevant relays to load shedding have acted [45]. The thresholds and the relevant amount of load shed are determined off-line, based on practical experiences and numerical simulations. Generally conservative settings are applied in traditional load shedding method due to the unknown scale of the disturbance [46]. Although this scheme is efficient during small disturbances, it can not differentiate between the normal and abnormal oscillations. For example, in this scheme, the frequency fall due to a generator outage is treated same as frequency drop of a normal wind speed oscillation in a wind turbine. Therefore, it sheds relatively lesser loads at large disturbances, which generally can not be seen as a comprehensive solution for widespread range of disturbances.

In the traditional UFLS, the load shedding places are already determined independent of disturbance location. As, the load curtailment is not carried out necessarily at the areas with active or reactive power shortage, the risk of tie line over loading and voltage instability issues exists following an improper load shedding [35]. Load curtailment at locations with relatively lower voltage and hence greater reactive power requirement, will improve voltage stability of the overall system and consequently aid the system to retrieve its stability following a serious combinational event.

In [47] a hierarchical genetic algorithm (GA) based technique was proposed to calculate the Under Frequency Load Shedding (UFLS) relay settings. The time delays and number of stages were considered as dependent and independent variables, respectively [47]. In [48], the fuzzy load model and the first fit heuristic was employed to calculate the relay settings. The load shed amount determined based on a closed form of voltage changes gradient in [49]. Selecting of demonstrative operation and incident scenarios was considered in layout of 81L UFLS relays in [50]. Several scenarios considering the intermittent nature of renewable energies and different outages were considered in calculation of shed load at each stage by taking into account of each scenario probability in [42].

3.1.2 Semi-Adaptive Load Shedding

The semi-adaptive load shedding scheme utilizes the frequency drop rate as an indicator of the active power shortcoming [4]. The amount of load shed is proportional to ROCOF when the frequency arrives to a specific threshold. Hence, this algorithm measures the ROCOF just after the threshold is crossed. Generally, the ROCOF value is employed only once at the first frequency threshold, the rest are treated as traditional scheme. The ROCOF thresholds and the amount of load shed at each stage are determined off-line based on simulation and experience. The scheme is adapted to the disturbance magnitude due to proportionality of load shed amount to the ROCOF value.

3.1.3 Adaptive Load Shedding

The active power shortage can be estimated based on measured initial ROCOF, just after power imbalance occurred. The system generators do not decelerate at a same rate. Therefore, the frequency is not unique through out the entire power system at least for first several cycles. To achieve the average frequency of the hole system, the Center of Inertia (COI) technique is used to get more accurate estimation [44, 51]. Moreover, it seems vital since the locally measured frequency does not contain precise information of system just after incident.

Adaptive aspect of UFLS has been presented to enhance the performance of traditional load shedding methods in [46, 52–54]. All of these methods calculate the active power shortcoming, following an incident, based on the equivalent system model presented in [52]. However, only frequency data is employed in the load shedding strategy.

By taking into account of voltage dependency of loads and exploiting of this fact in estimating of active power deficit, the scheme was improved to some extend [36, 44]. Load characteristic dependency to voltage and frequency have been taken into account in [54] in order to anticipate the frequency decline after an event. Coordination of frequency and ROCOF in UFLS method has been employed under a self-healing strategy in [46]. The adaptive schemes in [52, 53, 55] are based on using the initial frequency gradient following an event to determine the active power shortage in the power system.

In the above research studies, the voltage information was not directly involved in load shedding application. A precise evaluation demonstrates that the total load shedding deficit in the system is solely determined based on the frequency stability. The references [51, 55] equipped the adaptive load shedding scheme with the capability of determining the load shedding distribution using pre-fault V-Q sensitivity factors or voltage magnitude. The stability problem is the concern of all of aforementioned methods in adaptive UFLS. However, in reference [56] has been stated that occurrence of a severe contingencies, in a highly stressed power system, may also lead it to the voltage instability. In order to cope with such incidents, a centralized load shedding has been proposed in [55] to coordinate the UVLS along with UFLS. The UVLS scheme is triggered after falling down of load bus voltages below a specific threshold. Practically,

a voltage amplitude based UVLS plan is not secure enough versus voltage instability resulting from a severe event [51]. Ideally, a self-healing strategy should guarantee both voltage and frequency stability, following an event.

Different indexes have been reported for voltage instability in [57–59]. These indexes need to on-line calculation of either the network admittance matrix [57,58] or a Thevenin equivalent of the power system [59] to predict voltage collapse. A Voltage Stability Risk Index (VSRI) which has been proposed in [37, 51], addresses the voltage instability by employing the time series data of bus voltages to determine the vulnerability of the power system at each bus after a contingency. Despite of other indexes, there is no need to input from the other buses for the calculations. Therefore, this scheme can be implemented by PMUs to evaluate the transient voltage stability of the power system. The main effort of [51] is to drive the control actions considering the voltage dynamic changes regardless of disturbance. The work carried out in [37] advocates of exploiting the reactive power together with active power directly in the load shedding process. This approach deals with the coordination of voltage and frequency information instead of independent methods.

3.1.4 Distributed Load Shedding

In [47] a hierarchical genetic algorithm (GA) based technique was proposed to calculate the Under Frequency Load Shedding (UFLS) relay settings. The time delays and the number of stages were considered as dependent and independent variables, respectively [47]. In [48], the fuzzy load model and the first fit heuristic was employed to calculate the relay settings. Different LS methods including a fixed maximal load to shed and proportionality of shed load to the ROCOF were investigated in [60]. Calculation of UFLS relay setting based on Monte-Carlo simulation method for autonomous power systems were carried out in [61].

The main effort of [62] was focused on dynamically adjustment of the UFLS relay parameters using the frequency and ROCOF information, whereas the adaptive LS with even shed load at each stage may cause long-term transients. The authors in [63] have suggested the tuning of relay parameters according to practical conditions using an Artificial Neural Network (ANN). It should be noted that the scheme with only one stage of LS may result a serious overshoot frequency. The work reported in [64] utilizes ANNs to directly evaluate the parameters of most effective LS scheme considering system stability. There is the risk of over LS in case of following the single objective of maximum lowest frequency. The work carried out in [65] addresses the estimation of frequency and ROCOF using a non recursive Newton type procedure and in the next step, determination of the disturbance magnitude, whereas for estimation of the disturbance magnitude inertia constants should be known. Additionally, the minimization of total amount of shed load was not considered in [62–64].

The paper [49] developed an intelligent LS algorithm for scheduled islanding, ac-

companied by an algorithm for grid reconnection. That work also tried to determine the load shed amount based on a closed form of voltage changes gradient. Selecting of demonstrative operation and incident scenarios was considered in layout of 81L UFLS relays in [50].

Large power systems, to some extend, deal with similar daily pattern of load, whereas microgrids experience significantly different scenarios due to intermittent behavior of renewable energies and this fact was not considered for traditional relays in [47,48,60,61], and adaptive relays in [62–65]. The schemes with single objective of minimal shed load [50] may lead to a significant undershoot in frequency. Reference [42] advocates calculation of shed load at each stage of under frequency relay (81L) in a stand-alone micro grid based on historical meteorological data and the Markov two-state model. Furthermore, the shed load is minimized and the lowest swing frequency is maximized using the GA.

3.1.5 Centralized Versus Distributed Load Shedding

In [53,55], different types of centralized load shedding have been introduced to rank and select the best loads to interrupt during voltage or frequency stability. Centralized load shedding is supposed to be the best solution for coordination of dispersed loads and generators in power system. However, centralized method needs to collect and transmit the measured informations and to distribute the decisions throughout the system. This strategy has several disadvantages such as implementation expenses of communication system and vulnerability of communication link due to eventually natural failures or Cyber Security attacks, which have been introduced in [66]. Besides, the centralized scheme is unable to adapt itself to any structural changes in power system configuration, therefore it should be redesigned again when any load, generator or transmission line is installed or removed.The stochastic and variable nature of Renewable Energy Sources (RES) causes intermittent behavior of them in connection to the power system. Alteration of power system topology proliferates the duty of centralized control schemes. As distributed approach is able to prevail these weaknesses, decentralized control scheme seems to be a better solution to deal with RESs and to reach a more affordable and reliable power system.

Nowadays, Multi Agent System (MAS) is widely used as a suitable solution for decentralized control algorithms [67]. The MAS can process the distributed data and tolerate single point failures, which makes it faster in decision and operation and more efficient in duty distribution. A decentralized MAS load shedding algorithm has been proposed in [66] to achieve an effective load shedding scheme based on collected global information. The global informations are earned based on information exchange merely between neighbor agents. Total generation and demand can be identified accurately. The load shedding commands, can be issued according to the available informations.

In the decentralized load shedding, decisions are made based on locally measured

voltage and frequency signal at the relevant relay. In this method, load shed are determined based on the failure place either directly or indirectly. On the other hand, as the load shedding process is taken place utilizing locally measured information, no communication system is required. Therefore, implementation of these methods is much more easy and affordable than the centralized load shedding approaches which require rapid communication links [35].

3.1.6 The Role of PMU in Power System Stability

Standard [68] defines the synchrophasor as a complex number representation of either a voltage or a current, at the fundamental frequency, using a standard time reference. The power system variables are measured by phasor measurement units (PMUs) and are broadcasted with the Wide Area Monitoring and Control Systems (WAMCS). Therefore, the power system stability issues may be supervised more carefully than before. PMUs are able to dedicate synchronized measurements, which include the magnitude and phase angle of voltages, currents, frequency and ROCOF [69]. These collected information may aid to trace the dynamical behavior and provide useful data for both voltage and frequency stability evaluation. Additionally, the phase angle data ease early and more accurate recognition of voltage instability. However, they have not been utilized yet in current load shedding schemes [69].

3.2 Summary

In this chapter, different load shedding methods were classified in term of being centralized/distributed from a control strategy aspect of view, adaptive/nonadaptive capability regarding online updating of its parameters based on the measured power system variables and last, but not least, flexibility to overcome unpredicted changes of power system structure/topology.

Most of centralized methods introduced in this chapter are based on the SFR method, which is no longer accurate in case of synchronous machine outage during cascading events and/or in presence of renewable energy sources. Moreover, the recent fast-growing Cyber Security concerns regarding intentional sabotages with the aim of collapsing the communication system and hence the energy system seriously emphasizes that merely relying on a centralized control strategy may not be fully reliable following losing the communication link due to any reason.

Furthermore, almost all of adaptive methods are solely based on frequency data to estimate the active power deficit. The frequency is a common variable throughout the whole power system and it does not contain any useful information about the event location. Therefore, the load shedding is uniformly fulfilled in whole power system regardless of event location, resulting interruption of the loads that are inside the safe regions with the voltage inside the normal range.

The decentralized load shedding, which is an efficient solution for the case of communication lost situations has not been properly investigated in the existing literatures. At the present, the settings of protection relays are determined manually, offline, constant and independent of event location and magnitude, based on simulation and/or practical experiences of utility operators, which may not be a comprehensive countermeasure for all possible combinational and cascading events.

3.3 The Main Contributions of Thesis

This thesis addresses the decentralized control strategy of load shedding as a low level of a hierarchal control system implemented for protection system to reduce the burden of control center in receiving, processing and transmitting the Big Data of large power systems and therefore, distribution of protection decisions to the protection devices. Besides of its technical/practical possibility/difficulty, there is the risk of losing the communication with the control center due to Cyber Security attacks, a topic that became more relevant recently.

The frequency set points and stage time delays of load shedding relays are updated online and are adaptive to the magnitude and location of perturbation following the disturbance/s. The proposed schemes are coordinated with the existing plant protection relays to recover the frequency before their trigger and hence reducing the occurrence of more cascading events by outage of synchronous machines.

The power flow direction of feeders are considered in the suggested methods to avoid wrong disconnection of feeders, which support the grid stability by injecting either active or reactive power from dispersed generation, e.g. renewable energy sources into the load feeders.

The LS and the LFC participation of wind turbines are localized using locally measured voltage drop data following the disturbance/s. The loads/wind turbines closer to the event location are participating more in the LS/LFC comparing to distant loads/wind turbines. By this mean, transferring the required power from faraway generation units to the disturbance point is reduced as much as possible and the demand power is locally provided if the local and standby spinning reserve belong to the units located in the vicinity of event is still available.

Moreover, the efficiency of the proposed methods are evaluated in the presence of high share of wind power, which remarkably reduces the total system inertia and as a consequence yields improper estimation of active power deficit. The aforementioned load-generation imbalance is precisely approximated following each triggered load shed stage using locally measured pre and post-disturbance rate of frequency change and the shed load of disconnected feeder.

Chapter IV

Wind Turbine Ancillary Services and Challenges

4.1 Decentralized & Adaptive Load-Frequency Control

The recent global environmental concerns augment the development of renewable energies, especially wind power [9, 10, 70]. Installation of more wind turbines challenges operation and control of power system [14, 71]. With high share of wind power, the stochastic behavior and intermittent dispatch and connectivity of wind power penetrates into the power system. Moreover, rampancy of harmonics in the power system state variable and decrement of total network inertia which are the consequences of employed power electronic converters in wind turbines, should be considered beside the above weaknesses of wind turbines [72].

The wind turbines typically do not participate in the load-frequency control to support the grid during the disturbances. The wind turbines are basically set to operate at Maximum Power Point Tracking (MPPT) point to achieve maximum efficiency [22]. Hence, they are unable to produce more power to support the grid in case of frequency decline events [14, 73]. Moreover, the built-in power electronic converter decouples the rotor and turbine inertia from the grid and hence, the kinetic energy available in the rotor may no longer be used as a primary frequency control following the disturbances [8, 15, 22].

In the grids with high share of wind power, the load-frequency control task is inevitably assigned to the wind turbines. Hence, in order to provide the load-frequency control capabilities in wind turbines, the two above weaknesses should be fixed. Therefore, some spinning reserve needs to be foreseen in the wind turbines by shifting their operating point from MPPT to a sub-optimal point, which is well-known as wind turbine de-loading [9, 15, 22, 74, 75]. This reserved capacity may be utilized to support the grid at the time of frequency decline.

The wind turbine de-loading is basically done fulfilled by two different ways. The first way, which is called rotor over-speeding is out of thesis scope due to its disadvantages. In the over-speeding method, the kinetic energy of rotor is increased by slightly increment of rotor speed above its nominal value. According to the power-speed characteristic of the wind turbine depicted in Fig. 4.1, the operating point is shifted from MPPT to another right side sub-optimal point with a higher rotor speed and less produced power [9, 73]. Due to the mechanical limitation of rotor speed, this method may not be a concise solution for all possible conditions. Excessing the input mechanical torque of output electrical power due to abrupt load decline or a wind speed higher than rated value undesirably accelerates the rotor speed, which may damage the turbine and/or generator [9, 22].

The wind turbine de-loading can also be done using pitch control. In this way some of extractable wind energy is curtailed by increasing the pitch angle and this standby power can be utilized during frequency events.

The second weakness of wind turbines, i.e. decoupled inertia of wind turbine from

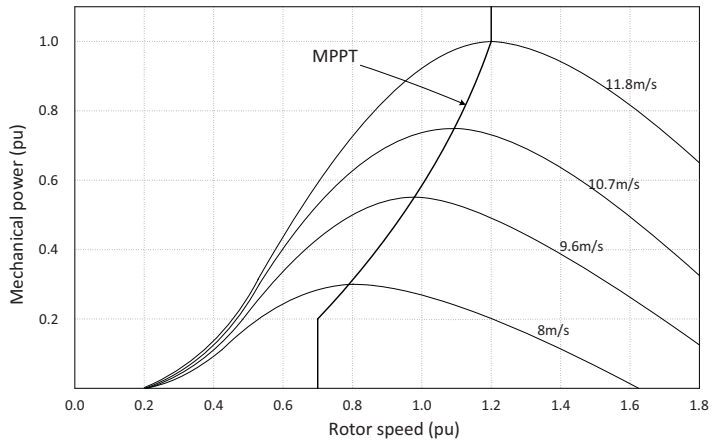

Fig. 4.1: The power-speed characteristic of wind turbine

the grid frequency can be recovered by proper control loops inside the converter. The load-frequency contribution of wind turbines can be recovered by emulating the inertial response of conventional synchronous machines [10, 70].

4.1.1 The Control Structure of Wind Turbine

4.1.1.1 The Pitch Angle and Rotor Speed Control

The pitch angle and rotor speed controller of wind turbine is indicated in Fig. 4.2. The controller should be able to track the optimal speed of the rotor (ω_{ref}), which lies between the maximum and minimum rotor speed equal to 1.2 and 0.7 pu, respectively [14, 15, 22]. According to the MPPT characteristic curve, the maximum efficiency of wind turbine is achieved at rotor speed equal to ω_{ref}. The desired value of ω_{ref} at or above the rated wind speed, is 1.2 pu, while for the power below 75% of rated power of wind turbine, the reference speed should track the curve defined as below [15, 22, 76]:

$$\omega_{ref} = -0.67P^2 + 1.4P + 0.51 \tag{4.1}$$

For the wind speeds beyond the rated value, the mechanical power overpasses the electrical power and hence the rotor speed is increased. According to Fig. 4.2, the pitch angle is increased to bypass the surplus mechanical power to keep the rotor speed tunned on the optimal value.

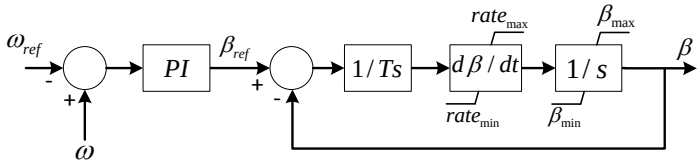

Fig. 4.2: The rotor speed controller

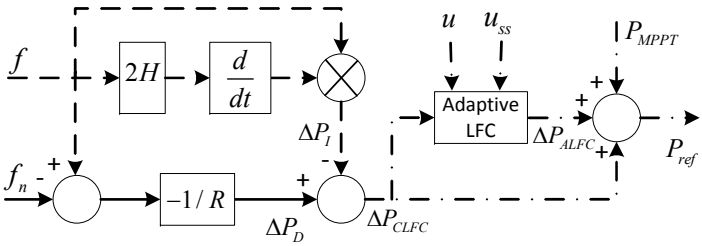

Fig. 4.3: The conventional & proposed load-frequency control

4.1.1.2 The Conventional load-frequency control Scheme

The rotor speed control, voltage regulation and load-frequency control provide the favorable performance of a wind turbine. Since this section addresses the load-frequency control capability of wind turbines, the structure of conventional method studied in [14, 22] and demonstrated in Fig. 4.3 is investigated as a background for the proposed method with a special attention to the droop and inertia characteristic of wind turbine. The active power reference of Rotor Side Converter (RSC) (i.e. P_{ref}) is tunned to obtain an optimal load-frequency control by adjusting the frequency at its nominal value (f_n).

4.1.1.3 The Inertial Support Scheme

The term ΔP_I indicated by dashed line in Fig. 4.3 represents the inertial response of wind turbine. This signal is determined using rate of frequency change and makes the wind turbine able to temporarily support the power system during the disturbances by injecting the spinning reserve power into the grid. The term ΔP_I is mathematically defined as below [9, 10, 70]:

$$\Delta P_I = 2 \cdot H \cdot f \cdot \frac{df}{dt} \tag{4.2}$$

where H is the equivalent inertia time constant of rotor and turbine and f is the grid frequency.

4.1.1.4 The Frequency Droop Control

The signal ΔP_D indicated by solid line in Fig. 4.3 represents the droop control of wind turbine, which is determined using frequency deviation from its nominal value as follows [15, 22]:

$$\Delta P_D = -\frac{f - f_n}{R} \tag{4.3}$$

where R is the speed adjustment rate of rotor.

The participation share of wind turbine in the load-frequency control (ΔP_{CLFC}) can be specified as below:

$$\Delta P_{CLFC} = \Delta P_D - \Delta P_I \tag{4.4}$$

The active power reference of rotor side converter (P_{ref}) is calculated in (4.5) using summation of MPPT term (P_{MPPT}) and the load-frequency control term (ΔP_{CLFC}). Since the rare of frequency change and frequency deviation signals in (4.2) and (4.3), respectively are zero in steady state, their corresponding terms in (4.4) are equal to zero, which means that in the steady state condition, the wind turbine is optimally tunned at MPPT.

$$P_{ref} = \Delta P_{CLFC} + P_{MPPT} \tag{4.5}$$

According to equations (4.2) and (4.3), the active power reference is augmented during the frequency decay, in order to support the grid by injecting more active power. Increment of generator load, causes deceleration of rotor. Hence, in order to return the rotor speed to its desired value, the pitch angle needs to be reduced to increase extracted mechanical power from the wind. The applicability of this solution is limited to the wind speed above or at least equal to rated value in order to have some spinning reserve by pitch angle value greater than zero [9, 10, 22].

4.1.2 The Proposed load-frequency control Scheme

4.1.2.1 Voltage Drop Data as an Alternative Criterion of Electrical Distance

Since the decentralized load-frequency control of wind turbine is studied in this section, no communication system is available between wind turbines. Therefor, voltage is the only measurable variable, which contains useful information about proximity event location.

The voltage collapse has a local behavior is generally limited to the vicinity of the failure point/s [4, 22, 35]. The proximity to the event place can be determined using electrical distance of any arbitrary point from the disturbance location. The electrical distance indicates the electrical proximity of any pair buses in the network using voltage sensitivity. The magnitude of the event is affected by the topology of grid and the

electrical distance from the disturbance location. The voltage interaction between buses i and j regarding occurrence of event at bus j can be determined as below [22, 39, 77]:

$$\Delta v_i = \alpha_{ij} \Delta v_j \tag{4.6}$$

The electrical distance between bus i and j is mathematically defined as follows:

$$D_{ij} = D_{ji} = -\log(\alpha_{ij} \cdot \alpha_{ji}) \tag{4.7}$$

The correlation between electrical and physical distance is not often strong [77]. It means that a pair of buses, which are close physically, may be distant electrically.

In the decentralized strategy, the voltage drop data at the event location (Δv_j) and parameters α_{ij} in (4.6) are not accessible , but Δv_i (the left side in (4.6)) is available by locally measurement and can be employed in the proposed method. The term Δv_j is the voltage deviation in the failure bus, which is unique and same for all of studied buses and the differences in the terms Δv_i is due to the diversity in their α_{ij}. Therefore, according to (4.6), the voltage decline of buses during the event has a direct relationship with their electrical distance from the event location.

4.1.2.2 The Adaptive load-frequency control Scheme Using Voltage Drop Data

According to the section 4.1.1.2, the conventional load-frequency control scheme is merely determined using frequency. The frequency is a common and same variable across the network [4, 39, 74]. It means that the participation share of all of wind turbines (ΔP_{CLFC} in (4.4)) in the load-frequency control is same, independent of event location. In other words, during the load-generation mismatch, same amount of active power is produced by close and faraway wind turbines, which are contributing in the load-frequency control plan.

Transferring the power from distant units to the event location, may cause worse voltage profiles, over loading of transmission lines and power factor decline [22, 40, 78], whereas enough spinning reserve may be available as standby power in the wind turbines located in the vicinity of the failure point. The load-frequency control scheme should be adaptive to the scale and place of event. Therefore, the load-frequency control should be modified so that the wind turbines nearby the event place should inject more power than the faraway units.

According to the electrical distance concept elaborated in section 4.1.2.1, the voltage decay can be a proper measure of the term *local* in the load-frequency control plan. The voltage deviation from its pre-disturbance value is defined as the difference between the steady state value (v_{ss}) and post-disturbance value:

$$\Delta v = 100 \cdot \frac{v_{ss} - v}{\Delta v_{max}} \tag{4.8}$$

In order to achieve an adaptive load-frequency control, the equation (4.5) can be modified using voltage deviation:

$$\Delta P_{ALFC} = K_{GOV} \cdot \Delta v \cdot \Delta P_{CLFC} \tag{4.9}$$

$$P_{ref} = \Delta P_{ALFC} + \Delta P_{CLFC} + P_{MPPT} \tag{4.10}$$

where the term K_{GOV} represents the classical contribution of wind turbine in the load-frequency control plan and is selected equal to 1 pu to be same as the corresponding gain of governor of conventional synchronous machines (IEEE standard governor GOV-IEESGO). If K_{GOV} of wind turbine is selected more than corresponding value of synchronous machines, the contribution of wind turbine in the load-frequency control exceeds the synchronous machine participation share. In this way, the dependency of operation of power system to the stochastic nature and intermittent behavior of wind energy is increased,which may reduce the system reliability. Contrariwise, the smaller value of K_{GOV} for wind turbines compels the grid to rely on synchronous machines that are no longer dominant in the network in case of high share of wind power penetration.

According to (4.10), the wind turbines, which are electrically closer to the event location and therefore experience larger voltage decay following perturbation, produce more active power to the network. The contribution share of wind turbine in load-frequency control scheme is adjusted according to their electrical distance to the incidence place. If the spinning reserve of wind turbine located in the neighborhood of disturbance place depletes by fully utilization of its capacity, the load-frequency control may keep running by distant wind turbines, which still have some spinning reserve until is recovered to the permissible range in time.

4.1.3 Simulation Setup

To assess the efficiency of proposed method, the 9 bus IEEE standard test system is selected as case study (Fig. 4.4) [10,39,70]. The static and dynamic data of the test system can be found in [6]. Synchronous generators are equipped with the IEEE standard governor GOV-IEESGO and automatic voltage regulator AVR-IEEEX1. To increase the share of wind power in the network up to 51%, the active power set point of G1, G2 and G3 equal to 71, 163 and 85 MW are declined to 55, 63 and 45 MW, respectively. The required active power demand is produced by three DFIG wind turbines with the active power reference equal to 52 MW connected to the buses 5, 6 and 8.

The wind speed can be assumed constant and equal to 14 m/sec [10,70,79] for typical period of interest up to tens of seconds. The control type of wind turbines are selected as PV bus to procure frequency and voltage regulation capability. The operating point of wind turbines are tunned on a sub-optimal operating point equal to 90% of their rated power to provide 10% spinning reserve [14, 22, 80].

The voltage and frequency dependency model of the load's active and reactive power

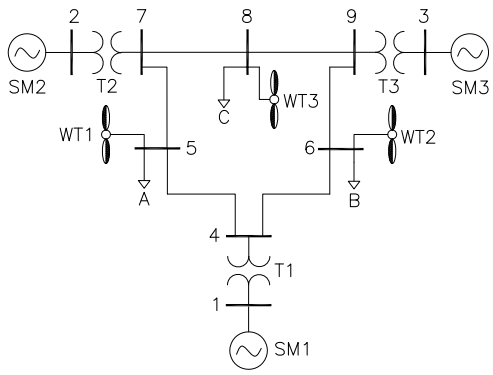

Fig. 4.4: The 9 bus IEEE test system

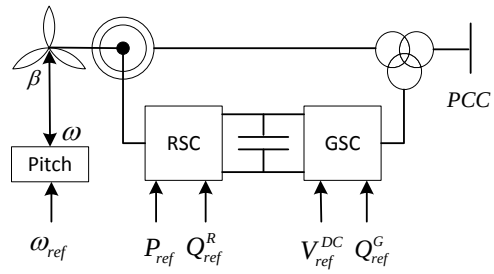

Fig. 4.5: The control structure of DFIG

Table 4.1: The Voltage & Frequency Dependency of Loads

load type	contribution(%)	p_v	p_f	q_v	q_f
CZ	**10**	**1.6**	**0.0**	**0.0**	**0.1**
CC	**20**	**1.2**	**-1.0**	**3.0**	**-2.8**
CP	**70**	**0.1**	**2.8**	**0.6**	**1.8**

specified in [8, 40, 74] is considered in the simulation. Moreover, the contribution of different type of loads in the load modeling including Constant Impedance (CZ), Constant Current (CC) and Constant Power (CP) is selected according to [4, 39, 74] in Table. 4.1 for all of existing loads (A, B and C).

Fig. 4.5 indicates the control structure of DFIG wind turbine. The active and reactive power of the wind turbine are independently determined by four-quadrant operation of back-to-back voltage source converters using vector control techniques in the dq-reference frame.

4.1.4 Simulation Results and Discussion

The efficiency of the proposed method is evaluated using numerical simulation conducted in DIgSILENT PowerFactory 15.0 software. 10% step increase of both active and reactive power of the Load A (4% of the total system load) at 1 s with the capacity equal to 12.5 MW/5 Mvar connected to the bus 5 is simulated as a disturbance.

Figs. 4.6-4.11 demonstrate the simulation results including electrical and mechanical variables throughout 10 second of simulation. Prior to the perturbation at 1 s, the power system variables are stable at steady state inside their permissible range. The

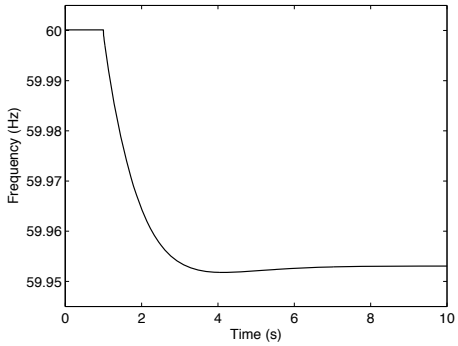

Fig. 4.6: The grid frequency

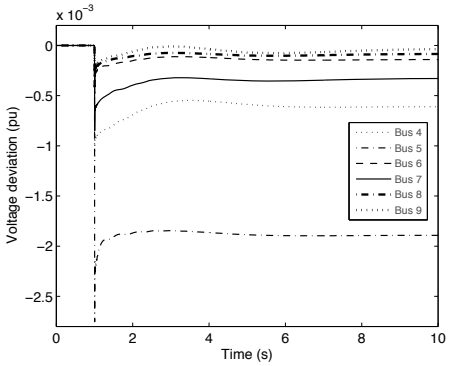

Fig. 4.8: The bus voltage deviation

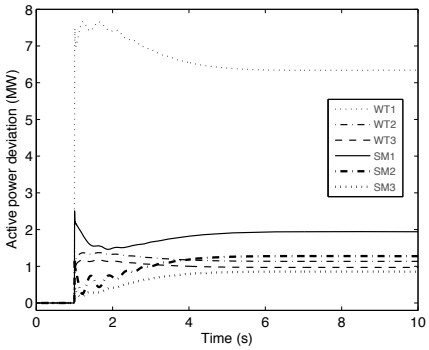

Fig. 4.7: The active power deviation

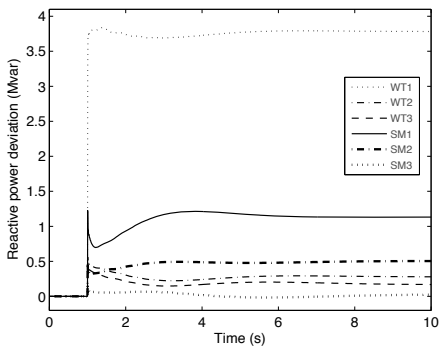

Fig. 4.9: The reactive power deviation

determinant variables are intentionally indicated with respect to their steady state values to highlight their variations and to simplify their comparison.

Before the disturbance at 1 s, the bus voltages are inside the normal operating boundary of 0.95 pu - 1.05 pu (Fig. 4.8) and the frequency is flat at 60 Hz (Fig. 4.6). The surplus wind power is bypassed by pitch angle about 9.9 deg (Fig. 4.11) to procure 10% spinning reserve in wind turbines. The optimal rotor speed equal to 1.2 pu as the input signal in Fig. 4.2 and depicted in Fig. 4.10 is calculated according to (4.1) based on the active power reference and required spinning reserve of wind turbine.

Following the load event at 1 s, the load voltages (Fig. 4.8) decline almost instantly, whereas the frequency starts to drop almost smoothly (Fig. 4.6). The voltage variations are often sharp comparing to the frequency behavior, since the frequency/active power is relevant to the governor and pitch dynamics of synchronous machines and wind tur-

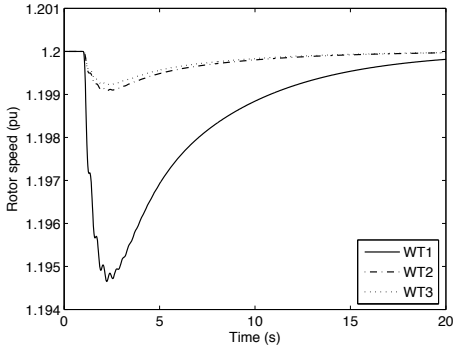

Fig. 4.10: The rotor speed

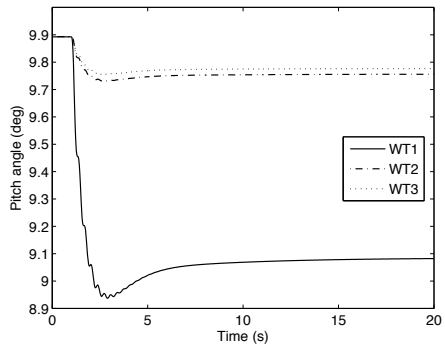

Fig. 4.11: The blade pitch angle

bines, respectively [22,37,40], whereas the voltage dynamics are determined by electrical devices of field excitation circuits, which are intrinsically fast comparing to mechanical dynamics. According to 4.6, since the voltage deviation is directly associated with the scale of the disturbance and hence the electrical distance from the event location, the bus 5 experiences more voltage drop than other buses (Fig. 4.8).

Since the under voltage events are often a local phenomena in the power system [4, 22, 35, 39], each individual generation unit is responsible for voltage regulation of its bus bar (neighborhood) to recover the bus voltage to the per-disturbance value as much as possible, therefore the control type of generating units either synchronous machines or wind turbines are defined as PV bus to procure the voltage regulation/reactive power support. Thus, the injected reactive power of wind turbine 1 (Fig. 4.9) to the grid is more comparing to the other wind turbines due to measuring more voltage drop at its bus (Fig. 4.8).

The load-frequency control loop of wind turbine demonstrated in Fig. 4.3 promptly reacts to the frequency decline in Fig. 4.6. Despite of conventional load-frequency control scheme in which the distant and nearby wind turbines are equally participating in the load-frequency control plan, the proposed method differentiates between the distinct wind turbines proportional to their electrical distance from the event location associated with the voltage decay data. Fig. 4.8 confirms that the wind turbine 1, which experiences more voltage drop, produces more active power following the disturbance at 1 s (Fig. 4.7).

Fig. 4.8 shows that the minimum voltage drop happens at bus 9, which corresponds to the maximum electrical distance from the failure bus 5, i.e. the farthest bus from the event place (bus 5). Therefore, minimum reactive power (Fig. 4.9) is injected by corresponding synchronous machine 3. While the voltage drop is augmented from bus 9

toward the disturbance place at bus 5 (Fig. 4.8), the reactive power provision (Fig. 4.9) is gradually increased.

According to the proposed adaptive load-frequency control method, similar to the reactive power, the active power provision (Fig. 4.7) increases from the distant generators (synchronous machine 3) toward the closest generators to the failure point (wind turbine 1) due to the increase in the voltage decline. Therefore, the major part of required active power is produced locally by wind turbines at vicinity of disturbance. It means that the frequency regulation capability of the wind turbine is made adaptive to the scale and place of event.

The magnitude of the disturbance at load A nearby to the wind turbine 1, causes abrupt augmentation of electrical load in wind turbine 1. The new quantity of term P_{ref} produced by load-frequency scheme in Fig. 4.3 following the disturbance decelerates the rotor speed, since the power electronic converter of wind turbine is much faster than mechanical dynamics of pitch and rotor, which possess a smooth and tardy physical process. Therefore, the rotor speed is gradually recovered with some delay after an initial decline (Fig. 4.10). The emulated inertial response of wind turbine, i.e. releasing the kinetic energy stored in the rotor may temporarily be available during the incipient phase of event. Hence, sufficient reaction time is transiently provided by emulated inertial response for pitch dynamics to increase the input mechanical power extracted from wind power. According to (4.1),the active power increase of wind turbine 1 to a value close to its rated power, causes higher rotor speed around its maximum mechanical boundary eaual to 1.2 pu in Fig. 4.10.

By comparison of Figs. 4.6-4.9, the electrical variables such as frequency, voltage, active and reactive power are stabilized at a new steady state values in less than 5 s, while reaching the steady state of mechanical variables such as pitch angle and rotor speed depicted in Figs. 4.10-4.11 lasts almost 20 s. Hence, the simulation time of interest about 20 s is selected according to the dynamics of mechanical state variables rather than electrical.

4.1.5 Summary

In the networks with high share of Wind Power, assigning the burden of load-frequency control to wind turbines is inevitable. Both inertial response and droop control of conventional load-frequency control schemes either in the synchronous machines or wind turbines are based on the frequency and since the frequency is a common factor across the whole power system, the participation share of distant and nearby wind turbines in the load-frequency control scheme is same, whereas sufficient spinning reserve may be available in the wind turbines located in the vicinity of event location. According to the electrical distance concept, the voltage drop is a proper measure of closeness to the disturbance location. The decentralized and adaptive load-frequency control scheme of wind turbines using locally measured voltage information to make the conventional

scheme adaptive to the scale and location of disturbance was done in this chapter. The wind turbines with more voltage decline, contribute more in load-frequency control plan. In other words, the contribution share of wind turbines in load-frequency control scheme is determined according to their electrical distance from event location.

4.2 Malfunction Operation of LVRT During Islanding

Rapid development of energy demand and abundant public concerns regarding global warming phenomena steers the energy production toward Renewable Energy Sources (RESs), particularly the wind power, which is recently in the center of attention in terms of growth [9, 70, 74]. The wind energy is the most popular and affordable source of energy comparing to the other sources. As the share of RESs in the grid is increased, its consequences, i.e. the impacts on operation and control of power system may not be neglected anymore. The stochastic behavior and intermittent nature of RESs applies the uncertainty to the availability of sources, which diminishes the reliability of power system [14, 22].

Widespread development of RESs enforces the utility operators to codify a set of regulations and technical standards called *grid codes*, which should be respected by RESs during their connection status to the grid. The grid codes include of a full range of ancillary services similar to conventional synchronous machines to support the network during the disturbance/s [10, 81]. The grid code requirements for new generation of RESs are strictly legislated or revised to achieve an efficient and comprehensive for different operating states of RESs and power system [71, 82].

Both static and dynamic requirements are encompassed by technical description of grid code. The static requirement dealing with the operation of RES in its steady state e.g. power flow at PCC, while the dynamic requirement i.e. the most important part, addresses the performance of RES during the transient state resulting from disturbance and/or fault conditions. The dynamic requirements basically covers many features and ancillary services such as voltage, frequency and power factor regulation an/or Fault Ride Through (FRT) capability.

The FRT feature is a widespread and general capability, which also covers LVRT and over speed ride through in RESs. The LVRT constitutes the principal requirement of FRT grid code and determines the connectivity of RES to the grid during short-term and transient voltage dips at its PCC, which may happen due to temporary decline of wind speed. In fact, the LVRT is dealing with how the RES can handle a significant reduction in the input energy, e.g. wind and solar plants. The LVRT grid code compels the RESs to stay connected to the grid for a specified time period, although the PCC voltage becomes zero or close to it due to the voltage sag/plunges.

The Permanent Magnet Synchronous Generator (PMSG) type of WT is gradually going to be dominant comparing to the other WT types particularly in the offshore applications due to the underneath advantages:

- High efficiency operation in Full range of wind speed
- Self excitation independent of grid or plant dynamics

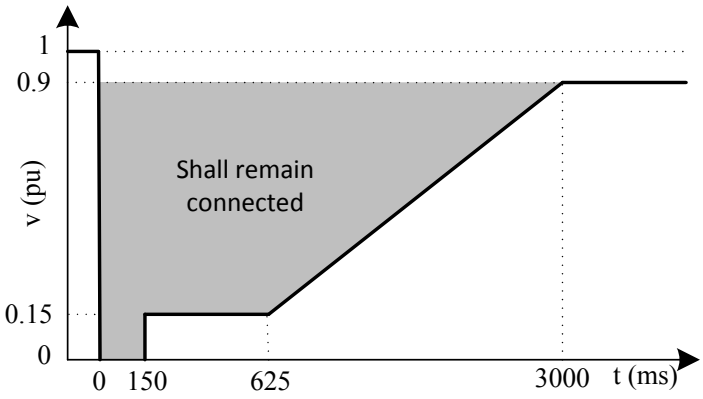

Fig. 4.12: Typical LVRT requirement [2]

- Reactive power support even during short circuit faults
- Gearboxless
- Low noise

The PMSG type of WT is indirectly connected to the grid via power electronic converters, as indicated in Fig. 4.13. The LVRT behavior of PMSG during event/s is mainly determined by grid side converter, as electrical and mechanical dynamics of generator are fully decoupled from the grid by employed converters [2, 83].

The majority of converter control loops are executed using conventional PI controllers, which are basically adjusted for steady state operation rather than transient state. Generally, the PI controllers may not be efficient at all operation conditions, i.e. severe transient dynamics of voltage sags resulting from short circuits. The inrush current of grid side converter may not be properly limited even with the controlled DC link voltage inside the permissible boundary, which may harm the grid side converter of PMSG and rotor side converter of Doubly Fed Induction Generator (DFIG) [2, 73].

4.2.1 LVRT Grid Code Requirements

A more reliable interconnection of high share of wind power with power system may be achieved if the WTs are equipped with LVRT capability. The LVRT compels the WTs to stay connected to the grid and support the network stability, similar to conventional synchronous machines during the voltage dip/sags resulting from various faults [81, 82]. The WTs should continuously contribute in active and/or reactive power support of the network following the grid faults in order to able to participate in load-frequency control and/or voltage regulation. The connectivity of WT to the grid is determined

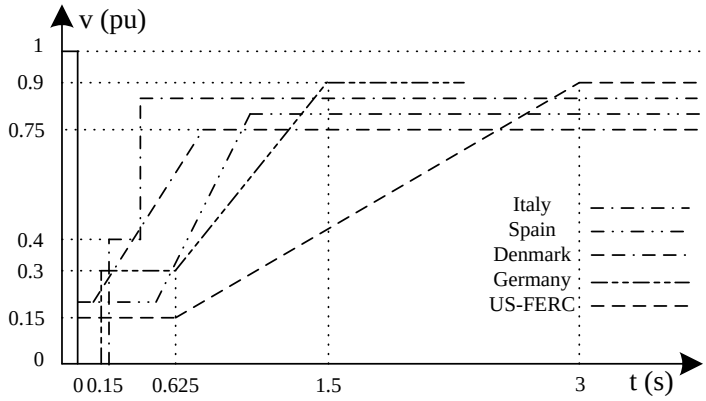

Fig. 4.13: The LVRT of different countries [3]

based on a specific voltage-time characteristic pattern, which depends on both voltage sag magnitude and its time duration measured at PCC. As can be seen from Fig. 4.12, the LVRT grid code is basically specified by a voltage versus time characteristic, stating the minimum required safety of WT regarding the grid voltage sags. The WT can be decoupled from the grid in case of any of following conditions [2, 73]. The PCC voltage is:

- equal to zero and is lasting for more than 150 ms
- less than 0.15 pu for more than 475 ms
- crossing the ramp line at any time between 625 ms and 3000 ms
- less than 0.9 pu for more than 3000 ms

As the WTs normally operate at Maximum Power Point Tracking (MPPT) condition with maximum efficiency or a nearby point to procure some spinning reserve, they are adjusted on a point close to their full capacity and therefore sufficient spinning reserve is not available to be used in case of more demand of active/reactive power [22, 71]. According to LVRT grid code, under the fault conditions, the active power set point of WT is intentionally declined to a lower value to provide some capacity for reactive power support and hence voltage regulation. The priority of grid support is assigned to the voltage regulation instead of load-frequency control and/or MPPT operation point in case of voltage magnitude less than 0.9 pu [73, 81].

4.2.2 LVRT Deficiency in Case of Islanding

Diverse LVRT patterns, depicted in Fig. 4.13, have been approved by Transmission and Distribution System Operators (TSO & DSO) of different countries, which are generally issued according to the practical experiences achieved from monitoring of power system operation/behavior. Despite of diversity in the LVRT profiles, the goal of all is to support the grid with RESs as much as possible in order to achieve a stable, safe and reliable power system following various grid faults [84].

The LVRT patterns may be categorized in term of two major pattern characteristics: Depth and duration of voltage sags. According to Fig. 4.13, the depth of voltage sag is less disperse than their duration, which implicitly indicates close agreement of various grid codes on this item. Furthermore, the LVRT capability has been originally issued to deal with severe faults such as short circuit/s at PCC of RESs and to pass the power system through their transient period to the normal condition following the clearance of fault in time or to inevitably disconnect the unit. The short circuit faults at PCC, generally and almost independent of power system topology, lead to a very low voltage magnitude close to zero, which brings the different grid codes to agreement on a narrow range and therefore, less diversity in depth of voltage sag. The least modifications applied to the depth of voltage sag in the successive revisions of LVRT grid code of different countries emphasizes on the aforementioned agreement stronger than before. Therefore the range of short circuit voltage at PCC is relatively narrow, which causes close agreement of different grid codes on less diversity in the depth of voltage sag of LVRT grid code.

The major difference between distinct LVRT patterns is in the time duration, in which the RESs are requested to withstand the fault and stay connected to the grid. It may depend on power system topology and geographical scale, the penetration level of RESs, availability of strong neighbor networks and so on. However, there is no comprehensive and deterministic pattern proved to be efficient in practice for all possible incidents especially contingencies other than short circuit failures e.g. cascading events and/or islanding condition. The performance/behavior of LVRT grid code has been rarely investigated under cascading events leading to islanding condition.

The nature of short circuit fault and consequently the reaction of power system to it is completely different from other types of faults like the outage of a generating unit or a transmission line. The voltage magnitude during a short circuit fault often falls into the lower 50% boundary of its nominal value, whereas in the outage type of faults, the voltage mostly lies in the upper half of the nominal value. When a short circuit occurs at or nearby the PCC of RESs, some locally variables in the vicinity of fault location, such as grid side converter currents, may exceed their normal range and can cause intolerable stress out of converter's apparent power damaging the power electronic elements, which is prevented by LVRT capability in time. In case of outage events, the relevant variables such as terminal voltages at PCC do not deviate much from the nominal values and therefore, the stress on the converter is not severe as it is in a short circuit situation.

This means that the RES may remain connected for a longer period of time without sacrificing either the reliability of power system or the life time of the converter.

This section addresses the active and/or reactive power support provided to the grid by RESs in presence of high wind power penetration, which is improperly interrupted by LVRT regardless of the fault type and the grid support ability of WT. It means that the RES is disconnected in both cases of short circuit with a severe voltage sag around 1 pu (v=0 pu) and islanding condition with a slight voltage sag around 0.1 pu (v=0.9 pu). In the latter case the voltage magnitude is not faraway from the nominal value and hence the apparent power burden on the converter is still less than its full range of MVA. In other words, the RES may still remain connected to the grid, keep on providing ancillary services and contribute in the stabilization of the power system [81].

A strict and non adaptive LVRT pattern, which is selected independent of disturbance type and standby support capacity available in the WT, may not be a comprehensive and effective solution for widespread range of possible incidents. Improper and early disconnection of a beneficial grid support capacity, which is safely available in RESs as standby, may not be logic and affordable and it may even initiate cascading events and lead the power system toward worse status and further instability.

Small voltage drop during the islanding condition generally demands a low level of reactive power injection comparing to the short circuit fault situation, which causes a severe voltage drop close to zero. Therefore, islanding conditions are completely different from short circuit faults for the voltage sag magnitude and hence, reactive power deficit aspect of view. The LVRT capability is unable to differentiate between islanding and short circuit situations. As a result, the LVRT needs to be revised in order to be efficient under all possible disturbance/s and not just in case of short circuit faults. The LVRT behavior should be investigated for islanding situations as well, which are improperly disconnected despite of their standby and safe capacity available to support the grid.

4.2.3 Simulation Setup

The 39 bus IEEE standard test system depicted in Fig. 4.14 is selected to study the behavior of LVRT in islanding condition [40, 85]. The 4th order mathematical model of synchronous machine, the IEEE standard governor IEESGO and Automatic Voltage Regulator (AVR) IEEEX1 are considered for all synchronous machines. The details of the system data can be accessed in [80]. The dependency of load's active and reactive power to the voltage and frequency in term of different type of loads is defined in (4.11) and (4.12) [8,39]. Moreover, the relevant parameters and the Share (s) of different types of loads such as type i, c and p in the load model is given in Table. 4.2 of Appendix [4].

$$P = P_0 \cdot [s_i \cdot (v/v_0)^{e_i^{pv}} + s_c \cdot (v/v_0)^{e_c^{pv}} + s_p \cdot (v/v_0)^{e_p^{pv}}] \cdot [s_i \cdot (f/f_0)^{e_i^{pf}} + s_c \cdot (f/f_0)^{e_c^{pf}} + s_p \cdot (f/f_0)^{e_p^{pf}}] \quad (4.11)$$

Table 4.2: The Voltage & Frequency Dependency of Loads

Load type	Share (s)(%)	pv	pf	qv	qf
Light bulb (i)	10	1.6	0.0	0.0	0.1
Fluorescent bulb (c)	20	1.2	-1.0	3.0	-2.8
Asynchronous motor (p)	70	0.1	2.8	0.6	1.8

$$Q = Q_0 \cdot [s_i \cdot (v/v_0)^{e_i^{qv}} + s_c \cdot (v/v_0)^{e_c^{qv}} + s_p \cdot (v/v_0)^{e_p^{qv}}] \cdot [s_i \cdot (f/f_0)^{e_i^{qf}} + s_c \cdot (f/f_0)^{e_c^{qf}} + s_p \cdot (f/f_0)^{e_p^{qf}}] \quad (4.12)$$

Some of existing synchronous machines are replaced with Permanent Magnet Synchronous Machine (PMSG) type of WT to achieve integration of wind power into the power system. Different scenarios indicated in Fig. 4.14 with various wind power penetration levels are defined to assess malfunction operation of LVRT grid code. The Federal Energy Regulatory Commission (FERC) LVRT pattern from Fig. 4.13 is employed in simulations.

4.2.4 Simulation Results

Numerical simulations are conducted in DIgSILENT PowerFactory 15.1 software. Distinct scenarios consisting of islanding and/or cascading events are defined in different areas of power system (Fig. 4.14) to demonstrate the malfunction operation of WT LVRT in case of islanding.

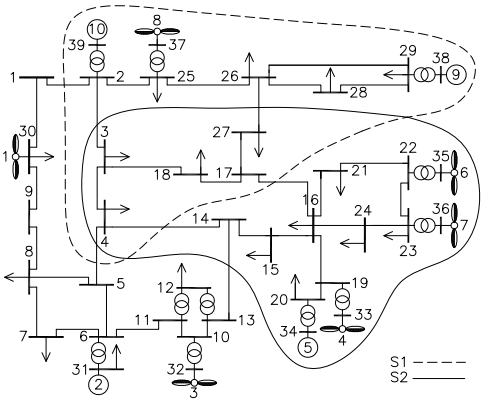

Fig. 4.14: Islands in 39 bus system

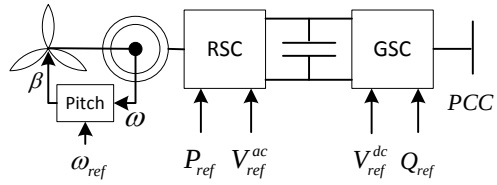

Fig. 4.15: Control structure of PMSG

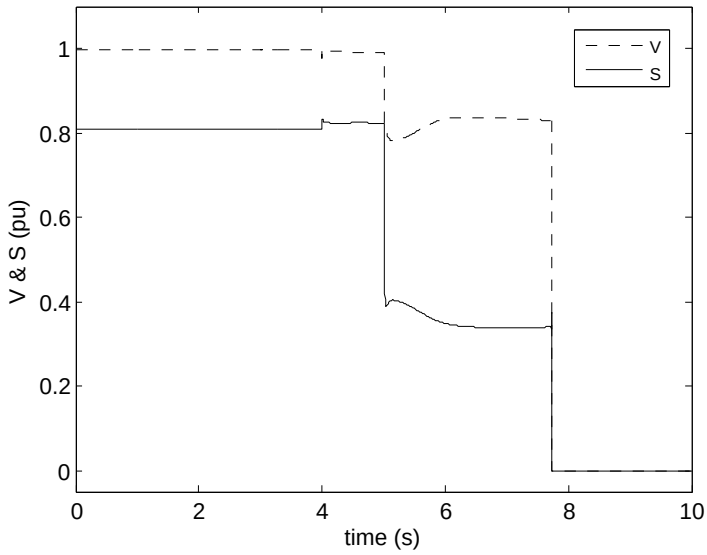

Fig. 4.16: The voltage and apparent power of WT8

4.2.4.1 Scenario 1:

In this scenario, outage of G10 at 2 s triggers some cascading events including loss of transmission lines 1-2 at 3 s, 4-5 at 4 s and both 16-17 & 4-14 at 5 s, which separates an island from the power system indicated by S1 in Fig. 4.14. By replacing G8 with a PMSG wind farm, 39% wind power penetration is achieved.

Fig. 4.16 shows the PCC voltage and apparent power of WT8 throughout 10 seconds of time simulation. The cascading events are started at 2 s and the islanding happens at 5 s. The PCC voltage falls below 0.9 at 5 s and the active power reference p_{ref} and therefore, the utilized capacity of WT8 is reduced to a lower level. In this case, not only the WT is not overloaded at all and there is no stress on the grid side converter, but also the WT8 is down regulated to a point less than half of its rated power. The LVRT is unable to differentiate between severe short circuit faults and the disturbances with a PCC voltage close to the normal range. Under such a circumstances, although there is plenty of stand by capacity in the WT8 to support the grid without any difficulty, the WT8 is improperly disconnected by LVRT before 8 s.

4.2.4.2 Scenario 2:

The solid line in Fig. 4.14 shows the islanding scenario S2, which is corresponds to an outage of tie-line 13-14 at 2 s, lines 4-5, 2-3 and 26-27 at 3 s, 4 s and 5 s, respectively.

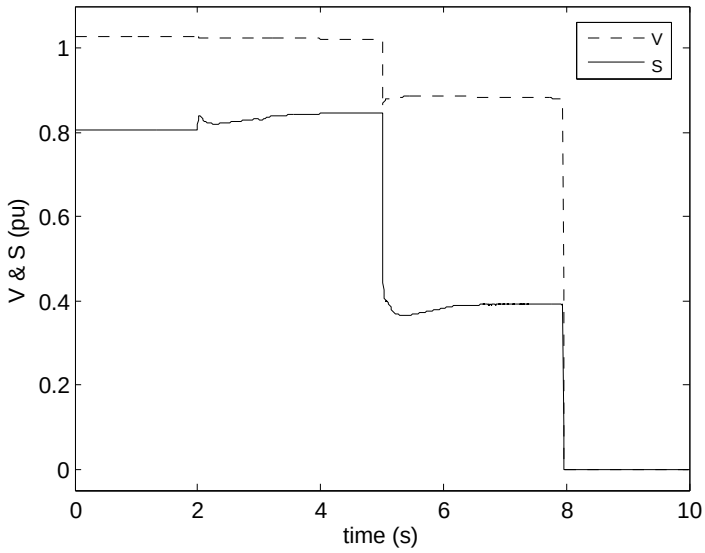

Fig. 4.17: The voltage and apparent power of WT4

After islanding, the wind power share in the network reaches 78%, which is a relatively high level of wind power penetration.

Fig. 4.17 presents the voltage and apparent power of WT4. In this scenario, WT4, WT6 and WT7 are suddenly disconnected around 8 s following the islanding condition at 5 s, which causes a slight voltage drop below the lower level of normal range at 5 s, which makes it different from short circuit fault situation. Although, same as the first scenario, all available WTs are improperly lost in a short period of time, the lost WTs in this scenario constitute the major part of total existing generation, which may lead the island to a much worse case or even blackout. Regardless of standby spinning reserve (S curve of WT4 in Fig. 4.17) available in the WTs during the disturbance/s provided via reducing the active power set point and allocating the released capacity to the reactive power support, the WTs without any stress on its converters, mechanical and electrical parts are improperly disconnected from the island, which may not only be logic and affordable, but also may further deteriorate the situation.

4.2.5 Summary

Although the LVRT pattern i.e. a voltage versus time characteristic curve may be efficient at short circuit faults, which generally cause a deep voltage drop close to zero and therefore, are accompanied by a huge reactive power deficit, it may not be effective in case of cascading events and islanding, which post-disturbance voltage is slightly below

the normal range and hence less reactive power support is expected from RESs. LVRT merely considers the voltage drop magnitude and its duration regardless of standby capacity available in the WT to support the grid for a longer time. This section demonstrates improper operation of LVRT in case of disturbances with small voltage sags (e.g. islanding situations) in which the WT is improperly disconnected sooner than the latest possible time.

Chapter V

Decentralized Load Shedding

5.1 Integration of Frequency and Voltage Thresholds

For a smooth growth of the load, unit governors measure the speed decline and increase the input power of the generator. Therefore, overload is compensated by using already provided spinning reserve (the unused capacity of the generator). If all generators are operating at maximum production capacity and hence there is no available spinning reserve, the governors may be unable to relieve extra loads. In any case, the fast frequency plunges that accompany serious overloads require impossibly rapid governor and boiler reaction. To prevent such a drop in frequency, it is compulsory to intentionally and automatically release a portion of the load equal to or greater than the extra load.

When a LS procedure is designed for a given power system, several key factors must be determined to achieve the most effective and optimal solution. Several key parameters should be carefully determined to minimize the amount of load to be curtailed, due to their significant effect on the LS process. The total amount of shed load, the number of LS stages, the amount of load to be shed at each stage, frequency thresholds, the delay between stages and the location of load curtailment are important decision parameters which affect the LS process [7, 38, 40, 74].

5.1.1 Load Shedding Trigger Criteria

Although relay manufactures provide underfrequency and undervoltage LS scheme in the single module with multiple steps for each one, the coordination between them has not been anticipated and they operate in the power system independently. Coordination of two independent schemes is necessary to prevent both under voltage and frequency events to avoid moving the power system toward jeopardy. Therefore, the UVLS scheme may be employed as a complementary part of UFLS scheme in a new combinatorial scheme in order to benefit from both voltage and frequency information. for the emergency control purposes, voltage and frequency are two suitable observable variables that could illustrate the state of system following an event. The state variables corresponding to frequency and voltage deviation in *pu* are defined as below, respectively:

$$x_f = \frac{f - f_0}{f_0} \qquad , \qquad y_v = \frac{v - v_0}{v_0} \tag{5.1}$$

where f_0 and v_0 are the nominal frequency and voltage at the relay busbar before contingency, respectively. By assigning the x axis to the state variable x_f and the y axis to the state variable y_v, the state trajectory can be plotted in the state plane (Fig. 5.1).

In the UFLS scheme, when the frequency exceeds one of the predetermined thresholds, some portion of the load is automatically discarded. There are similar thresholds for voltage in the UVLS scheme. The Table 5.1 indicates the normal region and the successive thresholds for both frequency (b_f) and voltage (b_v) in *p.u.* One way to merge the thresholds and make a new combinational threshold for the new scheme, is to use

Table 5.1: Frequency and Voltage Thresholds in *pu*

boundaries	b_f	b_v
N	0.30/60	0.050
S1	0.50/60	0.100
S2	0.75/60	0.125
S3	1.00/60	0.150
S4	1.25/60	0.175

each set of the thresholds in the Table 5.1 as the focus points of an elliptical boundary (Fig. 5.1) as follows:

$$\left(\frac{x_f}{b_f}\right)^2 + \left(\frac{y_v}{b_v}\right)^2 = 1 \tag{5.2}$$

In the new LS program, the number of LS steps is absolutely same as the former schemes and each new step is precisely triggered when the state trajectory crosses the corresponding elliptical boundary. In the classic UFLS/UVLS plans, the load relief is merely done when the frequency/voltage is less than the nominal values. The only area which meets both above conditions (negative value of both x_f and y_v) in the state plane is the third quarter. The Load curtailment in the buses with the voltage greater or equal to the value prior the contingency (the area indicated with angle α in Fig. 5.1) may cause locally reactive power shortcoming and exacerbate the situation [6]. Similarly, during the voltage dips which frequency is still in the normal range (the area indicated with angle β in Fig. 5.1), the load release should be avoided [6]. Since there is no comprehensive method or criteria for determining α and β, the frequency threshold indicated by vertical dotted line in Fig. 5.1 is considered as trigger criterion of Load shedding. Therefore, the alloted region to the LS plan is confined to the area located in the left side of vertical line. Both frequency and voltage affect the LS decision making and the proposed scheme is able to detect both voltage and frequency events at the same time. Besides, in order to block the malfunction operation of an underfrequency relay, an undervoltage inhibit function can be implemented in the present scheme of the relay [8].

5.1.2 Distribution of Shedding Amount

In conventional LS methods, all of the load buses are involved in load curtailment without selection, since these kind of classic plans are solely founded on using frequency information and frequency is a common factor throughout of the whole power system [4]. In the large scale power systems which may have thousand of load buses, contribution

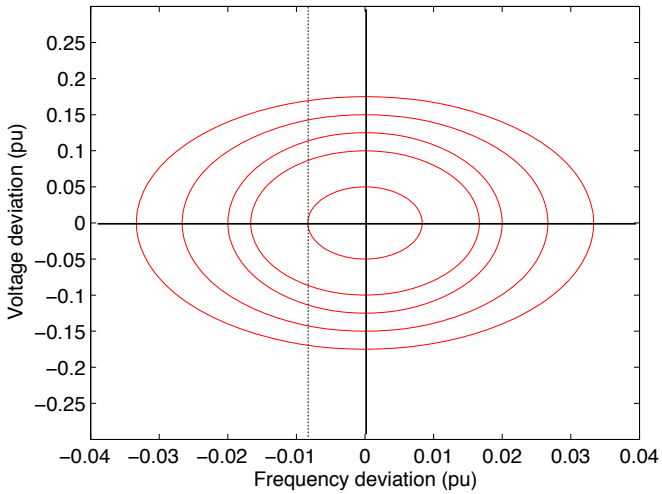

Fig. 5.1: The Boundaries of the New LS Scheme

of all loads in the LS scheme is not practical [37]. The LS zone should be bounded to a specific area in the vicinity of disturbance location [8, 37, 41]. For instance, when a generator is lost, it makes sense that the loads which are located around this generator and are supplied by it are shed first.

Following a contingency in the network, the bus voltages inherently contain useful information about the location of the event [36]. The buses nearby the failure point generally experience more voltage drop than the others and the closer they are, the more they decrease. The present proposed scheme uses frequency and voltage decline at the corresponding load bus. Although the frequency decay may be same for all load buses, the magnitude of voltage drop can be different depending on the electrical distance to the event location. The buses with more voltage drop may reach the LS boundaries sooner than the others and consequently are shed first. Therefore, during the incipient phase of the LS program, a limited area in the neighborhood of the incident place is covered and discarding some portion of the loads are initiated from this region. If either the frequency, voltage or both continue to further decline, the farther loads may gradually get closer to their corresponding elliptical boundaries and fire the related LS step. This deployment may radially propagate in the network until not only the frequency and voltage collapse are prevented, but they return back to their permissible values [8, 42].

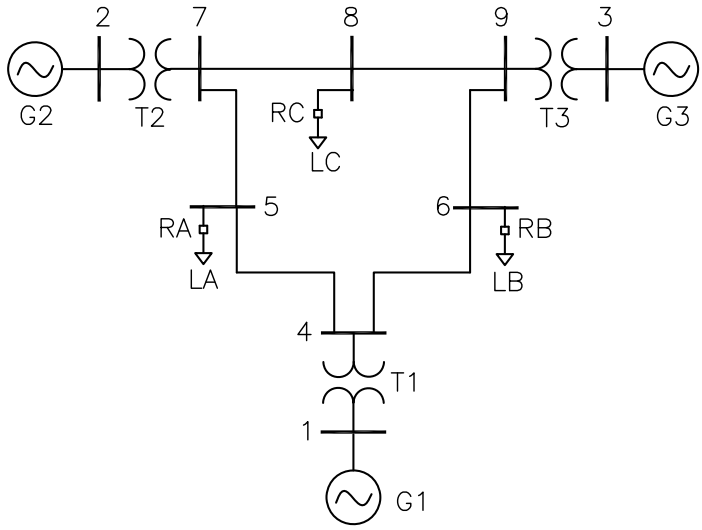

Fig. 5.2: 9 bus IEEE standard test system

5.1.3 Simulation Setup

5.1.3.1 Test System

In order to evaluate the superiority of proposed control scheme, the WSCC 3-machine system which is well-known as P.M Anderson 9-bus is chosen as case study. The power system contains of 3 generators, 6 lines, 3 two winding power transformers and 3 loads as depicted in Fig. 5.2. The static and dynamic data of the system can be found in [86]. Synchronous generators are equipped with the IEEE standard governor GOV-IEESGO and automatic voltage regulator AVR-IEEEX1.

5.1.3.2 Synchronous Machine Modeling

The correct modeling of Synchronous Machine (SM) is a very important issue in all kinds of studies of electrical power systems. PowerFactory provides highly accurate models which can be used for the whole range of different analysis, from simplified models for load-flow and short-circuit calculations up to very complex models for transient simulations. Basically there are two different representations of the SM:

- The round rotor generator or turbo generator
- The salient rotor generator

The generators with a round rotor are used when the shaft is rotating with or close to synchronous speed of 1500 to 3000 *rpm*. These types are normally used in thermal or nuclear power plants such as G2 and G3 in this paper. Slow rotating SMs with speed of 60 to 750 *rpm*, which are for example applied in diesel or hydro power plants, are realized with salient rotors such as G1.

It is assumed that SMs are operating in full capacity of their rated power and there is no reserve capacity available for either active or reactive power in synchronous machines in order to demonstrate the merit of the proposed scheme [44]. It is strongly recommended by some literatures that the LS scheme should be able to bring the frequency to the permissible range above the nominal frequency. There are two logical reasons behind this fact. Firstly, the SMs generally react to frequency drop with some delay due to tardiness of their prime mover which can be type of hydro or steam power plant. Secondly, there is the possibility that the generation increase may not be available due to full scale operation of SMs [8].

5.1.3.3 Load Modeling

The active power shortage is often escorted by reactive power shortage, which affects the voltage profile of the system. Many papers strongly emphasize on considering the voltage dynamics on the load's behavior [36, 55]. Hence, the sudden reaction of the load to the voltage variation cannot be practically neglected. The influence of frequency variations on the load in comparison to the voltage effects is insignificant and therefore, the load dependence on frequency can be almost neglected [36]. The voltage dependency of real and reactive power of loads in PowerFactory software is modeled using three polynomial terms as shown in (5.3) and (5.4), instead of only one polynomial term.

$$P = P_0 \left(c_1 . \left(\frac{v}{v_0} \right)^{e_1} + c_2 . \left(\frac{v}{v_0} \right)^{e_2} + c_3 . \left(\frac{v}{v_0} \right)^{e_3} \right) \tag{5.3}$$

$$Q = Q_0 \left(c_4 . \left(\frac{v}{v_0} \right)^{e_4} + c_5 . \left(\frac{v}{v_0} \right)^{e_5} + c_6 . \left(\frac{v}{v_0} \right)^{e_6} \right) \tag{5.4}$$

where $c_3 = 1 - c_1 - c_2$ and $c_6 = 1 - c_4 - c_5$. The subscript 0 indicates the normal operating point values. The quantities P, Q and v are standing for real power, reactive power and voltage of corresponding busbar, respectively. In order to simulate a mixture of three different type of loads, the exponents in (5.3) and (5.4) can be extracted from [8]. For example, selecting the exponent equal to 1 yields the constant current loads such as discharge lighting and the cumulative lumped load of many commercial establishments. The exponent equal to 2 yields the constant impedance loads such as resistors and the exponent value of 0 stands for constant power loads such as motors. The coefficients c_1, c_2 and c_3 determine the share of different type of loads in active power part of resulting load in *pu*. Analogously, the coefficients c_4, c_5 and c_6 play the same role for reactive

power part. Hence, a combination of different type of loads may be included in the load model as can be seen in practice from busbar aspect of view.

5.1.4 Simulation Results and Discussion

The numerical simulation is conducted in DIgSILENT PowerFactory 15.0.2 software. The outage of generator G3 is considered as a serious disturbance with the capacity almost equal to 27% of system load at 0.5 s. Figs.5.3-5.6 and Tab.5.2 show the simulation results throughout 10 seconds of time duration of simulation. Before the contingency at 0.5s, the power system is in the steady state and all of the variables are in range such as the frequency which is equal to 60 Hz as can be seen in Figs.5.4-5.6. In Fig. 5.3, the deviation of voltage has been plotted it term of frequency deviation which has been de-

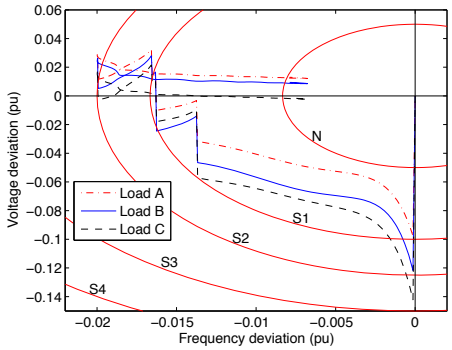

Fig. 5.3: State trajectory of loads

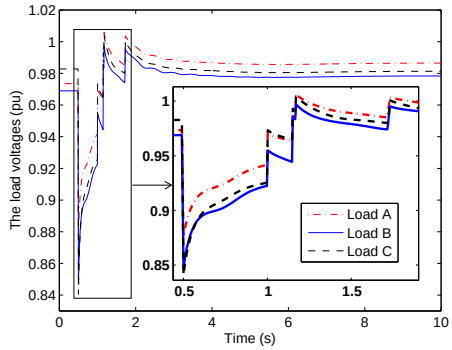

Fig. 5.5: Voltage profile of loads

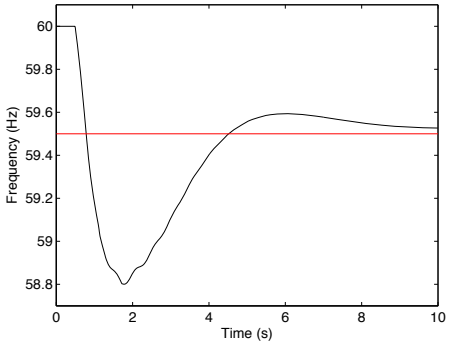

Fig. 5.4: Grid frequency

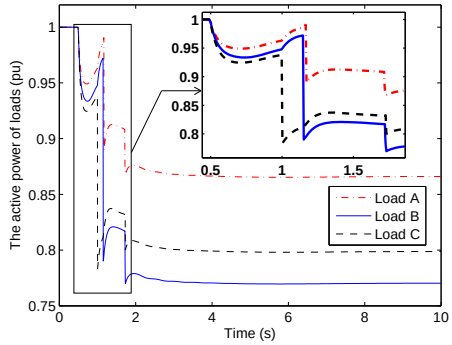

Fig. 5.6: Active power of loads

Table 5.2: The time sequence and percentage of load shed

Time (s)	Load A	Load B	Load C
1.00	-	-	16.7%
1.15	-	18.9%	-
1.17	10.4%	-	-
1.71	4.1%	-	-
1.72	-	4.8%	-
1.73	-	-	3.3%
Total	14.5%	23.7%	20.0%

fined in (5.1). The x and y axis show the state variables of x_f and y_v in pu, respectively. The terms $S1$ to $S4$ are standing for the first to forth step of the LS relays which are employed in this research. The Fig. 5.3 displays the state trajectory of the loads A to C.

Following the G3 trip at 0.5 s, bus voltages fall almost instantly as can be seen in Fig. 5.3 and Fig. 5.5, whereas frequency is still in the normal range in Fig. 5.4. The variation of the voltage is always much larger and faster than the frequency changes [37]. The state trajectories may intersect the LS boundaries depending on the magnitude of the event and as well as the electrical distance to the fault location. According to the proposed scheme which is implemented based on both frequency and voltage deviations, and regarding to the fact that frequency is same across the entire network [4], the distances between the trajectories are due to difference in the voltages. The more drop of load bus voltage, the more relevant trajectory far from the origin and therefore, crossing the boundaries sooner than the other loads. The state trajectory of the load C crosses over the first and second elliptical boundaries, but the corresponding curve of the load B only exceeds the first boundary (Fig. 5.3). Although the state curves cut the boundaries and relays detect this event, the relays do not react in this situation, which is called undervoltage block level, since this region has been located in the left side of vertical dotted line in the Fig. 5.1 and discussed in details in the section 5.1.1.

After the G3 outage at 0.5 s and before the first LS step at 1.0 s (Tab.5.2), two different phenomenas with same origin are noticeable in Figs.5.5-5.6. First, the voltage drop just after the generator outage which instantaneously affect the active and reactive power of the loads [35, 36] and hence active power of the loads gradually decline due to the voltage dependency of the loads which discussed in details in section 5.1.3.3 as can be observed in Fig. 5.6. Second, due to the loads active power decrease, the voltages tend to recover toward nominal values to some extend. The new upward trend of the

voltages causes augmentation of the active power of the loads again. Although, the effect of the voltage deviation on the loads behavior alleviates the shortage of the active power, it can not be sufficient to balance the load-generation level, thus the power system still suffer from active power deficit and frequency continues to decline steadily (Fig. 5.4).

During the voltage recovery phenomena (Figs.5.3 and 5.5), the load C has the maximum voltage drop and by gradually decline of frequency meets the first checkpoint ($S1$) sooner than the other loads. As a result, the first step of load C is triggered at 1.0 s with 16.7% load shed (Tab.5.2). The first shedding step of the load C has a major influence on the state trajectories, voltage profile and active power of the loads and it returns the state variables back into the limited area called $S1$ boundary. The relevant voltage and active power jumps are noticeable. Since the aforementioned shed load is not enough to make a balance between load and generation, the frequency still drops but with a lower value of ROCOF in comparison to before the first LS step of the load C, thus the state trajectory of the other loads get gradually closer to the $S1$ boundary. The state curve of load B and A meets the first boundary $S1$ at 1.15 s and 1.17 s with 18.9% and 10.4% of shed load, respectively. The trigger sequence of relays are visible in Fig. 5.6. The next phase of the shedding steps associated with the second boundary has been demonstrated in Tab.5.2.

Finally, the frequency reaches the steady state in another operation point greater than the minimum value of the permissible range. In the steady state, the state variables revert to the normal elliptical boundary N as mentioned in Fig. 5.2 and Tab.5.1 . The maximum shed load of 23.7% is discarded in the load B (Fig. 5.6) which is one of closest load to the event location. The second place in term of magnitude of the shed load belongs to load C with 20.0% and the last place is associated with load A with minimum amount of shed load about 14.5% as indicated in the Tab.5.2. Supremacy of the proposed LS scheme is obvious in localizing the load curtailment in the vicinity of event location.

5.1.5 Summary

In order to localize the LS scheme close to the disturbance place, the voltage drop information is utilized to shed the loads with higher voltage decay first. Therefore, this approach deals with coordination of voltage and frequency information instead of independent methods. The proposed undervoltage load shedding plan is utilized as a complementary part of the conventional underfrequency load shedding plan. The existing voltage and frequency thresholds, which are used in under voltage and frequency load shedding schemes, respectively, are combined together to achieve their coordination under an integrated plan. The aforementioned thresholds are considered as the center points of an ellipse, since the deviations of voltage and frequency from their pre-disturbance value in pu resulting from a given event may not be same for both.

Therefore, the load load shedding is initiated from the vicinity of incident place and is radially propagated in the power system until the from toward the center of it.

5.2 Adaptive Frequency Thresholds Using Voltage Drop Data

Power systems consist of numerous equipments with nonlinear dynamics and may not be properly protected by constant and prespecified settings of Under Frequeny Load Shedding (UFLS) relays which are independent of the location and magnitude of the disturbance [35, 53]. Moreover, there is the risk of simultaneous operation of different relays distant from the event location due to having the same frequency set point settings which may worsen the situation. To the best knowledge of authors, there is no comprehensive and widely used method to set the UFLS relay settings [47].

Dropping the loads distant from the disturbance place, may cause transmission line over loading, worse voltage profiles and power factor decline [35, 78]. Contrariwise, the load relief close to the event point is strongly recommended [8,37,41]. The buses nearby the failure place often experience larger voltage reduction. The voltage is an available variable to measure locally in all load bus relays. Thus, voltage drop information may be employed as a proper criterion of proximity to the failure point in power system analysis [5,36,41,51]. As a result, the loads may be classified to shed based on their voltage decay, which means the loads with higher voltage drop are discarded first. According to the proposed criterion, the Load Shadding (LS) process is initiated from the vicinity of the event location and radially propagates in the power system, so that not only the frequency collapse is prevented in time, but also the frequency returns back into the normal range [8, 42].

According to [35, 36, 51], the voltage deviation of load buses may be a proper and effective criterion of proximity to the event location. In order to find the most appropriate locations for LS plan, the frequency set point of LS relays are almost instantly determined based on the voltage drop magnitude at their load bus. The present work benefits from locally measured frequency and voltage informations and hence implementation of proposed method is more affordable and simpler than the centralized LS methods which require fast and reliable communication systems [35].

5.2.1 The Role of Voltage Dynamics in Power System Stability

Nowadays, the growing concern about the incidents initiated by voltage root causes has located in the center of attention [87]. Besides, assigning a separate category of instability classification to the voltage instability shows the importance of voltage dynamical behavior in the power system stability area [4]. The significance of voltage profile was stressed from different aspect of views in many literatures which are briefly reviewed in this section [8, 44].

The shortage of active power is often accompanied by deficit in reactive power and the lack of active/reactive power is reflected in the voltage profile of the load buses [36]. Any LS scheme in which the dependency of the loads to the voltage variation is over-

looked may not be effective in practice.

According to [4], the voltage instability is a phenomena of a local nature and if it is not prevented in time by proper control actions, it may spread to neighbor areas and even to the entire power system. Since the frequency which is measured locally at load buses is a common factor across the whole network and does not contain useful information about the event location, the voltage instability and its geographical region may be detected only based on the voltage data.

In the decentralized control strategy which is the main effort of the present work, there is no communication link between relays involved with LS scheme. Therefore, the magnitude and location of the event are unavailable. Although, the aforementioned information are unknown and unaccessible in a decentralized LS scheme, the voltage deviation is linearly determined by them [77]. Hence, a more accurate and reliable measure of sensitivity to the scale and place of perturbation is the voltage deviation of load buses, i.e. a quantity that is locally available. The sensitivity of each individual load bus to a given incident may be reflected via their voltage deviation. It means that the load buses with more sensitivity to the disturbance, experience a larger voltage drop. Therefore, the load buses may be classified in term of their voltage drop which is proportional to their sensitivity.

Utilizing the voltage drop data in the centralized strategy of the LS program have been proposed by numerous literatures as an appropriate and efficient criterion for determining the location of disturbance [35, 36, 41, 51], but application of voltage decay has rarely been employed in the decentralized strategy, especially for on-line and dynamically determining the frequency set points of the LS relays.

5.2.2 Decentralized and Adaptive UFVLS Approach

5.2.2.1 Adaptive Frequency Thresholds Using Voltage Drop Data

In the decentralized LS there is no communication between LS relays and hence only local variables including voltage and frequency are involved in the scheme. In the existing relays, the instant values of voltage are measured to calculate the frequency and the *rms* value of voltage for under voltage blocking function. Therefore, all data required to be involved in the proposed approach are already available in the existing relays. No extra hardwares/equipments are needed and just updating their code programming is sufficient to implement the proposed method [39, 40, 43].

The feeders for load shedding are automatically selected based on the voltage deviation from their steady state value. Despite of classical relays, manual setting of frequency set points is no longer necessary. A dynamic frequency set point is calculated on line and assigned to the relay stages rather than a constant, static and prespecified frequency set points against widespread possible perturbations. The frequency set points of distinct relays are continuously updated using voltage decay data. The loads with larger voltage drop are relatively attributed higher frequency set points, which are

reached by dropping frequency earlier than the others during the events. Therefore, the relevant feeders are disconnected sooner. Depending on the relative voltage decay of load, the frequency set points of different load relays may be faraway, have some overlap or even exactly located on each other [71, 74].

The idea is formulated as below for a frequency relay with m stages. The voltage deviation (Δv) from the steady state value (v_{ss}) can be determined as below:

$$\Delta v = v_{ss} - v \tag{5.5}$$

Since the voltage spikes resulting from penetration of power electronic converters in to power system or produced by noise or measurement techniques may not be taken into account properly by power system analysis softwares, therefore in order to achieve a practical and efficient method, this kind of practical fluctuations seen in real power systems should be suppressed by an appropriate low pass filter to merely pass the real voltage dynamics [39, 40, 88].

Each relay has a base frequency set point (f_b^{th}), which relatively determines the frequency set point of given relay comparing to the others in the frequency range and is calculated as below:

$$f_b^{th} = f_H - \Delta f_b^{th} \tag{5.6}$$

where f_H is the trigger frequency of LS scheme. The base frequency set point offset (Δf_b^{th}) in (5.6) indicates the proximity of the base frequency set point (f_b^{th}) of the current relay to the trigger frequency of the LS scheme (f_H), and changes proportional to the voltage drop of corresponding load bus (Δv):

$$\Delta f_b^{th} = (f_H - f_L) \cdot (\Delta v_{\max} - \Delta v)/\Delta v_{\max} \tag{5.7}$$

where f_L the lower limit of permissible frequency range. The frequency set point of distinct stages are determined using base frequency set point (f_b^{th}) and local frequency set point offset (Δf_l^{th}):

$$f_i^{th} = f_b^{th} - (i-1) \cdot \Delta f_l^{th} \quad \forall i \in \mathbb{N}, 1 \leq i \leq m \tag{5.8}$$

According to (5.8), the successive stages of the relay have a same local frequency set point offset (Δf_l^{th}), which is also determined in term of voltage decay of the load bus (Δv):

$$\Delta f_l^{th} = (f_n - f_H) \cdot \Delta v/\Delta v_{\max} \tag{5.9}$$

The feeders of a given load bus may be prioritized in term of their importance by connecting them to the relay outputs with higher index of i, i.e. lower frequency set points [8, 74]. Therefore, they are considered as the last feeders to be interrupted in the corresponding load bus.

Allocating a smaller frequency set point to a given stage causes its delayed interruption, since frequency needs more time to reach this frequency set point. Changing

the frequency set points, implicitly changes the stage delays. Hence, there is a strong relationship between determinant parameters of the relay, i.e. frequency set point and the stage time delay, which confirms they are not completely independent variables [40].

5.2.2.2 The Time Delay Between Consecutive Stages

The time delay between successive triggered stages of relay is one of determinant factor, which affects the LS process [74]. The delays should be minimized to avoid delayed load shedding, which may not only cause longer stay of frequency out of safe range, but also may even allow the frequency to decline further and cross over the permissible frequency range of the LS scheme (f_L to f_H). Minimized time delay causes fast recovery of frequency to the continuous operating range in time [8, 39, 42, 71].

If the frequency is not recovered in time by available control actions, the plant protection relays are triggered, which causes fast disconnection of generation units, cascading events and even blackout [8, 74]. The power system will experience a much worse situation, which is more rigorous to manage due to the complex dynamics of power system.

In contrast, too short time delay between consecutive stages is not recommended, since serious transient dips in the frequency curve, which may happen in such a short time may not be properly ignored to consider the average frequency trend [8, 39, 83]. Besides, according to the relevant standards, after any triggered stage the time duration of 10 to 14 cycles regarding the relay and circuit breaker operating times are typically required to be respected as the minimum time delay [8, 40, 71]. This period is associated with the time gap between reaching the frequency to a given set point and when the load is exactly disconnected.

The time delays are not directly calculated by the proposed scheme, but depending on the Rate of Change of Frequency (ROCOF) and local frequency set point offset (Δf_l^{th}), they may vary from a few cycles to several seconds [8, 74]. The minimum time delay between consecutive stages regarding relay and circuit breaker operating times can be taken into account in the suggested method as follows:

$$\Delta t \geq N \cdot T = N/f_n \tag{5.10}$$

where T, N and f_n are the cycle time, number of cycles and nominal frequency of power system, respectively. The time between successive stages (Δt) can be approximated using measured and the local frequency set point offset (Δf_l^{th}) calculated in (5.9) as follows [8]:

$$\dot{f} \cong \Delta f_l^{th}/\Delta t \tag{5.11}$$

By calculating the term Δt from (5.11) and substituting in (5.10), the lower boundary of Δf_l^{th} is estimated:

$$\Delta f_l^{th} \geq N \cdot \dot{f}/f_n \tag{5.12}$$

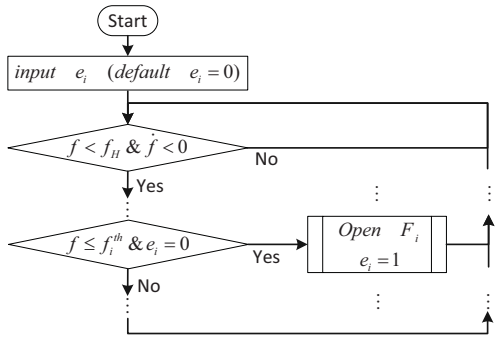

Fig. 5.7: The flowchart of the proposed LS scheme.

The quantity of Δf_l^{th} calculated in (5.9) should also satisfy the inequality expressed in (5.12) as below:

$$\Delta f_l^{th} = \max\left\{(f_n - f_H) \cdot \Delta v / \Delta v_{\max}, N \cdot \dot{f} / f_n\right\} \tag{5.13}$$

5.2.2.3 The Load Shedding Trigger Criterion

The flowchart of the suggested LS scheme is demonstrated in Fig. 5.7. In the steady state situation prior to the disturbance, all of feeders (F_i) are connected to the bus bar with the connection status bits, i.e. e_i equal to zero. In the first check point of the flowchart the sign of ROCOF is assessed, which should be negative ($\dot{f} < 0$) to pass through condition. More conditions are required to be met to trigger the LS scheme, since negative sign of ROCOF is possible even inside the normal range of frequency.

Since the ROCOF may sometimes be misleading, its supervision by another independent variable such as frequency is recommended to achieve a more reliable LS scheme [8, 40, 74]. Therefore, to supervise the ROCOF, in addition to the negative sign of ROCOF, the frequency should cross over f_H, as the second check point of flowchart. Reaching the frequency to f_H provides sufficient reaction time for available primary/secondary controls [8, 22, 70], as the LS scheme is the last and most expensive solution against frequency collapse [39, 44, 74].

The rest of checkpoints are relevant to the frequency set points of different stages of the relay, i.e. f_i^{th} calculated in section 5.2.2.1. Each feeder is interrupted when the frequency reaches its frequency set point with the status bit equal to zero ($e_i = 0$).

The number of considered set points is same as the number of existing stages in the relay (m) [40, 44, 71]. By default, the larger frequency set points (associated with lower index of i in (5.8)) are assigned to the feeders with less priority, unless the utility operators demand other choices for any particular reasons. Since the descending arrangement of frequency set points may be altered to obtain a special priority choice, during the

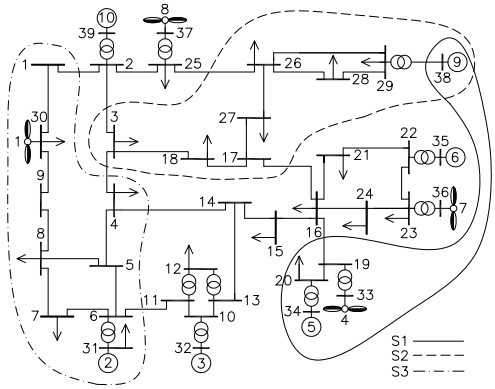

Fig. 5.8: The 39 bus IEEE test system.

Table 5.3: The Voltage & Frequency Dependency of Loads

Load type	Share (s)(%)	pv	pf	qv	qf
Light bulb (i)	10	1.6	0.0	0.0	0.1
Fluorescent bulb (c)	20	1.2	-1.0	3.0	-2.8
Asynchronous motor (p)	70	0.1	2.8	0.6	1.8

installation process, as can be seen in the flowchart, all of checkpoints regardless of their priority are regularly checked in any iteration. Howsoever, the smaller set points must be assigned to the feeders with higher priority of power supplying. In order to avoid disconnection of uninterruptible loads under any conditions, their may be exempted form contributing in the load shedding by setting their status bit equal to one, i.e. $e_i = 1$ via either external switches on or user interface panel mounted on the module. The new applied settings affect the flowchart, and therefore the LS plan during the initialization phase of registers of relay microprocessor, which takes place when the microprocessor is restarted.

5.2.3 Simulation Setup

The 39 bus IEEE standard test system indicated in Fig. 5.8 is chosen as case study to evaluate the efficiency of the suggested method in DIgSILENT PowerFactory 15.0 software [37,51,83]. The 4th order model is used for SMs. The IEEE standard governor GOV-IEESGO and automatic voltage regulator AVR-IEEEX1 are considered for SMs. The details of the system data can be accessed in [80].

The dependency of active and reactive power of loads to the voltage and frequency in term of different type of loads is defined in (5.14) and (5.15) [8]. Moreover, the relevant parameters and the Share (s) of different kind of loads such as type i, c and p in the load model is given in Table. 5.3 [4, 39, 74].

$$P = P_0 \cdot [s_i \cdot (v/v_0)^{e_i^{pv}} + s_c \cdot (v/v_0)^{e_c^{pv}} + s_p \cdot (v/v_0)^{e_p^{pv}}] \cdot [s_i \cdot (f/f_0)^{e_i^{pf}} + s_c \cdot (f/f_0)^{e_c^{pf}} + s_p \cdot (f/f_0)^{e_p^{pf}}] \quad (5.14)$$

$$Q = Q_0 \cdot [s_i \cdot (v/v_0)^{e_i^{qv}} + s_c \cdot (v/v_0)^{e_c^{qv}} + s_p \cdot (v/v_0)^{e_p^{qv}}] \cdot [s_i \cdot (f/f_0)^{e_i^{qf}} + s_c \cdot (f/f_0)^{e_c^{qf}} + s_p \cdot (f/f_0)^{e_p^{qf}}] \quad (5.15)$$

Despite of existing LS methods in which shedding a specific amount of estimated load is fulfilled, selection of proper feeders are addressed in the proposed method as it is done in practice. The loading rate of different feeders in pu in term of whole bus load is expressed in Table. 5.4. Since the simulation results of proposed method, i.e. Adaptive Under Frequency Voltage Load Shedding (AUFVLS) is compared to the conventional UFLS, the parameters of both methods are presented in Table. 5.5 [53].

5.2.4 Simulation Results and Discussion

Three different scenarios occurring in distinct areas of the power system including severe contingencies e.g. cascading events and islanding with different level of active/reactive power deficit are chosen as disturbance and the simulation results are compared with conventional UFLS. Recovery of power system variables, e.g. frequency and voltages to their continuous operating range in time is the aim of proposed method.

5.2.4.1 Scenario 1:

The disturbance in the first scenario is a set of cascading events including loss of generator G9 at 2 s followed by overloading and hence outage of transmission line 16-19 at 5 s (Fig. 5.8) as a serious contingency with 1970 MW load-generation mismatch (∼32% of system generation). Figs. 5.9-5.12 demonstrate 60 seconds of simulation results. All of variables including voltage and frequency are in the steady state inside of their continuous operation range prior the initiating event at 2 s.

An area including buses 19, 20, 33 and 34, generators G4 and G5 and the load 20 is separated from the rest of power system. Due to the surplus generation in the island, the frequency increases up to 62.5 Hz. Reduction of generation through relevant primary and maybe secondary control as a countermeasure of over frequency in the island (Fig. 5.9) to return back the frequency to the normal range is out of scope of the project and merely control of the rest of power system suffering from under frequency is the main objective of the suggested method.

Although the resultant voltage of both proposed AUFVLS and conventional UFLS schemes are acceptable and the UFLS even provides better voltage profiles, the UFLS is not successful in settling the post-disturbance frequency inside the permissible range above f_H. The UFLS method may trigger the plant protection relays leading to cascading events (outage of other SMs) in case of no or insufficient secondary control and maintaining the frequency for a while out of tolerable time period of under frequency protection relay of the SMs [8, 40, 74].

Another disadvantage of UFLS method is that it involves all of available loads (19

loads) in the LS plan, which is not practical and is not recommended by relevant literatures [37, 39, 71]. Distributing of shed load to all of loads yields less deviated voltages from their pre-disturbance. The AUFVLS method participates only 8 loads located inside the neighborhood of the event location, which are introduced in the legend of Figs. 5.10 and 5.12. The LS process indicated in Fig. 5.10 shows that the loads 16 and 24 are fully interrupted and the loads 25, 29, 21, 28, 23 and 15 are partially shed.

5.2.4.2 Scenario 2:

In the second scenario 4 cascading events including transmission lines 16-17, 25-26, 2-3 and 3-4 are successively tripped due to overloading and thermal limit condition at 2,

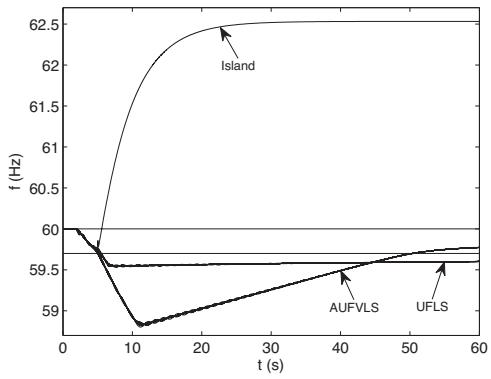

Fig. 5.9: Frequency

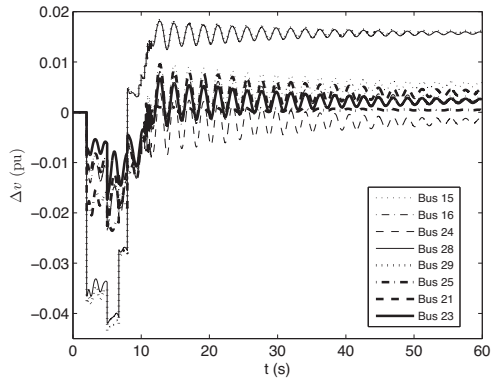

Fig. 5.11: Voltage deviation (AUFVLS)

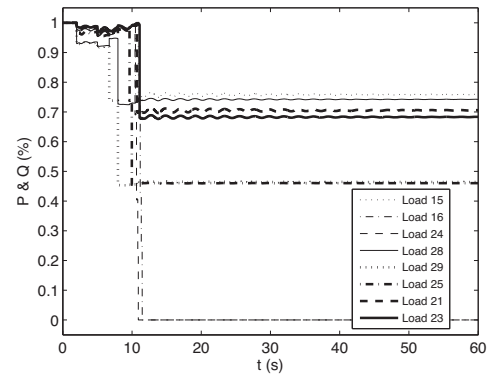

Fig. 5.10: Active power (AUFVLS)

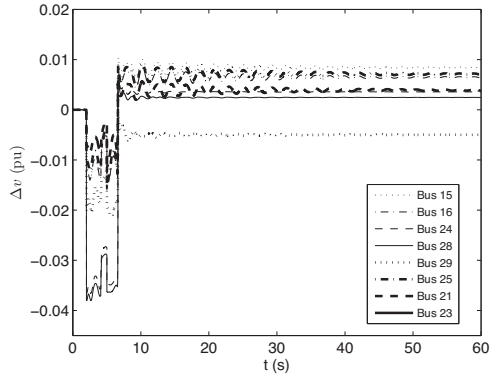

Fig. 5.12: Voltage deviation (UFLS)

4, 5 and 6 s, respectively (Fig. 5.8). A relatively big island including generator G9 and loads 29, 28, 26, 27, 18 and 3 is detached from the network with G9 as slack bus in the island. The active power imbalance in the island is about 564 MW (∼68% of remaining source), which is a severe contingency. The simulation results of scenario 2 for 60 seconds of time simulation are indicated in Figs. 5.13-5.16.

Despite of last scenario, in this case the rest of network suffers over frequency due to extra generation (Fig. 5.13) and the frequency of grid reaches the steady state at 61 Hz. The UFLS method reacts to the frequency decline sooner than AUFVLS method and even at a higher value of frequency, but it is unsuccessful in post-disturbance steady state value of frequency stabled beyond 63 Hz, whereas the AUFVLS method yields desired post-disturbance frequency and bus voltages. Comparison of voltage profile of AUFVLS

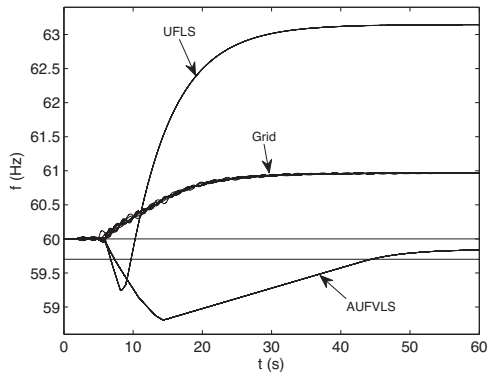

Fig. 5.13: Frequency

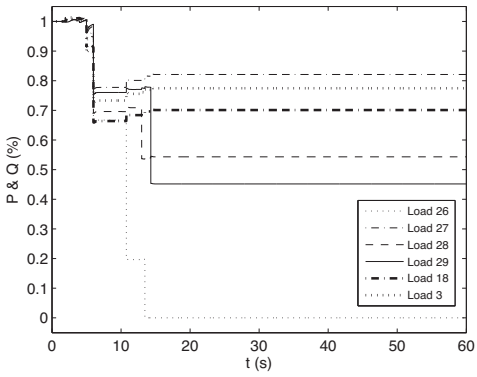

Fig. 5.14: Active power (AUFVLS)

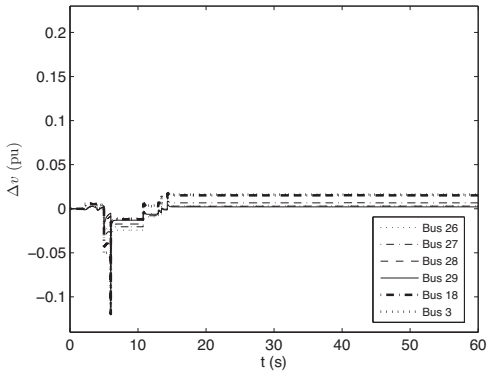

Fig. 5.15: Voltage deviation (AUFVLS)

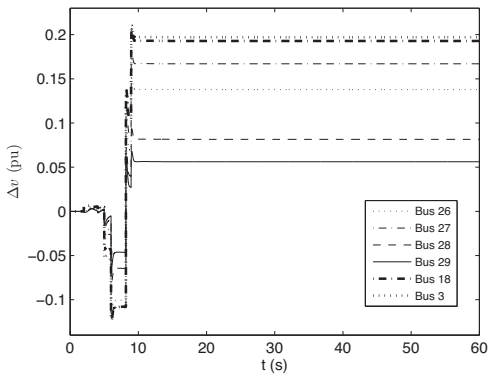

Fig. 5.16: Voltage deviation (UFLS)

and UFLS methods indicated in Figs. 5.15 and 5.16, respectively, reveals that proper LS locations are not always selected by UFLS method and shedding the loads with normal voltage is sometimes done. Improper distribution of shed load in UFLS method leads to over voltage beyond Δv_{max}, which may damage the electrical equipments.

Due to smallness of separated area, the set of loads, which contributing in the LS are almost same for both methods (loads 26, 27, 28, 29, 18 and 3), since all of loads are almost close to the disturbance places, i.e. tripped lines and are affected by the them. The method decisions are differ in feeder selection rather than load selection. In the UFLS method, regardless of event location, all of available loads are involved in the LS plan with the same number of feeders due to their equal and predefined frequency set points. In contrast, depending on the voltage drop magnitude, different number of feeders per load are interrupted in the AUFVLS method. In this scenario, 4 stages of load 26, 2 stages of loads 29 and 28 and one stage of loads 27, 18 and 3 are disconnected (Fig. 5.16).

5.2.4.3 Scenario 3:

The current scenario covers a part of power system far from the previous scenarios. Sudden outage of tie line 6-11 at 2 s followed by over loading and hence losing of line 4-14 at 4 s. In a same manner, the tine lines 1-39 and 3-4 are simultaneously lost at 5 s due to thermal limit protection. Finally, the region covering generator G1 and the loads 39, 4, 7 and 8 is separated at 5 s with generator G1 as the reference machine (slack bus) and active power deficit about 1347 MW ($\sim$135% of remained generation).

Figs. 5.17-5.20 show the simulation results of this scenario. According to the Fig. 5.17, similar to the last scenario, the UFLS method reacts to the frequency collapse faster than AUFVLS method an suffers form over load shedding by settling the frequency at slightly above 61.5 Hz, while the AUFVLS method provides a favorable post-disturbance frequency inside the permissible range.

Comparison of the voltage profiles of both UFLS and AUFVLS methods (Figs. 5.19 and 5.20) manifests that the AUFVLS method yields a relatively better post-disturbance voltages closer to the pre-disturbance values. AUFVLS method interrupts 4, 1 and 1 stages of the loads 4, 39 and 7, respectively (Fig. 5.18), while UFLS method disconnects the first two feeder of all loads (4, 7, 8 and 39). The total shed load in term of methods and scenarios is presented in Table. 5.6 to compare the performance of both AUFVLS with UFLS methods from total shed load aspect of view. Due to inadequate LS by UFLS method in scenario 1, the frequency is settled below the permissible range (Fig. 5.9) and in the scenarios 2 and 3, the UFLS method causes over LS (Figs. 5.13 and 5.17), which are not desired.

Comparison of frequency profile of distinct scenarios, shows that the AUFVLS method provides smooth frequency profile (advantage) due to assigning different frequency set points to distinct stages based on their voltage drop. In this way, rapid changes in the frequency resulting from simultaneous stage trigger of different loads due

to equal frequency set point is avoided as it happens in classical UFLS.

5.2.5 Summary

In the classical UFLS, the LS locations and the frequency set points of LS relays are already specified independent of event place, which may not be a comprehensive solution for widespread range of possible events. The voltage drop of loads is employed to calculate the frequency set points of LS relays. The loads closer to the event location experience higher voltage drop and need to be shed first. The higher frequency set points are atributed to the loads with larger voltage drop, which are often close to the disturbance place. The proposed method simultaneously benefits from UFLS and Under

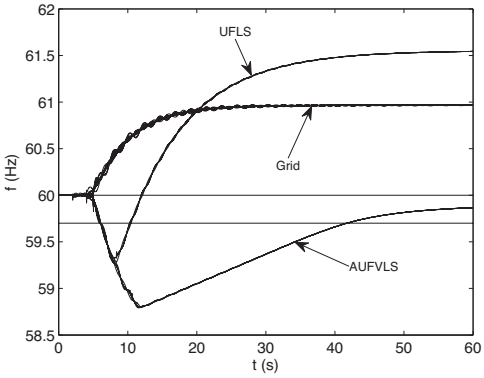

Fig. 5.17: Frequency

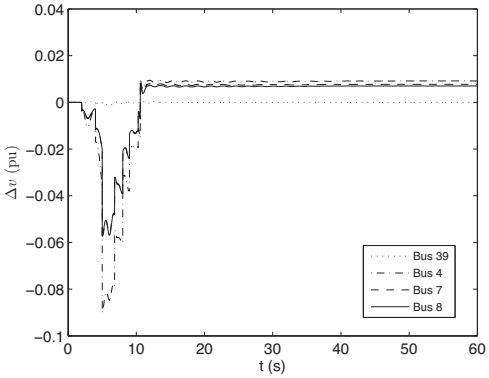

Fig. 5.19: Voltage deviation (AUFVLS)

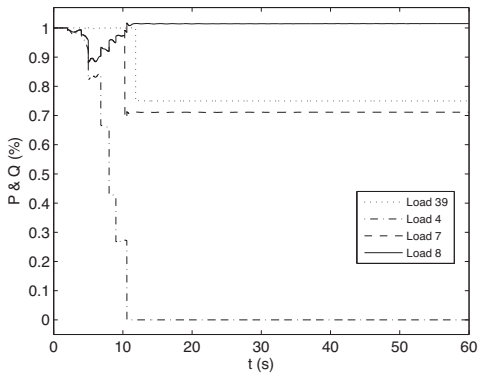

Fig. 5.18: Active power (AUFVLS)

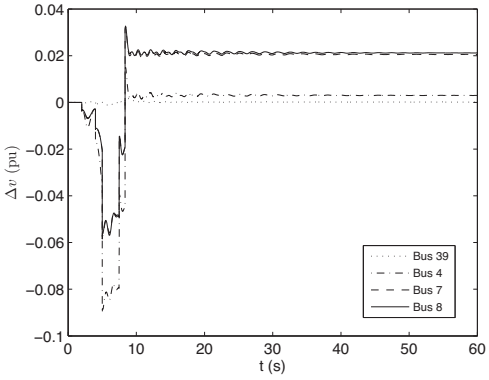

Fig. 5.20: Voltage deviation (UFLS)

Table 5.4: Feeder Loading %

Load	F1	F2	F3	F4	Load	F1	F2	F3	F4
3	25	30	20	25	**23**	32	16	28	24
4	25	29	18	28	**24**	30	29	19	22
7	30	29	19	22	**25**	25	29	18	28
8	18	30	23	29	**26**	30	23	27	20
12	28	18	30	24	**27**	19	29	18	34
15	25	29	18	28	**28**	28	18	30	24
16	25	32	17	26	**29**	22	33	25	20
18	32	18	23	27	**31**	19	29	18	34
20	18	30	23	29	**39**	25	28	27	20
21	30	23	27	20					

Table 5.5: The Simulation Parameters

Method	Parameters				
UFLS	f^{th} (Hz)	59.7	59.5	59.3	59.1
	T_d (cycle)	60	30	18	6
AUFVLS	f_n=60 Hz, f_L=57.9 Hz, f_H=59.7 Hz, m=4, N=12 and Δv_{max}=0.2 pu				

Table 5.6: The Total Shed Load (MW)

Method	Scenario 1	Scenario 2	Scenario 3
UFLS	1159	1036	1243
AUFVLS	1213	934	570

Voltage LS (UVLS) features which operate in the power system without coordination.

Chapter VI

Load Shedding with High Share of Wind Power

6.1 Active Power Deficit Estimation in the Presence of RESs

Conventional SMs temporarily utilize the kinetic energy stored in their rotor to compensate the frequency deviation following disturbance/s [14, 22, 70]. Most of RESs do not normally contribute to the system spinning reserve due to Maximum Power Point Tracking (MPPT). Furthermore, they do not even contribute to the Load-Frequency Control (LFC) (no inertial response) during load-generation mismatch, since their rotor inertia is decoupled from grid frequency by employed power electronic converters [9, 10, 15]. Therefore, the ROCOF quantity may not yield precise information about load-generation imbalance in the presence of RESs [8, 40, 74]. Besides, the voltage and frequency dependency of load's active and reactive power makes the active power shortage estimation more complicated, which means that it is crucial to predict how much load should be dropped at a specific time and/or location in the power system, due to variable composition of the loads [8, 39, 71].

6.1.1 Conventional Active Power Deficit Estimation

In the Center of Inertia (COI) method, the swing equation of multi machine system is replaced by an equivalent swing equation of a single machine with almost equal dynamical behavior to achieve an average frequency response [39, 51, 71]. The inertia time constant (H_{eq}) and apparent power (S_{eq}) of the resultant equivalent single machine are defined as below, respectively:

$$H_{eq} = \frac{\sum_{i=1}^{N} H_i \cdot S_i}{S_{eq}} \tag{6.1}$$

$$S_{eq} = \sum_{i=1}^{N} S_i \tag{6.2}$$

N is the number of generators. S_i and H_i are apparent power and inertia time constant of ith generator. The active power deficit is estimated by System Frequency Response (SFR) method [37, 39, 51]:

$$P_{def}(t) = \frac{2 \cdot H_{eq} \cdot S_{eq}}{f_n} \cdot \dot{f}(t) \tag{6.3}$$

where $P_{def}(t)$ is the active power deficit. f_n and $\dot{f}(t)$ are the nominal frequency of the power system and instantaneous value of ROCOF, respectively.

A major drawback of the SFR method is that it merely estimates the shortage of

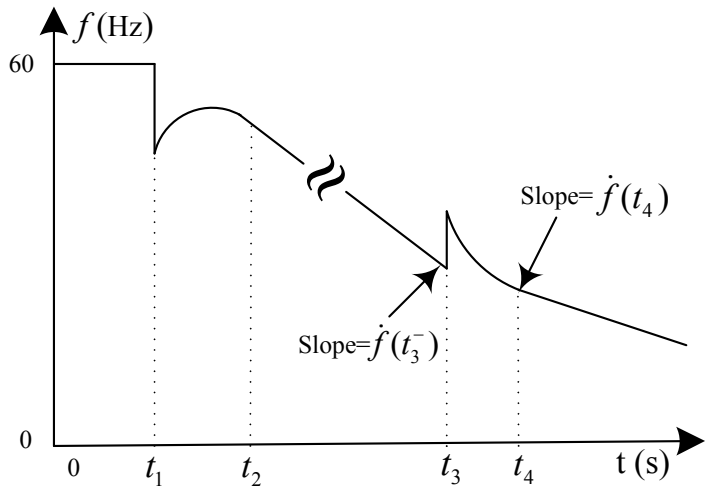

Fig. 6.1: Frequency behavior following an outage and LS

active power in order to achieve a load-generation balance, whereas the frequency may be settled at a value out of normal range [8, 74]. Moreover, in presence of RESs, the key parameters H_{eq} and S_{eq} are uncertain due to intermittent connectivity of RESs, which makes the active power deficit estimation inaccurate in practice.

6.1.2 Active Power Mismatch Estimation in Presence of RESs

The shed load resulting from disconnection of feeders are used to estimate the actual active power deficit regardless of type, penetration level and intermittent connectivity of RESs. It is assumed that proper selection of load feeders close to the event location is fulfilled based on the method, which discussed in section (5.2) details in using voltage drop data [39, 40].

Fig. 6.1 shows that the frequency declines following a frequency event at t_1. It is assumed that the LS plan is finally triggered due to unavailable, insufficient or unsuccessful primary and/or secondary control. t_2 is the first time in which the post-disturbance transients are almost suppressed and the frequency reaches a steady decline. It is also assumed that a potion of system load equal to P_{shed} is shed at t_3 by control center based on voltage drop criterion elaborated in [40, 41, 74]. The pre-shed active power deficit estimated by classical SFR method ($P_{def}(t_3^-)$) can be expressed as follows:

$$P_{def}(t_3^-) = \frac{2 \cdot H_{eq} \cdot S_{eq}}{f_n} \cdot \dot{f}(t_3^-) \tag{6.4}$$

where the post-shed frequency gradient equal $\dot{f}(t_4)$ at t_3 can be available via measurement. The terms $H_{eq} \cdot S_{eq}$ and $P_{def}(t_3^-)$ are still assumed to be unavailable. Since numerous combinational/cascading events may occur at the period between t_1 and the first load shedding stage at t_3, the last quantity of the active power deficit ($P_{def}(t_3^-)$) and its corresponding ROCOF ($\dot{f}(t_3^-)$) just before the load shedding time (t_3^-) are considered by the proposed scheme. After the feeder disconnection with the amount of P_{shed} at t_3, the conventional SFR method similarly yields the following new equation about new active power imbalance just after the transient period:

$$P_{def}(t_4) = P_{def}(t_3^-) + P_{shed} = \frac{2 \cdot H_{eq} \cdot S_{eq}}{f_n} \cdot \dot{f}(t_4) \tag{6.5}$$

The shed load at t_3 reduces the active power deficit and yields a lower value of ROCOF equal to $\dot{f}(t_4)$, which can also be available via measurement and is valid after the transient time at t_4. The load shedding does not affect the equations (6.1) and (6.2), hence the term $H_{eq} \cdot S_{eq}$ is remained unchanged.

By substituting the term $P_{def}(t_3^-)$ extracted from (6.4) into (6.5) and rearrangement of the resultant equation, the term $H_{eq} \cdot S_{eq}$ can be easily calculated as follows:

$$H_{eq} \cdot S_{eq} = \frac{f_n \cdot P_{shed}}{2 \cdot (\dot{f}(t_4) - \dot{f}(t_3^-))} \tag{6.6}$$

All of right hand variables and parameters in (6.6) are available. Finally, the $P_{def}(t_3^-)$ can be determined by substituting the term $H_{eq} \cdot S_{eq}$ calculated in (6.6) into (6.4) as below:

$$P_{def}(t_3^-) = \frac{\dot{f}(t_3^-)}{(\dot{f}(t_4) - \dot{f}(t_3^-))} \cdot P_{shed} \tag{6.7}$$

The post-shed active power deficit following the transient period at t_4, i.e. $P_{def}(t_4)$ can be determined by substituting (6.7) in the left hand equation of (6.5) as follows:

$$P_{def}(t_4) = \frac{\dot{f}(t_4)}{(\dot{f}(t_4) - \dot{f}(t_3^-))} \cdot P_{shed} \tag{6.8}$$

It means that before any load shedding stage, the actual amount of pre-shed and post-shed load-generation mismatch is unknown, but both of them can be calculated using above equations following each load curtailment.

6.1.3 Simulation Setup

The 39 bus IEEE standard test system depicted in Fig. 6.2 is selected as case study to investigate the active power estimation in presence of RESs [8,73]. The IEEE standard Automatic Voltage Regulator (AVR) IEEEX1 and governor IEESGO are employed for

all SMs.

Some of existing SMs are replaced with a Wind Farm (WF) of Permanent Magnet Synchronous Machine (PMSG) type of WT to achieve 51% integration of WP into the power system. The comprehensive model of PMSG WT type, which is specially developed for grid frequency regulation and transient stability studies is employed in this work [2, 89].

Fig. 6.3 indicates the control structure of PMSG WT. The active power set point of PMSG is tuned on MPPT, which is determined independent of frequency deviation [10, 22]. It means that the PMSG does not participate in the LFC scheme.

The wind speed may be assumed constant For the typical period of interest in dynamic simulations (tens of seconds) [22, 70, 79]. Thus the wind speed is considered constant at 14 m/s.

Since, the voltage and frequency dependency of load's active and reactive power significantly affects the actual active power deficit and moreover, the relevant equations in (6.9)-(6.10) recommended by IEEE standard [8, 40] are considered, in order to make the proposed scheme efficient in practice. The equation parameters and the Share (s) of different types of loads mentioned in [40] in the composite model of system loads are given in Table. 6.1.

$$P = P_0 \cdot [s_i \cdot (v/v_0)^{e_i^{pv}} + s_c \cdot (v/v_0)^{e_c^{pv}} + s_p \cdot (v/v_0)^{e_p^{pv}}] \cdot [s_i \cdot (f/f_0)^{e_i^{pf}} + s_c \cdot (f/f_0)^{e_c^{pf}} + s_p \cdot (f/f_0)^{e_p^{pf}}] \quad (6.9)$$

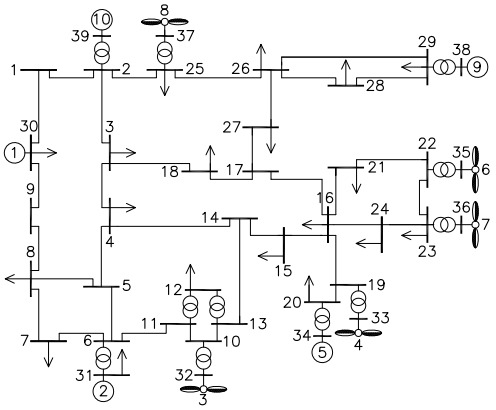

Fig. 6.2: The 39 bus IEEE test system

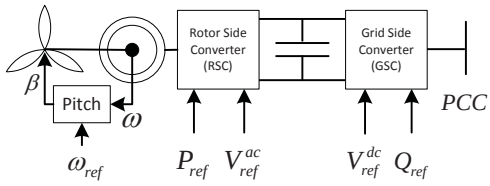

Fig. 6.3: Control structure of PMSG

$$Q = Q_0 \cdot [s_i \cdot (v/v_0)^{e_i^{qv}} + s_c \cdot (v/v_0)^{e_c^{qv}} + s_p \cdot (v/v_0)^{e_p^{qv}}] \cdot [s_i \cdot (f/f_0)^{e_i^{qf}} + s_c \cdot (f/f_0)^{e_c^{qf}} + s_p \cdot (f/f_0)^{e_p^{qf}}] \quad (6.10)$$

6.1.4 Simulation Results & Discussion

Numerical simulations are conducted in DIgSILENT PowerFactory 15.0 software. Outage of SM1 (Fig. 6.2) at 2 s with the capacity of 1012 MW almost equal to 16% of total system generation is considered as the disturbance. The profiles depicted in Figs. 6.4-6.7 indicate grid frequency, frequency gradient (ROCOF),the voltage and active power of loads, respectively. Before the contingency, the frequency is stable at 60 Hz in Fig. 6.4, which results zero value of ROCOF in Fig. 6.5. The voltage of buses are stabilized inside the normal range of 1 ± 0.05 pu in Fig. 6.6.

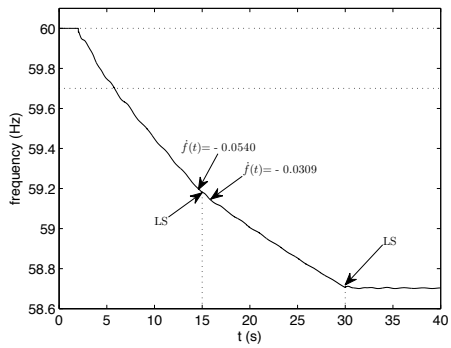

Fig. 6.4: The frequency

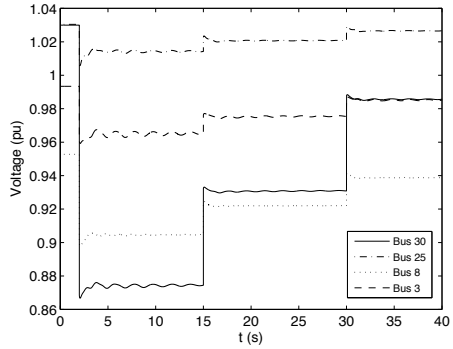

Fig. 6.6: The bus voltages

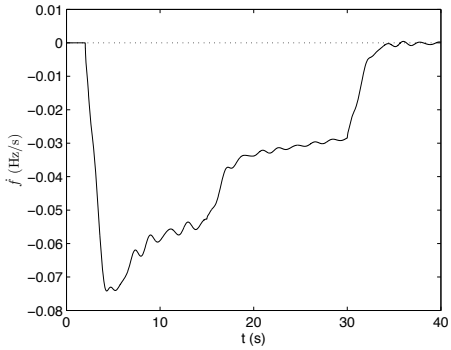

Fig. 6.5: The frequency gradient

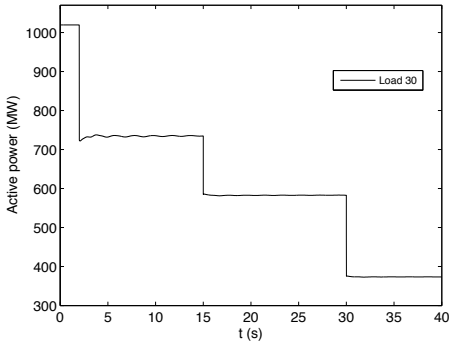

Fig. 6.7: Active power of loads

Following the event, the frequency declines with the rate of -0.0540 Hz/sec (Figs. 6.4 and 6.5) due to the shortage of active power. The abrupt reduction in bus voltages (Fig. 6.6), causes remarkable decrease of active power of loads, e.g. load 30 is decreases from 1025 MW to slightly above 700 MW in Fig. 6.7, which strongly reminds that if the voltage dependency of loads is overlooked in the estimation method, the resultant procedure may not be accurate in practice [35, 40].

The determinant parameters H_{eq} and S_{eq} of the SFR method may not be available properly, since the connectivity of RESs to the grid is unknown due to their stochastic and intermittent nature. Therefore, inaccurate value of the aforementioned parameters (H_{eq}=189 s and S_{eq}=7677 MVA) causes wrong estimation of active power deficit by SFR method equal to 2610 MW in this case considering the relevant ROCOF value given in Figs. 6.4 and 6.5.

Due to the dependency of load's active and reactive power, the active power deficit resulting from outage of SM1 with the rating power equal to 1012 MW is equal to 700 MW instead of its capacity, which demonstrates the complexity of power imbalance approximation. Taking into account of voltage dependency of the loads and the independency of the method on power system parameters i.e. H_{eq} and S_{eq}, which are often variable and/or unavailable are among the main advantages of the proposed method.

A feeder supplying 30% of load 30 is interrupted at 15 s (Fig. 6.7), which causes remarkably recovery of bus voltages (Fig. 6.6). Figs. 6.4 and 6.5 demonstrate reduction of ROCOF to a lower value equal to -0.0309. The SFR method estimates the active power deficit following the last shed load equal to 1493 MW, which is far from the actual value of 350 MW.

The proposed method yields more accurate pre and post-shed active power deficit equal to 701 and 401 MW, respectively. The estimation error regarding the actual power mismatch (350 MW) and its approximation (401 MW) at t=15 is due to the ROCOF fluctuations. since as can be seen in Fig. 6.5, the frequency gradient curve has some fluctuations around its average trend. It means that the last sampled value of ROCOF just before the load shedding may be any point between its peak to peak range. In order to improve the scheme by reducing the estimation error, the average value of ROCOF should be used by the method instead of its instantaneous value.

In order to assess the accuracy of the estimated post-shed active power deficit equal to 401 MW, a load portion equal to the approximated value is intentionally shed on load 30 at 30 s (Fig. 6.7). The frequency and its gradient are finally stabilized at almost 58.7 Hz and 0 Hz/s in Figs. 6.4 and 6.5, respectively, which confirms the precision of the proposed method and shows that the load and generation are now balanced.

6.1.5 Summary

The inertia of the power system is reduced in the presence of Renewable Energy Sources (RESs) due to their low or even no contribution in the inertial response as it is in-

Table 6.1: Chronological Order of Events and Resultant Active Power Deficit

	ΔP (MW)		
SFR Method	2610	1493	0
Proposed Method	701	401	0
Actual value	700	350	0
Time (s)	2	15	30
Occurrence	↑	↑	↑
Event	SM1 outage	first LS	second LS

herently provided in the Synchronous Machines (SMs). The total inertia of the grid becomes unknown or at least uncertain following loss of SMs during cascading events. Therefore, the active power deficit following the disturbance/s may not be properly estimated by existing conventional System Frequency Response (SFR) methods in which the total inertia of the power system is required to be available continuously. The dynamical behavior of power system is monitored during each load shedding stage to properly estimate the actual active power deficit following combinational and/or cascading event/s. The actual active power deficit is estimated using shed load amount, pre-shed and post-shed ROCOF, which are available in the centralized strategy of LS. Type, penetration level and intermittent connectivity of RESs do not challenge the accuracy of the proposed method and it is independent of grid inertia, type location and number of cascading events. Since the measured quantities of the ROCOF, employed in the proposed method are indirectly the result of voltage dependency of the loads, the type/composition of the system loads do not challenge the accuracy of the method.

6.2 Coordination of LS and Plant Protection in the Presence of RESs

Installation of RESs and/or replacement of existing conventional Synchronous Machines (SMs) by them causes significant issues in operation and control of power system [71,74]. The wind power impacts on the network have been rarely considered by existing LS methods and therefore, the available LS schemes proposed so far for conventional grids need to be revised in the presence of renewable energy sources.

Almost all of recent LS schemes ([90–92]) are based on System Frequency Response (SFR) to approximate the load generation imbalance using initial rate of frequency change following the event/s; a method that may no longer be valid in the presence of renewable energy sources or combinational/cascading disturbances including loss of SMs due to the unpredicted changes (unknown reduction) in the equivalent system inertia [71, 74, 83].

The decentralized control strategy can easily deal with the structural changes of the power system resulting from unpredicted connectivity of the renewable energy sources [10,66,70]. The distributed control strategy paves the way toward Plug-and-Play (PnP) operation enabling the addition and removal of system components in a modular fashion way by automatic and online tuning of hardware settings according to the current status of the power system with minimal human intervention. It makes sense especially in the large power systems, in which big data are required to be received, processed and transmitted in the control center besides the risk of communication failure, as well as recent Cyber Security issues and unscheduled dispatch of dispersed generations.

6.2.1 Estimation of Average Frequency Gradient

The frequency profile may have an oscillatory behavior following the event/s, that does not follow any particular pattern due to the complexity of power system dynamics [8,74]. Frequency oscillations may be relevant to either *local plant mode*, i.e. rotor angle oscillation of a single synchronous machine against the rest of generating units or *inter-area mode*, i.e. consonant swing of synchronous machines of an region against another area [5, 74].

The instantaneous frequency gradient, may be sometimes misleading due to the oscillatory behavior of the frequency associated with *local* and/or *interarea* oscillation modes [8] and as well as due to the recent high penetration of power electronic converters, which impose switching and rapid changes to the power system variables. [8,22,71]. In order to achieve more secure and reliable control decisions following under-frequency disturbances, supervision of frequency behavior by another variable, e.g. voltage, current, power flow direction, and/or frequency gradient is strongly recommended [8,39,40].

The overall trend of frequency in Fig. 6.8 and therefore its average rate of change may be approximately estimated by straight connection of inflection points of oscilla-

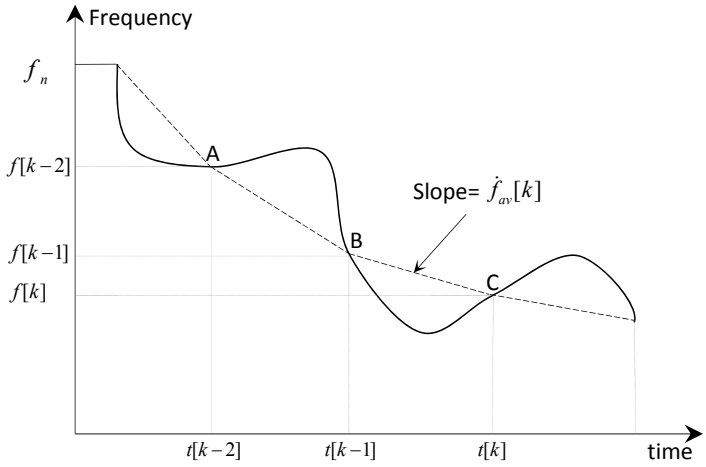

Fig. 6.8: Frequency trend estimation, solid: actual; dashed: estimated (line)

tions, i.e. the middle points A, B, C, etc. The sign of second derivative of the frequency changes at inflection points, i.e. the frequency curve switches from concave down to the concave up, or vice versa. The second derivative becomes zero at any inflection point, but not vice versa [74]. The successive inflection points of the frequency curve may be recognized as follows:

$$(t[k], f[k]) = (t, f(t))\,|_{-\overset{\ddot{f}(t)}{\longleftrightarrow}+} \tag{6.11}$$

where, t and $f(t)$ are the time and the instantaneous value of frequency, and $t[k]$ and $f[k]$ are their sampled values, respectively, when the second derivative of the frequency ($\ddot{f}(t)$) changes its sign. The average frequency gradient between each successive inflection points, e.g. between B and C may be linearly determined using the *backward difference* method as below:

$$\dot{f}_{av}[k] \cong \frac{(f[k] - f[k-1])}{(t[k] - t[k-1])} \tag{6.12}$$

The time difference between each two consecutive inflection points is equal to the half period of frequency oscillation:

$$\frac{T_{os}[k]}{2} \cong t[k] - t[k-1] \tag{6.13}$$

Therefore, the frequency of each oscillation may be determined from (6.13):

$$f_{os}[k] = \frac{1}{2 \cdot (t[k] - t[k-1])} \tag{6.14}$$

The oscillatory modes of frequency following the events are generally categorized by frequency range of their oscillations, and each of them has their own oscillatory frequency and damping. The *interarea mode* oscillations normally have lower oscillatory frequencies, i.e. 0.2 to 1 Hz comparing to *local mode* with the range of 1 to 2 Hz ($=f_{lm}^{max}$) [4]. According to (6.13) and regardless of the measurement technique, the calculation of average frequency gradient and frequency of oscillations may take a long time, especially when the frequency oscillates at a low rate [8, 74].

In order to maintain the oscillation modes (*local* or *interarea*) and to reject the sharp/undesired changes of variables resulting from power electronic converters and/or measurement process, and moreover to obtain a practically effective approach, a carefully tunned low pass filter with the time constant of τ_f is required to the measure frequency:

$$\tau_f = \frac{1}{2 \cdot \pi \cdot f_{os}^{max}} \tag{6.15}$$

where f_{os}^{max} is the maximum value of the highest possible oscillation frequency (f_{lm}^{max}), which is typically associated with *local mode* oscillations and the measured frequency ($f_{os}[k]$) before filtering in (6.14):

$$f_{os}^{max} = \max\left\{f_{os}[k], f_{lm}^{max}\right\} \tag{6.16}$$

While penetration of renewable energy sources has an unfavorable effect of increasing the peak-to-peak value of the rate of frequency change oscillations, it favorably augments the frequency of ROCOF oscillations, which indirectly causes faster calculation of average ROCOF and its oscillation frequency [8, 74].

6.2.2 Coordination of Load Shedding and Plant Protection Schemes

Frequency, its rate of change, voltage and time are important factors, which are often used without coordination in the protection procedures [8, 39, 40, 93]. Moreover, since a load feeder may sometimes become a source feeder by injecting active and/or reactive power to the grid, interruption of these feeders should be definitely avoided to keep them supporting the system stability. The load shedding is done by disconnecting load feeders, which are chosen based on simultaneous considering frequency and voltage informations. Moreover, the frequency gradient is directly employed in the scheme to make the scheme adaptive to the magnitude of event/s and low inertia grids, which possess a faster frequency drop due to high share of renewable energy sources [8, 21, 71, 83].

The proposed method consists of two sub procedures that are appropriately coordinated with plant protection plan under a united/integrated scheme. The first sub procedure is a frequency based plan, which adjusts the frequency set points of the distinct relays online using voltage drop data at load buses to block the frequency fall from further decline [40, 71]. The second sub procedure is a time based plan and operates as a backup/complementary protection procedure by tunning the relay time delays according

to the voltage drop information in order to prevent the frequency from stalling and/or staying out of normal range for a long time out of tolerable time of plant protection relay, which may activate the plant protection relays [74].

6.2.2.1 Frequency Collapse Barrier Scheme

This sub plan dynamically adjusts the frequency set points of the load shedding relays based on the voltage drop magnitude measured locally at the load bus. The relays with larger voltage decline at their bus bar are relatively assigned higher frequency set points. Depending on the voltage decay, the frequency threshold curve of different relays may be far, close (Fig. 6.9), slightly overlapped (Fig. 6.10) or even exactly same. The voltage deviation ($\Delta v_i(t)$) from the steady state value (v_i^{ss}) following the event/s is determined as below:

$$\Delta v_i(t) = v_i^{ss} - v_i(t) \tag{6.17}$$

Despite of short circuit faults, which often have post-disturbances close to zero, the cascading events leading to islanding typically have a post-disturbance voltage close to normal range. Hence, in order to focus more on the voltages close to normal range, the logarithmic mathematical function of voltage is involved with the scheme instead of its normal value. In order to take into account of the post-disturbance voltages,

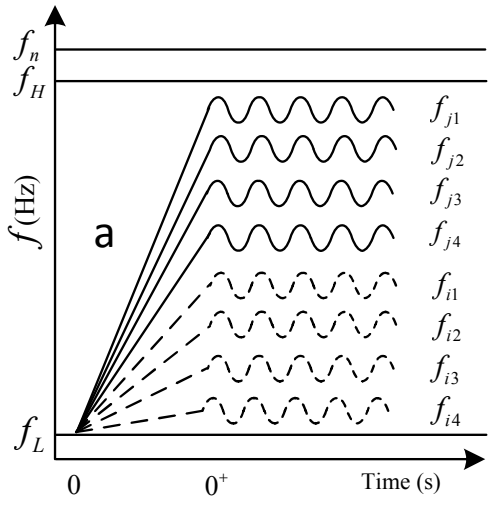

Fig. 6.9: different voltage drops (no overlap)

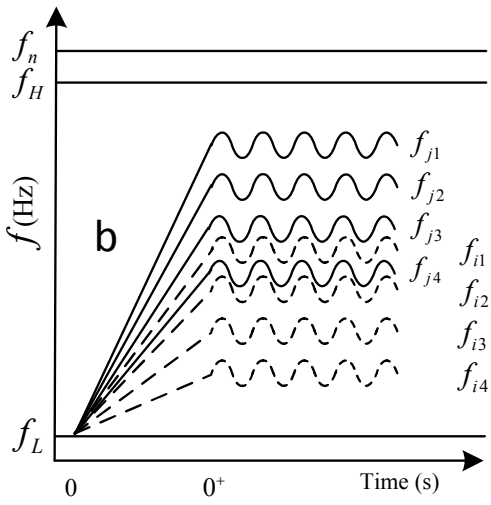

Fig. 6.10: close voltage drops (some overlap)

Fig. 6.11: Frequency threshold deployment of two LS relays

which may be sometimes greater than their steady state value due to already triggered load shedding stage/s ($-0.1 \leq \Delta v_i(t) \leq 1$), the voltage offset v^{of}=0.1 pu (the maximum permissible voltage magnitude above the nominal value) is applied to consider the above full range of possible voltage drop:

$$v^{of} - 0.1 \leq \Delta v_i(t) + v^{of} \leq 1 + v^{of} \tag{6.18}$$

Voltage deviations lower than 0.1%=10^{-p} pu (p=3) may be overlooked without challenging the method accuracy to avoid zero or negative values applied to the logarithm function. The resultant voltage range is expressed as below:

$$\Delta v_i^{log}(t) = 1 + \frac{log(\Delta v_i(t) + v^{of})}{p} \tag{6.19}$$

According to [40, 71, 93], all of the frequency set points should fall between f_H=59.5 Hz to f_l=58.4 Hz. To this aim, the frequency set point of the first relay stage i is determined as below:

$$f_{i1}(t) = f_L(t) + (f_H - f_L(t)) \cdot \Delta v_i^{log}(t) \tag{6.20}$$

According to [5, 74] both frequency collapse and its time duration are determinant in activating the plant protection scheme. In order to coordinate the proposed scheme with the plant protection plan, the lower boundary of frequency ($f_L(t)$) is limited according to [74, 93] in order to make sure that the frequency does not stay below f_h for a time period longer than T_h:

$$f_L(t) = \begin{cases} f_L = 58.0 & t \leq T_L = 2 \\ m \cdot \log(t) + b & T_L \leq t \leq T_h \\ f_h = 59.3 & t \geq T_h = 60 \end{cases} \tag{6.21}$$

where

$$m = \frac{f_h - f_L}{\log(T_h/T_L)} \quad , \quad b = f_h - m \cdot \log(T_h) \tag{6.22}$$

The load shedding scheme is triggered when the frequency declines below f_H, and therefore the corresponding time is selected as the origin of the time axis:

$$t = 0|_{f(t)=f_H \& \dot{f}(t)<0} \tag{6.23}$$

The frequency set point of stage j ($1 \leq j \leq$m=4) of relay i is determined as below:

$$f_{ij}(t) = f_{i1}(t) - (j-1) \cdot \Delta f_i(t) \tag{6.24}$$

where $\Delta f_i(t)$ is the frequency offset between each consecutive frequency set points of relay i and is calculated as below [40]:

$$\Delta f_i(t) = N^{min} \cdot \frac{\left|\dot{f}(t)\right|}{f_n} \tag{6.25}$$

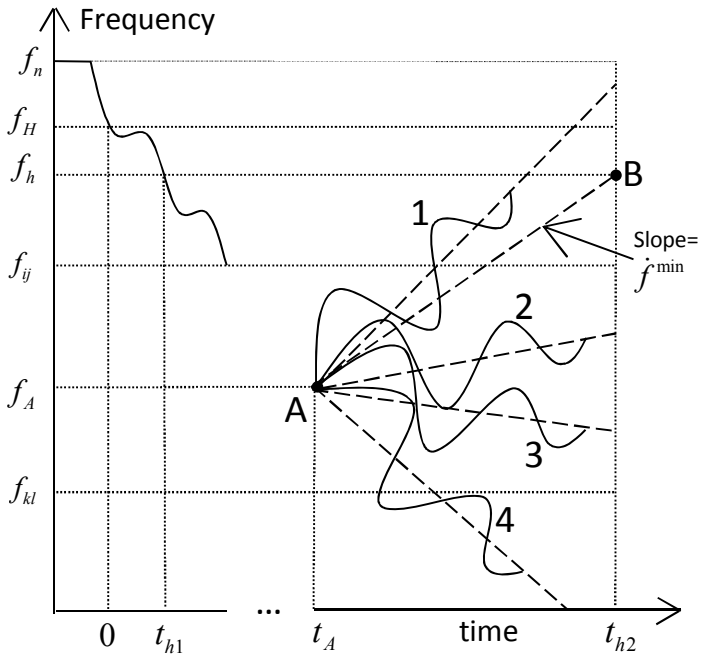

Fig. 6.12: Different possible trends of frequency following load shedding at A, 1: in time recovery; 2 and 3: frequency stalling; 4: able to reach lower stages

The f_n indicates the nominal frequency of grid equal to 60 Hz and N^{min} determines the minimum number of cycles (N) to be respected between each two consecutive frequency set points regarding relay and circuit breaker operation time, in which under any circumstances, should not be less than 6 cycles [8, 40, 71, 93]. A number of cycles in the range of $10 \leq N \leq 14$ is typically recommended by relevant IEEE standards [8].

The references [74, 93] clearly specifies the upper limit of $\Delta f_i(t)$ (Δf_i^{max}=0.5 Hz). Moreover, in order to respect the minimum tunning resolution of $\Delta f_i(t)$ proposed in the available frequency relays, e.g. ABB, SPAF 340 C3, the lower limit of $\Delta f_i(t)$ should be bounded to Δf_i^{app}=0.02 Hz:

$$\Delta f_i^{app} \leq \Delta f_i(t) \leq \Delta f_i^{max} \tag{6.26}$$

6.2.2.2 Frequency Stall Detection Scheme

Fig. 6.12 shows different possible scenarios of frequency following a load shedding at point A. t_{h1} and t_{h2} indicate the time, in which the frequency crosses over the value f_h during the drop and recovery conditions, respectively. According to the Under-frequency

Performance Characteristic mentioned in (6.21) and (6.22), the frequency should not stay below f_h=59.3 Hz for more than T_h=60 s to avoid excitation of plant protection relays [71, 74, 93]:

$$t_{h2} - t_{h1} \leq T_h \tag{6.27}$$

Following the load shedding at point A in Fig. 6.12, the frequency may reach the normal range above f_h in time (scenario 1), in which the anti stalling scheme is not triggered. In scenario 4, the frequency keeps on further drop toward a lower frequency set point ($f_{kl}(t)$) due to insufficient load shedding at point A.

In scenarios 2 and 3, the frequency cannot reach neither f_H nor the lower set point f_{kl} in time (before $T_h + t_{h1}$), resulting in the frequency stuck between two successive stages ($f_{ij}(t)$ and $f_{kl}(t)$) for a time period longer than plant protection time setting. The anti stalling procedure is to be used for scenarios 2 and 3 and even scenario 4 if the frequency collapse barrier scheme fails in control of frequency drop in time.

The frequency trend at inflection point A with the position (t_A, f_A) and its estimated average rate change $\dot{f}_A$ determined in (6.11) and (6.12), respectively, may be locally linearized as below:

$$f_{av}^{est}(t) = \dot{f}_A \cdot (t - t_A) + f_A \tag{6.28}$$

The anti stalling scheme is deactivated if both underneath equations associated with the frequency and time margins are simultaneously met:

$$t = t_{h1} + T_h \quad \Rightarrow \quad f_{av}^{est}(t) \geq f_h \tag{6.29}$$

$$f_{av}^{est}(t) = f_h \quad \Rightarrow \quad t = t_{h2} \leq t_{h1} + T_h \tag{6.30}$$

Otherwise, the anti stalling plan is triggered or remained activated until either proper recovery of the frequency ($\dot{f}^{min}$) or the minimum frequency quantity of f_H is detected in time.

6.2.2.3 Frequency Anti Stalling Scheme

While the frequency is stuck between two consecutive set points and the rest of lower set points are no longer triggered in time, the anti stalling scheme may recover the frequency by disconnecting extra feeders via automatic tunning of the stage time delays of the load shedding relay based on the voltage drop information.

In order to coordinate the anti stalling procedure as a complementary protection plan with the frequency collapse barrier scheme as the principle procedure, the anti staling plan is intentionally activated with $T_d^{min} = T_h/4$ time delay following the frequency collapse barrier scheme. Moreover, since the inertia of the power system may be reduced due to the eventually lose of synchronous machine/s, half of permissible time span ($T_d^{max} = T_h/2$) should be assigned to the recovery process to bring the frequency back

above f_H. Hence, the arrangement of the time delays, e.g. stage j of relay i ($T_{ij}(t)$) should fall into the following region:

$$T_d^{min} \leq T_{ij}(t) \leq T_d^{max} \tag{6.31}$$

The first stage time delay is calculated using the logarithmic function of voltage decay introduced in section 6.2.2.1 so that less time delay is allocated to the loads with higher voltage drop determined in (6.19):

$$T_{i1}(t) = T_d^{max} + (T_d^{min} - T_d^{max}) \cdot \Delta v_i^{log}(t) \tag{6.32}$$

The time delay of stage j ($1 \leq j \leq$m=4) is calculated as below:

$$T_{ij}(t) = T_{i1}(t) + (j-1) \cdot \Delta T_i(t) \tag{6.33}$$

where $\Delta T_i(t)$ is the time delay offset between successive stages, and as discussed in section 6.2.2.1, should be minimized to obtain a fast frequency recovery procedure:

$$\Delta T_i(t) = N \cdot T_n = \frac{N}{f_n} \tag{6.34}$$

The lower boundary of time delay is determined considering relay and circuit breaker operation time (T_{R+CB}), in which its number of cycles should be at least N^{min} cycles [8, 74, 93]:

$$T_{R+CB} = N^{min} \cdot T_n \leq \Delta T_i(t) \tag{6.35}$$

6.2.2.4 Considering the Power Flow Direction of Feeders

The design of conventional power systems are fulfilled based on single direction power flow from a central power plants toward load centers, rather than bidirectional power flow provided by installation of dispersed generation sources on load feeders. Nowadays, the load feeders may contribute in the frequency/voltage regulation, something that is rarely considered by existing load shedding methods.

The grid code Low Voltage Ride Through (LVRT) requires that optimal performance of renewable energy sources, i.e. Maximum Power Point Tracking (MPPT) or Load-Frequency Control (LFC), should be temporarily disabled during the disturbances by reducing the active power set point and assigning th released capacity to reactive power compensation/voltage regulation [2]. The required active power can be provided globally, whereas the reactive power has to be provided locally, since the reactive power can not be transmitted to the long distances. It means that interruption of feeders, which inject reactive power to the grid should be avoided, even if they consume active power.

Table. 6.2 shows all possible scenarios of a typical feeder in term of active/reactive power consumption/production. Disconnection of a consumer feeder (Q(t)>0, P(t)>0)

(scenario 1), generally improves both frequency and voltage profiles, and hence makes sense. Interruption of a producer feeder, whether P(t) or Q(t) (scenarios 2, 3 and 4), may deteriorate the situation by further decrease of frequency and/or voltage.

6.2.2.5 The Flowchart of the Proposed Scheme

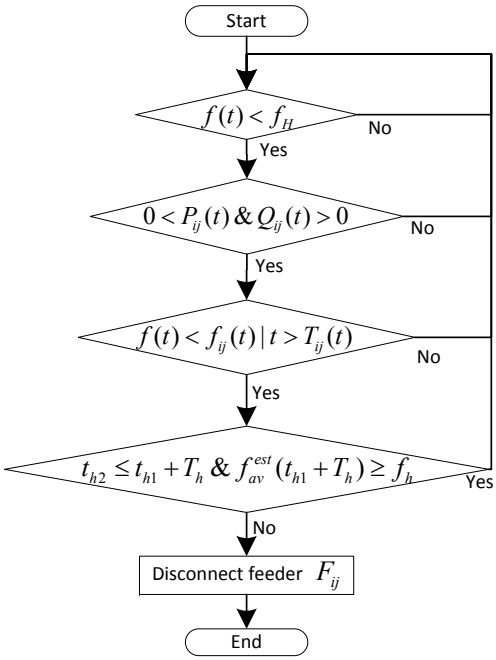

Fig. 6.13: The flowchart

Table 6.2: Feeder Disconnect Decision

Trip	Q(t)>0	Q(t)<0
P(t)>0	1: ✓	3: ×
P(t)<0	2: ×	4: ×

✓: Trip
×: Intact
>0: Consume
<0: Produce

Fig. 6.13 shows the flowchart of the proposed method including coordination of different sub schemes under an integrated plan. In the first checkpoint, crossing the frequency down over f_H is examined. Power flow direction of feeders, is checked in the second checkpoint as elaborated in section 6.2.2.4. The frequency set points and stage time delays are checked in the third checkpoint as explained in sections 6.2.2.1 and 6.2.2.3, respectively, which disconnects the relevant feeder (F_{ij}), unless the minimum recovery trend of the frequency approximated in (6.29) and (6.30) is recognized in the last checkpoint to prevent over load shedding.

6.2.3 Simulation Setup

The efficiency of the proposed scheme is validated in DIgSILENT PowerFactory 15.1 software. The 39 bus IEEE standard test system shown in Fig. 6.14 is chosen as case study [37,40,71]. The 4th order mathematical model of SM, the IEEE standard governor IEESGO and Automatic Voltage Regulator (AVR) IEEEX1 are considered for all SMs. The dependency of load's active and reactive power to the voltage and frequency and the contribution share of different type of loads including light bulb (10%), fluorescent bulb (20%) and asynchronous motor (70%) are defined according to [8, 40, 74].

The results are compared to the classical Under Frequency LS (UFLS) method in term of steady state value of frequency, the total amount of shed load, the number of loads and feeders involved with the LS scheme and the voltage deviation of the load buses from their predisturbance values. The parameters of both classical UFLS [40, 74] and the proposed scheme are available in Table. 6.5 of Appendix.

The relatively high share of wind power around 44% is integrated into the grid by replacing some of existing SMs by VSWTs as can be seen in Fig. 6.14. A comprehensive and standard model of Permanent Magnet Synchronous Machine (PMSG) type of VSWT including two mass shaft dynamic model, pitch control and voltage regulation by reactive power support is employed [2, 22, 70].

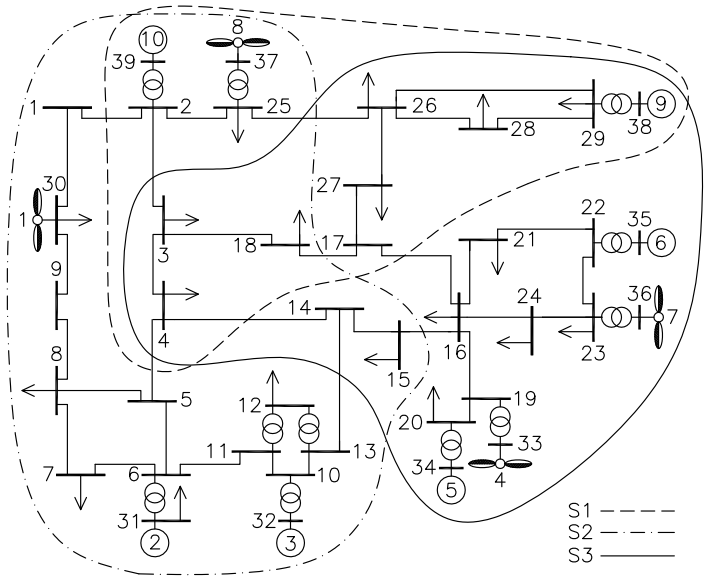

Fig. 6.14: The islanding scenarios defined in 39 bus IEEE standard test system

6.2.4 Simulation Results

Three scenarios depicted in Fig. 6.14 covering different areas of the 39 bus test system including cascading events leading to islanding with different level of load-generation imbalance (ΔP), Wind Power Penetration (WPP) share and ROCOF quantity are chosen as the disturbances.

6.2.4.1 Scenario 1:

In the first scenario, outage of transmission line 1-2 as an initiating event at 2 s causes overloading and hence cascaded outage of transmission lines 4-5 at 3 s, 4-14 at 4 s and 16-17 at 5 s, which lead to separation of almost a large part of power system from the rest of network called S1 and indicated by dashed line in Fig. 6.14. Figs. 6.15,6.16 and 6.17 show the simulation results throughout 60 seconds. Fig. 6.15 shows that the conventional UFLS leads to over load shedding and yields the frequency equal to 60.2 Hz, whereas the proposed Automatic Under Frequency and Voltage LS (AUFVLS) approach provides favorable post-disturbance frequency slightly less than 60 Hz.

The voltage profile of AUFVLS and UFLS methods are plotted in Figs. 6.16 and 6.17, respectively, but due to the large number of voltage profiles and limited number of line plot styles in each figure, they are intentionally plotted in two different figures located in same column with vertical axis range. The AUFVLS method results better voltage profiles comparing to UFLS technique by less deviation from their steady state value prior to the disturbance.

The AUFVLS technique totally sheds 507 MW of load by interrupting 6 feeders of 5 involved loads, whereas the conventional UFLS method curtailes 526 MW of load by disconnecting 8 feeders of all available 8 loads, which means the AUFVLS technique acts as an optimal LS scheme by shedding less loads and feeders, and as a localized LS scheme which concentrates on the faulty region, where the event occurs.

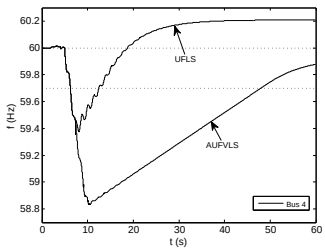

Fig. 6.15: Frequency

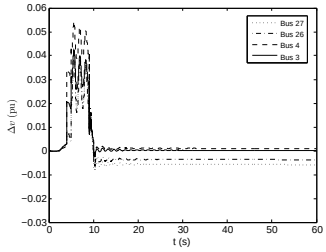

Fig. 6.16: Voltage deviation (AUFVLS)

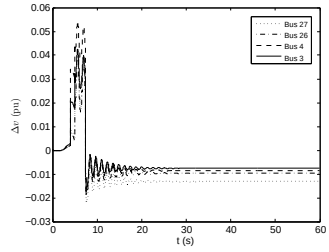

Fig. 6.17: Voltage deviation (UFLS)

6.2.4.2 Scenario 2:

The second scenario (S2) is indicated by dash-dot line in Fig. 6.14, which occurs in a different region of the power system with some overlap with the first scenario. Outage of G3, transmission lines 15-16, 17-18 and 25-26 at 2 s, 3 s, 4 s and 5 s, respectively, makes an island with the active power deficit equal to 1024 MW (30% of remaining generation) and higher rate of frequency change of -0.62 Hz/s. Replacement of G1 and G8 with Permanent Magnet Synchronous Machine (PMSG) augments the wind power penetration into the grid up to 43% of total generation.

Fig. 6.18 indicates that the power system is prone to frequency instability sooner than the previous scenario using classical UFLS method, whereas the AUFVLS technique stables the post-disturbance frequency inside the desired region slightly less than the nominal frequency (f_n=60 Hz).

The classical UFLS technique provides higher post-disturbance voltages due to the over load shedding and improper location of load shedding (Fig. 6.20), whereas the post-disturbance voltage of AUFVLS method demonstrated in Fig. 6.19 are favorable. The total shed load, number of involved feeders and loads in AUFVLS and UFLS methods are 1167 MW, 18 feeder, 9 loads and 1625 MW, 21 feeder and 10 loads, respectively. Despite of classical UFLS method, the shed load in the AUFVLS scheme is not uniformly distributed across the island, since the feeder selection is done based on voltage drop measure, which explicitly indicates the proximity of the loads to the event location [39, 40, 71, 90].

6.2.4.3 Scenario 3:

The islanding in scenario S3 indicated by solid line in Fig. 6.14 is initiated by loss of transmission line 13-14 at 2 s followed by cascading events such as outage of lines 4-5, 2-3 and 25-26 at 3 s, 4 s and 5 s, respectively. The wind power share equal to 38% together with 741 MW load-generation imbalance (19%) in term of total available supply

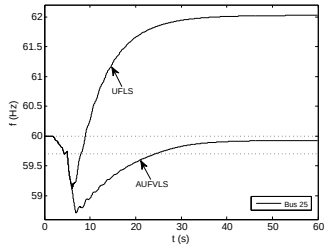

Fig. 6.18: S2: The island frequency

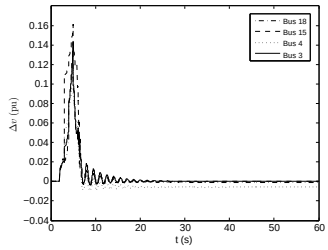

Fig. 6.19: S2: The voltage deviation (AUFVLS)

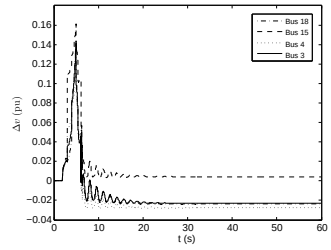

Fig. 6.20: S2: The voltage deviation (UFLS)

in the island results in a frequency downfall with the rate of -0.18 Hz/s.

By comparing the frequency and voltage profiles of both UFLS and AUFVLS methods plotted in Figs. 6.21, 6.22 and 6.23, acceptable performance of proposed method (AUFVLS) is explicitly revealed. Only 6 of 10 loads installed in the area S3 in Fig. 6.14 participate in the LS when the AUFVLS method is applied. The loads 3 and 18 are completely curtailed and the loads 4, 16 and 26 are partially discarded, which confirms the event location orientation of the AUFVLS scheme.

In the scenarios 1 and 2, the frequency collapse barrier scheme discussed in section 6.2.2.1 is merely enough to bring the frequency back to the permissible range in time, and hence the frequency anti stalling scheme elaborated in 6.2.2.3 is not activated. In scenario 3, as it is observable in Fig. 6.21, the frequency stall detection scheme explained in 6.2.2.2 diagnoses that despite of oscillations and minor incremental trend in the frequency between time 15 s and 27 s, its average trend may not reach the safe boundary in time same as the scenario 2 in Fig. 6.12. As it can be seen in Figs. 6.21 and 6.22, the anti stalling scheme interrupts one more feeder at 27 s to recover the frequency in time.

6.2.4.4 Comparison of Different Scenarios and Discussion

By comparing the frequency and voltage curves of different scenarios, some points are noteworthy while the wind power penetration is augmented in the power system: First, the frequency relatively falls faster (larger ROCOF values) due to lower inertia of resultant power system [83], which necessitates faster relevant control actions (e.g. less

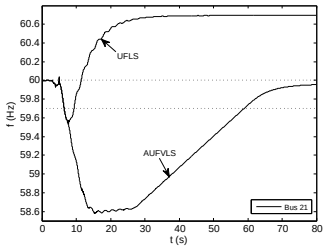

Fig. 6.21: S3: The island frequency

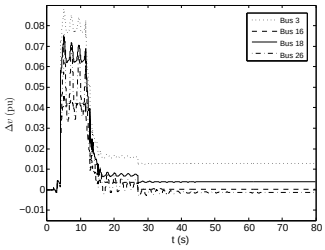

Fig. 6.22: S3: The voltage deviation (AUFVLS)

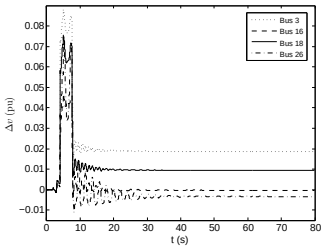

Fig. 6.23: S3: The voltage deviation (UFLS)

Table 6.3: The Comparison of Different Scenarios

Scenario	ΔP MW (%)	WPP (%)	ROCOF (Hz/s)
S1	454 (22)	33	-0.25
S2	1024 (30)	43	-0.62
S3	741 (19)	38	-0.18

stage time delays) [71]. Second, the period of frequency oscillations despite of their peak to peak value is reduced [8, 74]. Third, the flickers/spikes/plunges are relatively become prevalent in both frequency and voltage curves, which may improperly excite the protection relays, e.g. ROCOF relays [8, 22, 72]. In the SMs, the frequency/voltage variables are the result of mechanical rotation of rotor, which may freely deviate from their overall trend. Furthermore, the mechanical dynamics essentially have a smooth nature due to their inherent inertia, which causes prevention of sharp changes in frequency and voltage profiles, whereas the VSWTs are well-known as harmonic producers in the frequency and voltage profiles due to the employed power electronic converters, since converters are much faster than rotor mechanical motion and governor dynamics of SMs and may cause sharp variation of aforementioned variables [74].

In order to make the comparison of distinct scenarios easier, three determinant variables, i.e. the active power deficit (ΔP), Wind Power Penetration (WPP) share and initial value of ROCOF following the islanding have been collected in the Table. 6.3. The ROCOF has a direct relationship with both ΔP and WPP. Moreover, the performance of distinct UFLS and AUFVLS methods in different scenarios in term of total shed load, the number of involved loads and feeders is summarized in Table. 6.4. Table. 6.4 demonstrates that the continuous operation condition of the island following the severe cascading events is achieved by less shed load, involved loads and feeders in AUFVLS scheme in comparison to the classical UFLS method.

Comparing the performance of the AUFVLS and UFLS methods discloses that although the UFLS method reacts to the frequency collapse sooner and faster than the AUFVLS method and causes less stay of the power system states (variables) in the stressed operation condition far from the safe area, it suffers from over load shedding in all of scenarios, and hence fails in settling the frequency inside the acceptable region [40, 71]. In the UFLS method, the equality of corresponding frequency set points of different relays causes almost simultaneous trigger of aforementioned stages regardless of resultant total shed load and therefore frequency behavior, which may cause sharp changes in the frequency profile and even over load shedding. In contrast, in the AUFVLS technique, distributed deployment of frequency set points results gradual trigger of feeders, i.e. slightly delayed reaction of AUFVLS method is necessary to avoid over load shedding by providing enough time for the transient and sharp jumps of the frequency resulting from already triggered stages to be damped in order the frequency trend can be properly detected [74].

Table 6.4: Total Shed Load (MW) | No. Involved Loads | Feeders

Method	S1	S2	S3
UFLS	526 | 8 | 8	1625 | 10 | 21	996 | 13 | 13
AUFVLS	507 | 5 | 6	1167 | 9 | 18	809 | 5 | 12

Table 6.5: The Simulation Parameters of Different Methods

Method	Parameters				
UFLS	f^{th} (Hz)	59.7	59.5	59.3	59.1
	T_d (cycles)	60	30	18	6
AUFVLS	f_L	f_l	f_h	f_H	f_n
	58.0 Hz	58.4 Hz	59.3 Hz	59.5 Hz	60 Hz
	T_L	T_h	Δf_i^{app}	Δf_i^{max}	v^{of}
	2 s	60 s	0.02 Hz	0.5 Hz	0.1 pu
	N^{min}	N	m		
	6	12	4		

6.2.5 Summary

The average trend of frequency oscillations following the disturbance/s is estimated using inflection points of second frequency gradient profile. Moreover, a frequency collapse barrier procedure is set up by adaptive tunning of frequency set points of load shedding relays using voltage drop data coordinated with plant protection scheme. A frequency anti stalling scheme is developed to interrupt more load feeders in case of frequency stall/stuck between successive stages. The latter time-based approach tunes the time delay of the stages to interrupt the feeders with more voltage drop first, in order to push the frequency up to the normal range before activation of plant protection relays. To avoid over load shedding, the load drop is stopped if the frequency reaches the normal range in time. In addition, tripping of producer feeders, which inject active or reactive power to the network due to penetration of renewable energy sources into the load feeders is also avoided by considering the power flow direction of feeders in the proposed scheme.

6.3 Emergency Control with High Share of RESs

6.3.1 The Time Delay Between Successive Stages

The stage delay is one of important parameters, which significantly affects the LS procedure and needs to be considered carefully [40, 42, 71]. The upper limit of stage delay is specified to avoid unnecessary postponement in the LS process, which results not only tardiness of LS procedure, but may also allow the frequency to egress from the LS frequency zone (f_L to f_H) and therefore cause early trigger of undesired stages of other load relays that may be far from the event location [40, 74].

On the other hand, the stage delay should be minimized as much as possible to fast recovery of frequency to the permissible frequency reign (f_L to f_H) or at least continuous operating range of SMs (60±0.5 Hz) [8, 40, 42]. Moreover, the time delay between consecutive stages is intentionally employed to reject probabilistic transient dips in frequency, which may come to exist due to the inter area oscillations or measurement issues [8, 39, 71] and too short delays may fail to achieve the aforementioned goal.

Severe frequency plunges, sharp downfall of frequency or a high value of ROCOF may occur in a short time of several seconds due to two main reasons or both simultaneously [8]. First, the power system suffers from a large load-generation imbalance (ΔP), which may happen in the case of islanding. Second, the share of WP in the power system is high and hence the equivalent inertia time constant (H_{eq}) is low as illustrated in section 6.1.2. The last one may happen in close future if current growth of RESs in power system continuously keeps on development without a proper countermeasure for the reduced inertia.

In conventional power systems without RESs, the time delay between 10 to 14 cycles is suggested as the lower limit of stage delay to respect the relay and circuit breaker operation times [40, 71, 74]. But in low inertia power systems, the frequency profile is steepened further and hence the situation is worsened by remarkably increment of ROCOF quantity, especially in the case of high penetration of WP. Under such a circumstances, the reaction time of relevant control actions needs to be reduced in order to be efficient in time. Furthermore, with this rapid decline of frequency and respecting the minimum time delay between consecutive stages recommended by IEEE standard, the frequency may cross the important thresholds without encountering the reaction of protection devices such as LS relays [8, 93].

The 39 bus IEEE standard test system shown in Fig. 6.24 is chosen as case study and the system data can be found in [37, 40, 74, 80]. The 4th order mathematical model, the IEEE standard governor IEESGO and Automatic Voltage Regulator (AVR) IEEEX1 are considered for all SMs. The dependency of load's active and reactive power to the voltage and frequency and the contribution share of different type of loads including light bulb (10%), fluorescent bulb (20%) and asynchronous motor (70%) are defined according to [8, 40]. The parameters of both classical UFLS [40, 71] and the proposed

scheme (AUFVLS) are available in Tab. 6.8.

The wind speed is assumed to be constant (in this case 14 m/sec) for short period of time up to tens of seconds [10, 22, 79]. A high penetration of WP in the power system about 65% is achieved by replacing the existing SMs by VSWTs as can be seen in Fig. 6.24. A comprehensive model of Permanent Magnet Synchronous Machine (PMSG) type of VSWT shown in Fig. 6.25 is employed [70, 94] and its operating point is set at a suboptimal point equal to 90% of its rated power using pitch control to provide 10% spinning reserve [10, 14]. The real and reactive power of VSWT are independently controlled by four quadrant operation of back to back voltage source converters using vector control techniques in the dq reference frame. The parallel VSWTs inside the wind farm are aggregated into a single unit with the MVA equal to the summation of the apparent power of individual units.

6.3.2 Simulation Results

The efficiency of the proposed scheme is validated in DIgSILENT PowerFactory 15.0 software. Three distinct scenarios covering different parts of the power system (Fig. 6.24) including severe combinational perturbations such as islanding and/or cascading events with high level of load-generation imbalance (ΔP), various WP Penetration share (WPP) and ROCOF quantity are selected as the disturbance. The results are compared to the classical UFLS method in term of steady state value of frequency, the total amount of shed load, the number of loads and feeders involved with the LS scheme and the voltage deviation of the load buses from their per-disturbance values.

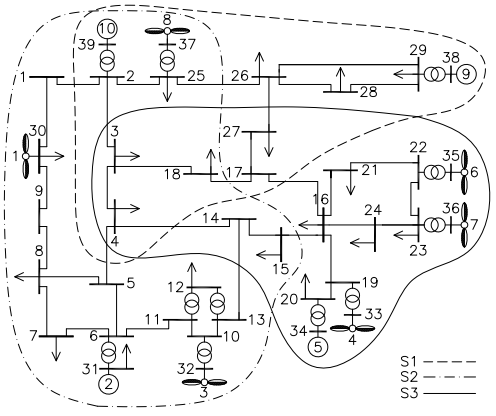

Fig. 6.24: The 39 bus IEEE test system

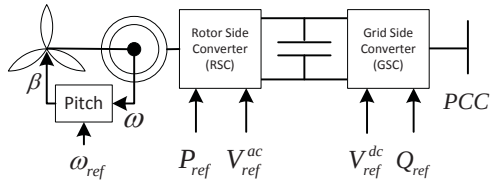

Fig. 6.25: Control structure of PMSG

6.3.2.1 Scenario 1:

In the first scenario, the G10 loss as the initiating event in 2 s causes tie-line overloading and hence cascading events including outage of tie-lines 1-2 at 3 s, 4-5 at 4 s and both 16-17 & 4-14 at 5 s, which result separation of almost a large island from the rest of power system indicated by dashed line and S1 region in Fig. 6.24. Since the G8 is replaced with a wind farm with the same capacity, just after the islanding at 5 s, 39% WP penetration, 740 MW of active power deficit (54% of remained generation) and ROCOF quantity of -0.42 Hz/s is registered.

The simulation results throughout 60 seconds of time are shown in Figs. 6.26-6.29. Fig. 6.26 indicates that the classical UFLS suffers from over LS and stables the frequency at 61.8 Hz, whereas the proposed AUFVLS yields a desired steady state frequency slightly less than 60 Hz. Fig. 6.27 demonstrates the chronological order of LS

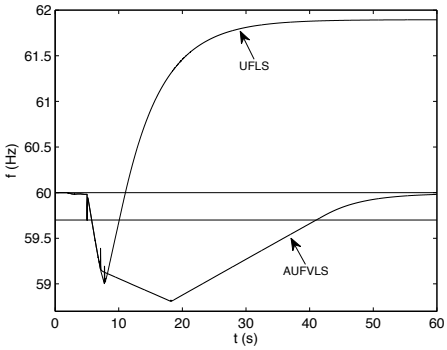

Fig. 6.26: Frequency

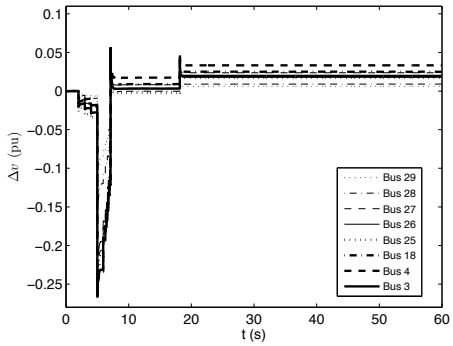

Fig. 6.28: Voltage deviation (AUFVLS)

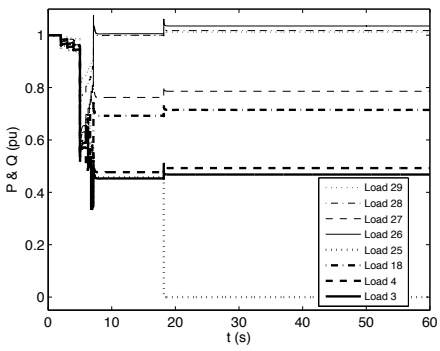

Fig. 6.27: Active power (AUFVLS)

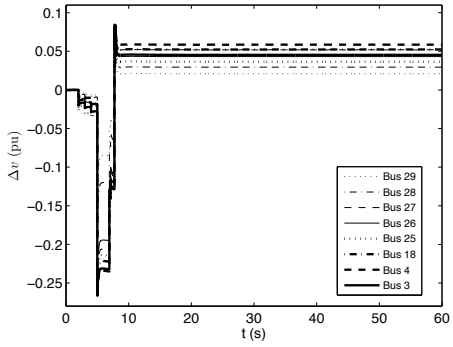

Fig. 6.29: Voltage deviation (UFLS)

plan in which just one stage of loads 27 and 18, two stages of loads 3 and 4 and all stages of load 25 are triggered.

The voltage profile resulting from AUFVLS and UFLS methods are depicted in Figs. 6.28 and 6.29, respectively, but due to the numerous voltage profiles in each figure and limited number of line styles, they are intentionally plotted in two different figures located in the same column. In order to simplify the comparison between two different column figures, the vertical axis range is deliberately selected same for both figures. The comparison of voltage profiles of AUFVLS and UFLS methods indicates better voltage profiles of AUFVLS method with less deviation from their steady state value prior to the disturbance.

Due to the high level of WP penetration and therefore large value of ROCOF, the recommended minimum time between consecutive stages elaborated in section 6.3.1 is inevitably violated at least for the incipient triggered stages, since each fired stage releases some portion of the system load and hence reduces the load-generation imbalance and as well as ROCOF quantity.

The AUFVLS method totally curtails 771 MW of load by disconnecting 10 feeders of 5 involved loads, whereas the classical UFLS drops 1095 MW of load by opening 16 feeders of 8 involved loads, which shows that the AUFLS scheme is a localized LS technique with focus of the event zone with less loads/feeders relief to retrieve to the normal condition. The comparison of pre and post-disturbance steady state values of frequency and voltages also confirms better performance of proposed method.

6.3.2.2 Scenario 2:

The second scenario (S2) specified by dash-dot line in Fig. 6.24 covers a different area of the power system partially overlapped with the first scenario. Outage of VSWT3 and transmission lines 15-16, 17-18 and 25-26 at 2 s, 3 s, 4 s and 5 s, respectively, forms the cascading events leading to the islanding situation with the load-generation mismatch equal to 1091 MW (48% of remaining generation) and faster frequency drop of -0.64 Hz/s. Replacement of G1, G3 and G8 SMs with alternative PMSG VSWTs increases the WP share percentage to 67% of total generation.

Fig. 6.30 shows that the classical UFLS leads the frequency to instability sooner than the previous scenario, whereas the AUFVLS method settles the post-disturbance frequency inside the permissible range slightly above the nominal frequency of the power system equal to f_n=60 Hz. The post-disturbance frequency at or above the nominal value is recommended by standards for the networks in which sufficient reserve capacity is not available to provide extra generation and bring the frequency up from a value inside the permissible range to the nominal value [8, 22, 74].

Despite of classical UFLS in which all 10 loads and 26 feeders of 40 available feeders in the S2 area are involved in the LS, the AUFVLS scheme merely contributes 8 loads and totally 18 feeders of them in the LS plan. Fig. 6.31 demonstrates that All of relay stages of loads 3 and 15 are consecutively triggered and the remaining 6 loads

contributing in the LS plan are partially curtailed. The shed load is non uniformly distributed across the island since the feeder selection is done based on voltage drop criterion and therefore proximity of the loads to the event location [22, 35, 36, 40, 41, 74]. In this scenario, the conventional UFLS method in addition to the over frequency, it even suffers from over voltage due to shedding the loads in improper locations, which further worses the situation (Fig. 6.33), whereas the post-disturbance voltage profiles of AUFVLS approach depicted in Fig. 6.32 are relatively desired. The total shed load, number of disconnected feeders and number of involved loads in AUFVLS and UFLS methods are 1257 MW, 18 feeder, 8 loads and 1958 MW, 26 feeder, 10 loads, respectively.

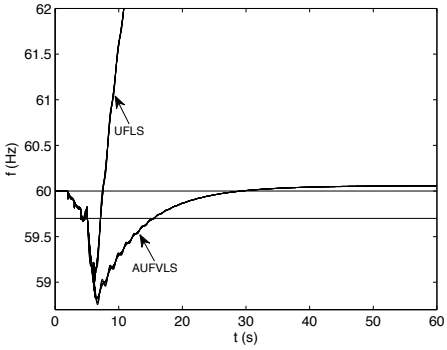

Fig. 6.30: Frequency

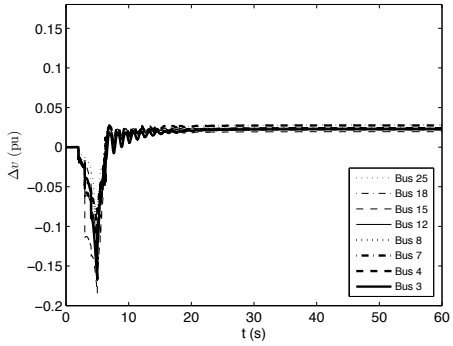

Fig. 6.32: Voltage deviation (AUFVLS)

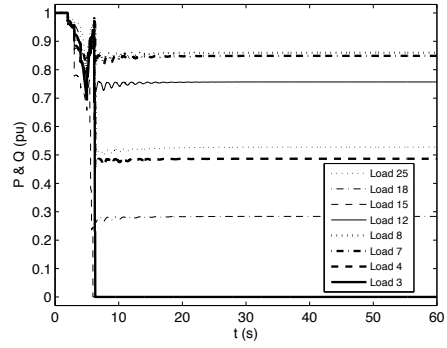

Fig. 6.31: Active power (AUFVLS)

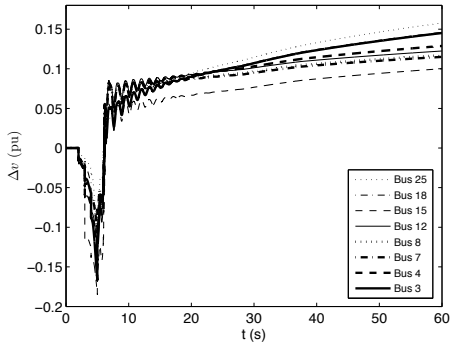

Fig. 6.33: Voltage deviation (UFLS)

6.3.2.3 Scenario 3:

The islanding in scenario S3 represented by solid line in Fig. 6.24 is initiated by loss of transmission line 13-14 at 2 s followed by cascading events such as outage of lines 4-5, 2-3 and 26-27 at 3 s, 4 s and 5 s, respectively. The highest WP share equal to 78% together with 996 MW load-generation imbalance (42%) in term of total available supply in the island results a relatively high value of ROCOF about -0.95 Hz/s.

By comparing the frequency and voltage profiles of both UFLS and AUFVLS methods plotted in Figs. 6.34, 6.36 and 6.37, acceptable performance of proposed method (AUFVLS) is explicitly revealed. Only 6 of 10 loads installed in the area S3 in Fig. 6.24 are participated in the LS by AUFVLS method. The loads 3 and 27 are completely curtailed and loads 4, 15, 16 and 18 are partially discarded (Fig. 6.35).

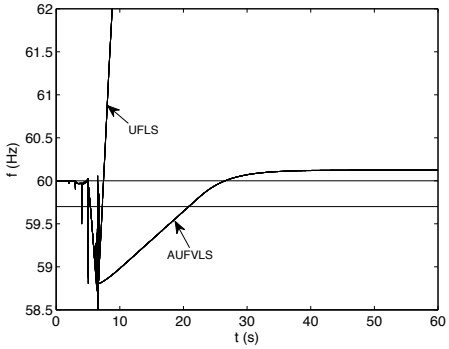

Fig. 6.34: Frequency

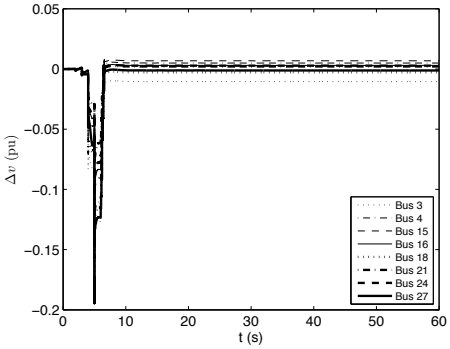

Fig. 6.36: Voltage deviation (AUFVLS)

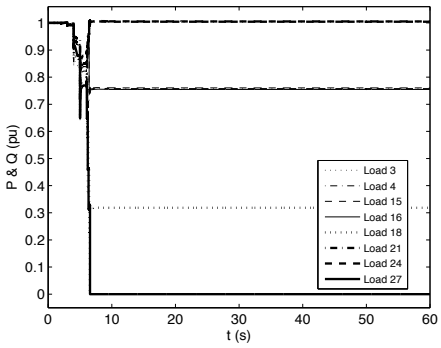

Fig. 6.35: Active power (AUFVLS)

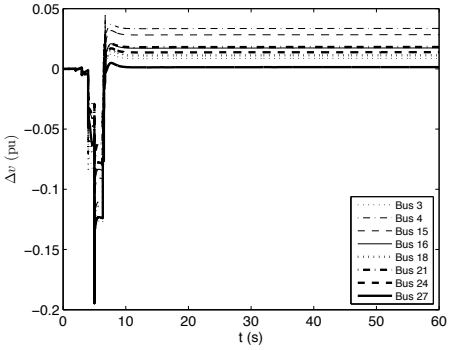

Fig. 6.37: Voltage deviation (UFLS)

6.3.3 Comparison of Different Scenarios and Discussion

By considering the frequency profiles of different scenarios, two differences are observable in the frequency behavior when the WP share is increased in the power system. First, the frequency inter-area oscillations, which are observable in the power systems with no RESs and deviate from the overall trend of frequency are reduced in the networks with high WPP. Second, the flickers/spikes/plunges are relatively increased in both frequency and voltage profiles, which may improperly trigger the protection devices e.g. ROCOF relays. They may be due to the differences in the nature of SMs and VSWTs. In the SMs, the frequency/voltage is the result of rotation of spinning masses (rotors) and these masses to some extent feel free to slightly deviate from overall frequency of power system. Furthermore, the mechanical dynamics essentially have a smooth nature due to their inherent inertia, which causes prevention of sharp changes in frequency and voltage profiles, whereas the frequency and voltage in VSWTs are directly determined by PECs, which are much faster than governor dynamics and rotor mechanical motion of SMs and may cause sharp variation of variables.

In order to simplify the comparison of different scenarios, three key variables i.e. the total shed load (ΔP), WP Penetration share (WPP) and initial value of ROCOF just after the islanding have been summarized in the Tab. 6.6. Although, the ΔP, WPP and ROCOF variables have an almost same increase trend from scenario 1 to scenario 2, but from scenario 2 to scanario 3, the ΔP is to some extent decreased whereas the WPP and ROCOF keep on same augmentation trend as before, which means that between ΔP and WPP (the two major factors that affect the ROCOF and discussed in section 6.3.1), the WPP is dominant in this case. The ROCOF equal to -0.95 Hz/s corresponding to 78% of WPP in scenario 3 indicates that if the relevant control actions do not react in time, the frequency reaches 58.0 Hz i.e. the trigger frequency of plant protection relay of SMs, which operates in 2 seconds and hence the power system encounters to more cascading events [95].

The performance of different UFLS and AUFVLS methods in distinct scenarios in

Table 6.6: The Comparison of Different Scenarios

Scenario	**ΔP MW (%)**	WPP (%)	ROCOF (Hz/s)
S1	740 (54)	39	-0.42
S2	1091 (48)	67	-0.64
S3	996 (42)	78	-0.95

Table 6.7: Total Shed Load (MW) | No. Involved Loads | Feeders

Method	S1	S2	S3
UFLS	1095 | 8 | 16	1958 | 10 | 26	1757 | 10 | 20
AUFVLS	771 | 5 | 10	1257 | 8 | 18	991 | 6 | 14

Table 6.8: The Simulation Parameters of Different Methods

Method	Parameters				
UFLS	f^{th} (Hz)	59.7	59.5	59.3	59.1
	T_d (cycles)	60	30	18	6
AUFVLS	f_L	f_H	f_n	Δv_{max}	m
	57.9 Hz	59.7 Hz	60 Hz	0.25 pu	4

term of total shed load, the number of involved loads and feeders is summarized in Tab. 6.7. Tab. 6.7 demonstrates that the normal status of the island following the severe cascading events is achieved by less shed load, involved loads and feeders in AUFVLS scheme.

6.3.4 Summary

There are two possible solutions to deal with the fast frequency drop. First, shedding the selected loads entirely at their first stage in case of high value of ROCOF especially in the incipient phase of event occurrence, which may cause sharp changes in the frequency profile and is not recommended at all. Second, disregarding the time delay between successive stages recommended by relevant IEEE standard. The time delay between two consecutive stages directly depends on how fast the ROCOF crosses the frequency threshold of the first stage and reaches the frequency threshold of the second stage. It means that the higher value of ROCOF yields less time delays, which may violate the minimum time delay recommended by IEEE standard.

Chapter VII

Conclusion

The intent of this chapter is to summarize the work, which has been done throughout this Ph.D. project, and to emphasize the main contributions of this project documented in this thesis - *A Power System Emergency Control Scheme in the Presence of High Wind Power Penetration.*

7.1 Summary

In *chapter I*, the scope of thesis including background, motivation, objectives and, last but not least, limitations are highlighted. Next, the thesis outline along with the list of corresponding publications are presented, respectively.

In *chapter II*, the power system stability states are briefly reviewed with more focus on emergency control and its countermeasures such as load shedding in the presence of high share of renewable energy sources, which is the main target of project. Afterward, the necessity of considering voltage dynamics along with frequency data to achieve coordination of under voltage and under frequency schemes is emphasized.

In *chapter III*, the recent, relevant and high-ranked literatures regarding the last research findings in this field are reviewed and classified based on their control strategy and flexibility, i.e centralized/distributed and adaptivity. Different proposed methods are compared from distinct aspects and their merits and disadvantages of each category are highlighted. The main contribution of current thesis in order to improve/advance the aforementioned state of the art is clarified at th end of chapter.

In *chapter IV*, the capabilities and ancillary services provided by variable speed wind turbines such as load-frequency control and reactive power support associated with frequency and voltage regulation following disturbance/s, respectively are studied. The aforementioned grid supports are improved to be adaptive to the magnitude and location of perturbation/s using integration of locally measured voltage drop data into the existing/conventional schemes, which implicitly indicates the electrical distance to the event location. Next, the new challenges regarding integration of high share of renewable energy sources into power system such as malfunction operation of LVRT grid code under the islanding condition, which may lead to successive outage of RESs and therefore, occurrence of cascading events is investigated.

In *chapter V*, simultaneous use of both voltage and frequency data to achieve coordination of corresponding under voltage and under frequency load shedding schemes, respectively are fulfilled. Two different methods are suggested to localize the load shedding scheme to be localized as much as possible on the event location using adaptive tunning of relay settings based on voltage drop data.

In *chapter VI*, the share of renewable energy sources in the power system is remarkably increased. Active power deficit estimation in unknown inertia power systems, i.e. in the presence of renewable energy sources and/or in case of cascading events including outage of synchronous machines is proposed. Coordination of proposed load shedding procedure with plant protection relays are carried out to prevent eventually outage of

more generation units.

7.2 Main Contributions

This dissertation addresses the decentralized power system emergency control scheme, using load shedding in the presence of high wind power penetration. The main objectives and contributions of current thesis are highlighted as below:

1. The impacts of high penetration of renewable energy sources, especially wind power on the system stability reflected in the key and determinant state variables such as frequency, voltage and frequency gradient was analyzed, and an overview of the key issues related with wind power in power system emergency control was addressed.

2. Reduction of equivalent system inertia, which is a consequence of penetration of renewable energy sources into power system and/or outage of synchronous machines during the cascading events and hence causes inaccurate estimation of actual active power deficit was investigated and considered in the proposed methods. A new method is suggested to approximate and update the actual load-generation imbalance following each load shedding stage using pre and post-disturbance rate of frequency change and the shed load amount.

3. The need for revising the tuning strategy of under frequency and voltage load shedding relays were also emphasized. The necessity of simultaneous considering frequency, voltage and rate of frequency change indices in designing a coordinated, integrated and effective load shedding procedure was shown.

4. Decentralized and automatic adjusting of frequency set points and stage time delays of load shedding relays based on voltage drop data were proposed to make the scheme adaptive to the magnitude and location of disturbance/s. In addition to its adaptive feature and easy Plug & Play installation, which handles variant topology of power system due to intermittent connectivity of RESs, a part of duty/burden of control center is assigned to the low level of hierarchal control system, i.e. distributed protection devices against Cyber Security attacks.

5. The voltage drop data were employed to localize the load shedding plan on the vicinity of event location. It means that the loads closer to the event location and experience more voltage drop participate more in the load shedding plan than distant and faraway loads.

6. In order to achieve a preventive approach, the proposed methods were coordinated with existing plant protection schemes. The frequency versus time characteristic of plant protection relays were considered in the proposed method to recover the

frequency to the permissible range in time before their activation, which causes outage of synchronous machine and therefore occurrence of more cascading events.

7. Distributed, adaptive and localized Load-Frequency Control (LFC) of variable speed wind turbines were proposed in such a way that the wind turbines with larger voltage drop at their PCC contribute more to the LFC. Localized LFC causes locally provision of demanded power as much as possible to avoid power transfer from distant generation units to the event location, which may overload transmission lines and hence lead to their outage due to the respective thermal limit.

8. The performance of LVRT grid code was investigated under the islanding condition. A much more reliable ancillary service provided by RESs during severe contingencies was proposed by changing the disconnection policy of existing LVRT grid code. The connectivity of RESs to the grid in case of having voltages close to the nominal value following the disturbances should be determined based on being the RES under mechanical or electrical stress, instead of voltage versus time characteristic of LVRT. Therefore, as far as the RES can support the grid safely by either active or reactive power, it should be remained connected to the grid.

Chapter VIII

Future Works

Although many issues have been documented in this thesis regarding power system stability and protection in presence of renewable energy sources, there are still a lot of possibilities for technology improvement. This chapter presents an outlook of the thesis topic in order to enrich the future research outcomes. Some issues of high interest for future investigations are listed below:

1. Due to the dependency of active and reactive power of loads to the voltage, the reduction of load voltage during the disturbance/s typically decreases the active and reactive power consumption. Discarding a given amount of load can be done by either disconnecting a big number of feeders with lower voltage and hence lower active power consumption than its rated value or by disconnecting a relatively smaller number of feeders with the voltage close to its nominal value and therefore rated power. The penalty cost of an interrupted feeder/costumer during load shedding is independent of its active power quantity during the disturbance. It means that despite of the fact that most of existing load shedding methods try to minimize the amount of total shed load in their proposed solution, the total cost of load shedding is not necessarily minimized by minimizing the total shed load in MW. In addition to the total shed load, the penalty cost of interrupted feeder/costumer should also be considered in the final cost function.

2. The grid code LVRT capability of Renewable Energy Sources (RESs), which may cause improper/early disconnection of them from the grid during islanding condition, should be improved by considering the available/standby/unused spinning reserve of RES, which is released for voltage regulation/reactive power support, by reducing the active power set point from MPPT to a operating point with lower efficiency during disturbances. It means that if the wind turbine still has some spinning reserve and it is not under any kind of mechanical or electrical stress, disconnection of wind turbine according to the LVRT characteristic just based on the voltage sag magnitude and/or its duration time may be an incorrect decision. Therefore, a revision of existing LVRT characteristic regarding the islanding condition is necessary.

3. The estimated active power deficit in presence of RESs needs to be examined with different scenarios including combinational and cascading events and islanding under distinct level of load-generation imbalance, wind power penetration on different power systems.

4. Nowadays, the operating points of transmission lines are close to their thermal limit due to fast growing energy demand and/or high penetration of dispersed generation into the distribution feeders. Therefore, the thermal limit of transmission lines connected to the PCC of wind turbine should be considered in the Load-Frequency Control (LFC) of wind turbines to avoid eventual outage of transmission line, which may further deteriorate the stability management.

bibliography

[1] G. W. E. C. GWEC. (2015) Global wind statistics 2014. [Online]. Available: http://www.gwec.net

[2] J. Chen, L. Jiang, W. Yao, and Q. Wu, "Perturbation estimation based nonlinear adaptive control of a full-rated converter wind turbine for fault ride-through capability enhancement," *Power Systems, IEEE Transactions on*, vol. 29, no. 6, pp. 2733–2743, 2014.

[3] Y. Yang, F. Blaabjerg, and H. Wang, "Low-voltage ride-through of single-phase transformerless photovoltaic inverters," *Industry Applications, IEEE Transactions on*, vol. 50, no. 3, pp. 1942–1952, 2014.

[4] P. Kundur, *Power system stability and control*. Tata McGraw-Hill Education, 1994.

[5] P. Kundur, J. Paserba, V. Ajjarapu, G. Andersson, A. Bose, C. Canizares, N. Hatziargyriou, D. Hill, A. Stankovic, C. Taylor *et al.*, "Definition and classification of power system stability ieee/cigre joint task force on stability terms and definitions," *Power Systems, IEEE Transactions on*, vol. 19, no. 3, pp. 1387–1401, 2004.

[6] H. Bevrani and A. Tikdari, "An ann-based power system emergency control scheme in the presence of high wind power penetration," in *Wind Power Systems*. Springer, 2010, pp. 215–254.

[7] H. Bevrani, T. Hiyama, and A. Tikdari, "On the necessity of considering both voltage and frequency in effective load shedding scheme," in *IEEJ Technical Meeting*, 2009.

[8] IEEE, "Ieee guide for the application of protective relays used for abnormal frequency load shedding and restoration," *IEEE Std C37.117-2007, Power System Relaying Committee*, pp. 1–43, 2007.

[9] P. Moutis, S. A. Papathanassiou, and N. D. Hatziargyriou, "Improved load-frequency control contribution of variable speed variable pitch wind generators," *Renewable Energy*, vol. 48, pp. 514–523, 2012.

[10] B. Hoseinzadeh, F. F. Silva, and C. L. Bak, "Coordination of voltage and frequency feedback in load-frequency control capability of wind turbine," *IEEE Industrial Electronics Society, IECON14*, pp. 5501–5507, 2014.

[11] G. Lalor, A. Mullane, and M. O'Malley, "Frequency control and wind turbine technologies," *Power Systems, IEEE Transactions on*, vol. 20, no. 4, pp. 1905–1913, 2005.

[12] G. Ramtharan, N. Jenkins, and J. Ekanayake, "Frequency support from doubly fed induction generator wind turbines," *IET Renewable Power Generation*, vol. 1, no. 1, pp. 3–9, 2007.

[13] J. Morren, S. W. de Haan, W. L. Kling, and J. Ferreira, "Wind turbines emulating inertia and supporting primary frequency control," *Power Systems, IEEE Transactions on*, vol. 21, no. 1, pp. 433–434, 2006.

[14] Z.-S. Zhang, Y.-Z. Sun, J. Lin, and G.-J. Li, "Coordinated frequency regulation by doubly fed induction generator-based wind power plants," *Renewable Power Generation, IET*, vol. 6, no. 1, pp. 38–47, 2012.

[15] D. Gautam, L. Goel, R. Ayyanar, V. Vittal, and T. Harbour, "Control strategy to mitigate the impact of reduced inertia due to doubly fed induction generators on large power systems," *Power Systems, IEEE Transactions on*, vol. 26, no. 1, pp. 214–224, 2011.

[16] E. Vittal, M. O'Malley, and A. Keane, "A steady-state voltage stability analysis of power systems with high penetrations of wind," *Power Systems, IEEE Transactions on*, vol. 25, no. 1, pp. 433–442, 2010.

[17] N. R. Ullah, T. Thiringer, and D. Karlsson, "Voltage and transient stability support by wind farms complying with the e. on netz grid code," *Power Systems, IEEE Transactions on*, vol. 22, no. 4, pp. 1647–1656, 2007.

[18] V. Akhmatov and P. B. Eriksen, "A large wind power system in almost island operation—a danish case study," *Power Systems, IEEE Transactions on*, vol. 22, no. 3, pp. 937–943, 2007.

[19] P. B. Eriksen, T. Ackermann, H. Abildgaard, P. Smith, W. Winter, and J. Rodriguez Garcia, "System operation with high wind penetration," *Power and Energy Magazine, IEEE*, vol. 3, no. 6, pp. 65–74, 2005.

[20] E. Vittal, M. O'Malley, and A. Keane, "Rotor angle stability with high penetrations of wind generation," *Power Systems, IEEE Transactions on*, vol. 27, no. 1, pp. 353–362, 2012.

[21] A. Zertek, G. Verbic, and M. Pantos, "A novel strategy for variable-speed wind turbines' participation in primary frequency control," *Sustainable Energy, IEEE Transactions on*, vol. 3, no. 4, pp. 791–799, 2012.

[22] B. Hoseinzadeh, F. F. Silva, and C. L. Bak, "Decentralized & adaptive load-frequency control scheme of variable speed wind turbines," *The 13th International Workshop on Large-Scale Integration of Wind Power into Power Systems as well as on Transmission Networks for Offshore Wind Power Plants*, pp. 747–753, 2014.

[23] H. Ahmadi and H. Ghasemi, "Maximum penetration level of wind generation considering power system security limits," *Generation, Transmission & Distribution, IET*, vol. 6, no. 11, pp. 1164–1170, 2012.

[24] C. Luo and B.-T. Ooi, "Frequency deviation of thermal power plants due to wind farms," *Energy Conversion, IEEE Transactions on*, vol. 21, no. 3, pp. 708–716, 2006.

[25] K. Antonakis, "Analysis of the maximum wind energy penetration in the island of crete," Ph.D. dissertation, Master's thesis, University of Strathclyde. Master in Science in Energy Systems and the Environment, 2005.

[26] E. Vittal, A. Keane, and M. O'Malley, "Varying penetration ratios of wind turbine technologies for voltage and frequency stability," in *Power and Energy Society General Meeting-Conversion and Delivery of Electrical Energy in the 21st Century, 2008 IEEE*. IEEE, 2008, pp. 1–6.

[27] A. Woyte, P. Gardner, and H. Snodin, "European concerted action on offshore wind energy deployment: inventory and analysis of power transmission barriers in eight member states," *Wind Energy*, vol. 10, no. 4, pp. 357–378, 2007.

[28] U.-C. P. S. O. T. Force, S. Abraham, H. Dhaliwal, R. J. Efford, L. J. Keen, A. McLellan, J. Manley, K. Vollman, N. J. Diaz, T. Ridge *et al.*, *Final Report on the August 14, 2003 Blackout in the United States and Canada: Causes and Recommendations.* US-Canada Power System Outage Task Force, 2004.

[29] G. Andersson, P. Donalek, R. Farmer, N. Hatziargyriou, I. Kamwa, P. Kundur, N. Martins, J. Paserba, P. Pourbeik, J. Sanchez-Gasca *et al.*, "Causes of the 2003 major grid blackouts in north america and europe, and recommended means to improve system dynamic performance," *Power Systems, IEEE Transactions on*, vol. 20, no. 4, pp. 1922–1928, 2005.

[30] C. Wang and M. H. Nehrir, "Analytical approaches for optimal placement of distributed generation sources in power systems," *Power Systems, IEEE Transactions on*, vol. 19, no. 4, pp. 2068–2076, 2004.

[31] B. R. Williams, W. R. Schmus, and D. C. Dawson, "Transmission voltage recovery delayed by stalled air conditioner compressors," *Power Systems, IEEE Transactions on*, vol. 7, no. 3, pp. 1173–1181, 1992.

[32] G. C. Bullock, "Cascading voltage collapse in west tennessee, august 22, 1987," in *Georgia Institute of Technology 44th Annual Protective Relaying Conference, May*, 1990.

[33] T. Van Cutsem and C. Vournas, *Voltage stability of electric power systems.* Springer, 1998, vol. 441.

[34] IEEE, "Ieee standard definitions for power switchgear," *IEEE Std C37.100-1992*, 1992.

[35] A. Saffarian and M. Sanaye-Pasand, "Enhancement of power system stability using adaptive combinational load shedding methods," *Power Systems, IEEE Transactions on*, vol. 26, no. 3, pp. 1010–1020, 2011.

[36] U. Rudez and R. Mihalic, "Analysis of underfrequency load shedding using a frequency gradient," *Power Delivery, IEEE Transactions on*, vol. 26, no. 2, pp. 565–575, 2011.

[37] J. Tang, J. Liu, F. Ponci, and A. Monti, "Adaptive load shedding based on combined frequency and voltage stability assessment using synchrophasor measurements," *Power Systems, IEEE Transactions on*, vol. 28, no. 2, pp. 2035–2047, 2013.

[38] H. Bevrani, G. Ledwich, and J. J. Ford, "On the use of df/dt in power system emergency control," in *Power Systems Conference and Exposition, 2009. PSCE'09. IEEE/PES.* IEEE, 2009, pp. 1–6.

[39] B. Hoseinzadeh, F. Faria Da Silva, and C. Bak, "Power system stability using decentralized under frequency and voltage load shedding," *PES General Meeting Conference Exposition, 2014 IEEE*, pp. 1–5, 2014.

[40] B. Hoseinzadeh, F. F. Silva, and C. L. Bak, "Adaptive tuning of frequency thresholds using voltage drop data in decentralized load shedding," *Power Systems, IEEE Transactions on*, vol. 30, no. 4, pp. 2055–2062, July 2015.

[41] M. Q. Ahsan, A. H. Chowdhury, S. S. Ahmed, I. H. Bhuyan, M. A. Haque, and H. Rahman, "Technique to develop auto load shedding and islanding scheme to prevent power system blackout," *Power Systems, IEEE Transactions on*, vol. 27, no. 1, pp. 198–205, 2012.

[42] Y.-Y. Hong, M.-C. Hsiao, Y.-R. Chang, Y.-D. Lee, and H.-C. Huang, "Multiscenario underfrequency load shedding in a microgrid consisting of intermittent renewables," *Power Delivery, IEEE Transactions on*, vol. 28, no. 3, pp. 1610–1617, 2013.

[43] A. Ghaleh, M. Sanaye-Pasand, and A. Saffarian, "Power system stability enhancement using a new combinational load-shedding algorithm," *Generation, Transmission & Distribution, IET*, vol. 5, no. 5, pp. 551–560, 2011.

[44] U. Rudez and R. Mihalic, "Monitoring the first frequency derivative to improve adaptive underfrequency load-shedding schemes," *Power Systems, IEEE Transactions on*, vol. 26, no. 2, pp. 839–846, 2011.

[45] W. A. Elmore, *Protective Relaying: Theory and Applications*. CRC Press, 2003, vol. 1.

[46] H. You, V. Vittal, and Z. Yang, "Self-healing in power systems: an approach using islanding and rate of frequency decline-based load shedding," *Power Systems, IEEE Transactions on*, vol. 18, no. 1, pp. 174–181, 2003.

[47] Y.-Y. Hong and S.-F. Wei, "Multiobjective underfrequency load shedding in an autonomous system using hierarchical genetic algorithms," *Power Delivery, IEEE Transactions on*, vol. 25, no. 3, pp. 1355–1362, 2010.

[48] Y.-Y. Hong and P.-H. Chen, "Genetic-based underfrequency load shedding in a stand-alone power system considering fuzzy loads," *Power Delivery, IEEE Transactions on*, vol. 27, no. 1, pp. 87–95, 2012.

[49] I. J. Balaguer, Q. Lei, S. Yang, U. Supatti, and F. Z. Peng, "Control for grid-connected and intentional islanding operations of distributed power generation," *Industrial Electronics, IEEE Transactions on*, vol. 58, no. 1, pp. 147–157, 2011.

[50] L. Sigrist, I. Egido, and L. Rouco, "A method for the design of ufls schemes of small isolated power systems," *Power Systems, IEEE Transactions on*, vol. 27, no. 2, pp. 951–958, 2012.

[51] K. Seethalekshmi, S. Singh, and S. Srivastava, "A synchrophasor assisted frequency and voltage stability based load shedding scheme for self-healing of power system," *Smart Grid, IEEE Transactions on*, vol. 2, no. 2, pp. 221–230, 2011.

[52] P. Anderson and M. Mirheydar, "An adaptive method for setting underfrequency load shedding relays," *Power Systems, IEEE Transactions on*, vol. 7, no. 2, pp. 647–655, 1992.

[53] V. V. Terzija, "Adaptive underfrequency load shedding based on the magnitude of the disturbance estimation," *Power Systems, IEEE Transactions on*, vol. 21, no. 3, pp. 1260–1266, 2006.

[54] M. Larsson and C. Rehtanz, "Predictive frequency stability control based on wide-area phasor measurements," in *Power Engineering Society Summer Meeting, 2002 IEEE*, vol. 1. IEEE, 2002, pp. 233–238.

[55] H. Seyedi and M. Sanaye-Pasand, "New centralised adaptive load-shedding algorithms to mitigate power system blackouts," *Generation, Transmission & Distribution, IET*, vol. 3, no. 1, pp. 99–114, 2009.

[56] I. Dobson, T. Van Cutsem, C. Vournas, C. DeMarco, M. Venkatasubramanian, T. Overbye, and C. Canizares, "Voltage stability assessment: Concepts, practices and tools," *IEEE Power Engineering Society, Power System Stability Subcommittee Special Publication*, vol. 11, pp. 21–22, 2002.

[57] V. Balamourougan, T. Sidhu, and M. Sachdev, "Technique for online prediction of voltage collapse," in *Generation, Transmission and Distribution, IEE Proceedings-*, vol. 151, no. 4. IET, 2004, pp. 453–460.

[58] G. M. Huang and N.-K. Nair, "Detection of dynamic voltage collapse," in *Power Engineering Society Summer Meeting, 2002 IEEE*, vol. 3. IEEE, 2002, pp. 1284–1289.

[59] M. Nizam, A. Mohamed, and A. Hussain, "Dynamic voltage collapse prediction in power systems using power transfer stability index," in *Power and Energy Conference, 2006. PECon'06. IEEE International*. IEEE, 2006, pp. 246–250.

[60] T. Tomšič, G. Verbič, and F. Gubina, "Revision of the underfrequency load-shedding scheme of the slovenian power system," *Electric power systems research*, vol. 77, no. 5, pp. 494–500, 2007.

[61] E. J. Thalassinakis and E. N. Dialynas, "A monte-carlo simulation method for setting the underfrequency load shedding relays and selecting the spinning reserve policy in autonomous power systems," *Power Systems, IEEE Transactions on*, vol. 19, no. 4, pp. 2044–2052, 2004.

[62] V. Chuvychin, N. Gurov, S. Venkata, and R. Brown, "An adaptive approach to load shedding and spinning reserve control during underfrequency conditions," *Power Systems, IEEE Transactions on*, vol. 11, no. 4, pp. 1805–1810, 1996.

[63] C.-T. Hsu, M.-S. Kang, and C.-S. Chen, "Design of adaptive load shedding by artificial neural networks," in *Generation, Transmission and Distribution, IEE Proceedings-*, vol. 152, no. 3. IET, 2005, pp. 415–421.

[64] E. J. Thalassinakis, E. N. Dialynas, and D. Agoris, "Method combining anns and monte carlo simulation for the selection of the load shedding protection strategies in autonomous power systems," *Power Systems, IEEE Transactions on*, vol. 21, no. 4, pp. 1574–1582, 2006.

[65] V. V. Terzija, "Adaptive underfrequency load shedding based on the magnitude of the disturbance estimation," *Power Systems, IEEE Transactions on*, vol. 21, no. 3, pp. 1260–1266, 2006.

[66] Y. Xu, W. Liu, and J. Gong, "Stable multi-agent-based load shedding algorithm for power systems," *Power Systems, IEEE Transactions on*, vol. 26, no. 4, pp. 2006–2014, 2011.

[67] M. Wooldridge, *An introduction to multiagent systems*. Wiley, 2008.

[68] IEEE, "Ieee standard for synchrophasor measurements for power systems," *IEEE Std C37.118.1-2011 (Revision of IEEE Std C37.118-2005)*, pp. 1–61, 2011.

[69] A. G. Phadke and J. S. Thorp, *Synchronized phasor measurements and their applications*. Springer, 2008.

[70] B. Hoseinzadeh and Z. Chen, "Intelligent load-frequency control contribution of wind turbine in power system stability," *EUROCON, 2013 IEEE*, pp. 1124–1128, 2013.

[71] B. Hoseinzadeh, F. Faria Da Silva, and C. Bak, "Decentralized power system emergency control in the presence of high wind power penetration," *PES General Meeting Conference Exposition, 2015 IEEE*, pp. 1–5, 2015.

[72] T. Kalogiannis, E. Muller Llano, B. Hoseinzadeh, and F. F. Silva, "Impact of high level penetration of wind turbines on power system transient stability," *Power Tech Conference Proceedings, 2015 IEEE*, pp. 1–6, 2015.

[73] B. Hoseinzadeh, F. F. Silva, and C. L. Bak, "Malfunction operation of lvrt capability of wind turbines under islanding conditions," *Power Tech Conference Proceedings, 2015 IEEE*, pp. 1–5, 2015.

[74] ——, "Decentralized coordination of load shedding and plant protection with high wind power penetration," *Power Systems, IEEE Transactions on*, 2015.

[75] A. Zertek, G. Verbic, and M. Pantos, "Optimised control approach for frequency-control contribution of variable speed wind turbines," *Renewable Power Generation, IET*, vol. 6, no. 1, pp. 17–23, 2012.

[76] N. W. Miller, W. W. Price, and J. J. Sanchez-Gasca, "Dynamic modeling of ge 1.5 and 3.6 wind turbine-generators," *GE-Power systems energy consulting*, 2003.

[77] H. Liu, A. Bose, and V. Venkatasubramanian, "A fast voltage security assessment method using adaptive bounding," *Power Systems, IEEE Transactions on*, vol. 15, no. 3, pp. 1137–1141, 2000.

[78] D. Prasetijo, W. Lachs, and D. Sutanto, "A new load shedding scheme for limiting under-frequency," *Power Systems, IEEE Transactions on*, vol. 9, no. 3, pp. 1371–1378, 1994.

[79] H. Ma and B. Chowdhury, "Working towards frequency regulation with wind plants: combined control approaches," *Renewable Power Generation, IET*, vol. 4, no. 4, pp. 308–316, 2010.

[80] H. Bevrani, F. Daneshfar, and R. Daneshmand, "Intelligent power system frequency regulations concerning the integration of wind power units," in *Wind Power Systems*. Springer, 2010, pp. 407–437.

[81] D. Xie, Z. Xu, L. Yang, J. Ostergaard, Y. Xue, and K. P. Wong, "A comprehensive lvrt control strategy for dfig wind turbines with enhanced reactive power support," *Power Systems, IEEE Transactions on*, vol. 28, no. 3, pp. 3302–3310, 2013.

[82] T. Vrionis, X. Koutiva, and N. Vovos, "A genetic algorithm-based low voltage ride-through control strategy for grid connected doubly fed induction wind generators," *Power Systems, IEEE Transactions on*, vol. 29, no. 3, pp. 1325–1334, 2014.

[83] B. Hoseinzadeh, F. Faria Da Silva, and C. Bak, "Active power deficit estimation in presence of renewable energy sources," *PES General Meeting Conference Exposition, 2015 IEEE*, pp. 1–5, 2015.

[84] V. Yaramasu, B. Wu, S. Alepuz, and S. Kouro, "Predictive control for low-voltage ride-through enhancement of three-level-boost and npc-converter-based pmsg wind turbine," *Industrial Electronics, IEEE Transactions on*, vol. 61, no. 12, pp. 6832–6843, 2014.

[85] H. Bevrani, M. Watanabe, and Y. Mitani, *Power system monitoring and control*. John Wiley & Sons, 2014.

[86] P. M. Anderson and A. A. Fouad, *Power system control and stability*. John Wiley & Sons, 2008.

[87] Y. Wang, I. Pordanjani, W. Li, W. Xu, and E. Vaahedi, "Strategy to minimise the load shedding amount for voltage collapse prevention," *Generation, Transmission & Distribution, IET*, vol. 5, no. 3, pp. 307–313, 2011.

[88] D. Karlsson and D. J. Hill, "Modelling and identification of nonlinear dynamic loads in power systems," *Power Systems, IEEE Transactions on*, vol. 9, no. 1, pp. 157–166, 1994.

[89] A. Uehara, A. Pratap, T. Goya, T. Senjyu, A. Yona, N. Urasaki, and T. Funabashi, "A coordinated control method to smooth wind power fluctuations of a pmsg-based wecs," *Energy Conversion, IEEE Transactions on*, vol. 26, no. 2, pp. 550–558, 2011.

[90] S. AbdElwahid, A. Babiker, A. Eltom, and G. Kobet, "Hardware implementation of an automatic adaptive centralized underfrequency load shedding scheme," *Power Delivery, IEEE Transactions on*, vol. 29, no. 6, pp. 2664–2673, 2014.

[91] L. Sigrist, "A ufls scheme for small isolated power systems using rate-of-change of frequency," *Power Systems, IEEE Transactions on*, vol. PP, no. 99, pp. 1–2, 2014.

[92] C. Reddy, S. Chakrabarti, and S. Srivastava, "A sensitivity-based method for underfrequency load-shedding," *Power Systems, IEEE Transactions on*, vol. 29, no. 2, pp. 984–985, 2014.

[93] N. A. E. R. C. (NERC), "Nerc prc-006, standard on automatic underfrequency load shedding," *Reliability Standards for the Bulk Electric Systems of North America*, pp. 1387–1461, 2014.

[94] I. D. Margaris, S. A. Papathanassiou, N. D. Hatziargyriou, A. D. Hansen, and P. Sorensen, "Frequency control in autonomous power systems with high wind power penetration," *Sustainable Energy, IEEE Transactions on*, vol. 3, no. 2, pp. 189–199, 2012.

[95] IEEE, "Ieee guide for ac generator protection," *IEEE Std C37.102, Power System Relaying Committee*, vol. 37, pp. 1–190, 2013.

Part II

Publications

Journal Papers

Publication J.1

(*Journal Paper*)

Decentralized Coordination of Load Shedding & Plant Protection Considering High Share of RESs

Bakhtyar Hoseinzadeh, Filipe Faria da Silva, Claus Leth Bak

The paper has been published in the
Power Systems, IEEE Transactions on,
pp. 1 –8, 2015.

Publication J.2

(*Journal Paper*)

Adaptive Tuning of Frequency Thresholds Using Voltage Drop Data in Decentralized Load Shedding

Bakhtyar Hoseinzadeh, Filipe Faria da Silva, Claus Leth Bak

The paper has been published in the
Power Systems, IEEE Transactions on,
pp. 1 –8, 2014.

Conference Contributions

Publication C.1

(*Conference Contribution*)

Decentralized Power System Emergency Control in the Presence of High Wind Power Penetration

Bakhtyar Hoseinzadeh, Filipe Faria da Silva, Claus Leth Bak

The paper has been accepted in the
Proceeding of IEEE PES General Meeting | Conference Exposition,
pp. 1 –5, July, 2015.

Publication C.2

(*Conference Contribution*)

Impact of High Level Penetration of Wind Turbines on Power System Transient Stability

Theodoros Kalogiannis, Enrique Muller Llano, Bakhtyar Hoseinzadeh, Filipe Faria da Silva

The paper has been accepted in the
Proceeding of IEEE PowerTech Conference,
pp. 1 –5, June, 2015.

Publication C.3

(*Conference Contribution*)

Active Power Deficit Estimation in Presence of Renewable Energy Sources

Bakhtyar Hoseinzadeh, Filipe Faria da Silva, Claus Leth Bak

The paper has been accepted in the
Proceeding of IEEE PES General Meeting | Conference Exposition,
pp. 1 –5, July, 2015.

Publication C.4

(*Conference Contribution*)

Malfunction Operation of LVRT Capability of Wind Turbines under Islanding Conditions

Bakhtyar Hoseinzadeh, Filipe Faria da Silva, Claus Leth Bak

The paper has been accepted in the
Proceeding of IEEE PowerTech Conference,
pp. xxx–xxx, June, 2015.

Publication C.5

(*Conference Contribution*)

Coordination of Voltage and Frequency Feedback in Load-Frequency Control Capability of Wind Turbine

Bakhtyar Hoseinzadeh, Filipe Faria da Silva, Claus Leth Bak

The paper has been published in the
Proceedings of the 40th Annual Conference of IEEE Industrial Electronics Society Conference, IECON 2014,
pp. 1 –7, June, 2014.

Publication C.6

(*Conference Contribution*)

Decentralized & Adaptive Load-Frequency Control Scheme of Variable Speed Wind Turbines

Bakhtyar Hoseinzadeh, Filipe Faria da Silva, Claus Leth Bak

The paper has been published in the
Proceeding of The 13th International Workshop on Large-Scale Integration of Wind Power into Power Systems as well as on Transmission Networks for Offshore Wind Power Plants,
Energynautics, pp. 1 –7, November, 2014.

Publication C.7

(*Conference Contribution*)

Power System Stability Using Decentralized Under Frequency and Voltage Load Shedding

Bakhtyar Hoseinzadeh, Filipe Faria da Silva, Claus Leth Bak

The paper has been published in the
Proceeding of IEEE PES General Meeting | Conference Exposition,
pp. 1 –5, July, 2014.

Publication C.8

(*Conference Contribution*)

Intelligent Load-Frequency Control Contribution of Wind Turbine in Power System Stability

Bakhtyar Hoseinzadeh, Zhe Chen

The paper has been published in the
Proceeding of IEEE EUROCON Conference,
pp. 1124 –1128, July, 2013.